AFRL-IF-RS-TR-2004-305
Final Technical Report
November 2004

WAVELET PACKETS IN WIDEBAND MULTIUSER COMMUNICATIONS

GIRD Systems, Inc.

AIR FORCE RESEARCH LABORATORY
INFORMATION DIRECTORATE
ROME RESEARCH SITE
ROME, NEW YORK

STINFO FINAL REPORT

This report has been reviewed by the Air Force Research Laboratory, Information Directorate, Public Affairs Office (IFOIPA) and is releasable to the National Technical Information Service (NTIS). At NTIS it will be releasable to the general public, including foreign nations.

AFRL-IF-RS-TR-2004-305 has been reviewed and is approved for publication

APPROVED: /s/
DAVID HUGHES
Project Engineer

FOR THE DIRECTOR: /s/
WARREN H. DEBANY, JR.
Technical Advisor
Information Grid Division
Information Directorate

REPORT DOCUMENTATION PAGE

Form Approved
OMB No. 074-0188

1. AGENCY USE ONLY (Leave blank)	2. REPORT DATE	3. REPORT TYPE AND DATES COVERED
	November 2004	**FINAL** **Jun 00 – Sep 04**

4. TITLE AND SUBTITLE

WAVELET PACKETS IN WIDEBAND MULTIUSER COMMUNICATIONS

5. FUNDING NUMBERS

C - F30602-00-C-0086
PE - 62702F
PR - 4519
TA - 42
WU - P2

6. AUTHOR(S)

Howard Fan

7. PERFORMING ORGANIZATION NAME(S) AND ADDRESS(ES)

GIRD Systems, Inc.
310 Terrace Ave.
Cincinnati OH 45220

8. PERFORMING ORGANIZATION REPORT NUMBER

N/A

9. SPONSORING / MONITORING AGENCY NAME(S) AND ADDRESS(ES)

AFRL/IFGC
525 Brooks Road
Rome NY 13441-4505

10. SPONSORING / MONITORING AGENCY REPORT NUMBER

AFRL-IF-RS-TR-2004-305

11. SUPPLEMENTARY NOTES

AFRL Project Engineer: David Hughes/IFGC/(315) 330-4122 David.Hughes@rl.af.mil

12a. DISTRIBUTION / AVAILABILITY STATEMENT

APPROVED FOR PUBLIC RELEASE; DISTRIBUTION UNLIMITED.

12b. DISTRIBUTION CODE

13. ABSTRACT *(Maximum 200 Words)*

Throughout the entire duration of this contract, the contractor has accomplished a number of tasks. First, we modeled communications channels using wavelet packets, for both time-invariant and time-varying channels. We then developed doubly orthogonal CDMA user spreading waveforms based on wavelet packets. We have also developed and evaluated a wavelet packet based multicarrier CDMA wireless communication system. In this system design a set of wavelet packets are used as the modulation waveforms in a multicarrier CDMA system. The need for cyclic prefix is eliminated in the system design due to the good orthogonality and time-frequency localization properties of the wavelet packets. Two new detection algorithms are developed to work in either time domain or wavelet packet domain to combat multiuser and inter symbol interferences. Compared with the existing DFT based multicarrier CDMA systems, better performance is achieved with the wavelet packet based system by utilizing the saved cyclic prefix overhead for error correction coding. Theoretical analyses as well as computer simulations are performed to support these claims.

14. SUBJECT TERMS	15. NUMBER OF PAGES
Wavelet packets, multicarrier modulation, CDMA, time-varying channels, channel modeling	120
	16. PRICE CODE

17. SECURITY CLASSIFICATION OF REPORT	18. SECURITY CLASSIFICATION OF THIS PAGE	19. SECURITY CLASSIFICATION OF ABSTRACT	20. LIMITATION OF ABSTRACT
UNCLASSIFIED	UNCLASSIFIED	UNCLASSIFIED	UL

TABLE OF CONTENTS

List of Figures

List of Tables

1. Introduction

Multicarrier Code Division Multiuser Access (CDMA) communication is a combination of the multicarrier modulation scheme and the CDMA concepts [1]-[8]. The basic idea to use multicarrier transmission in a CDMA system is to extend the symbol duration so that a frequency selective fading channel is divided into a number of narrow band flat fading channels, and the complex time domain equalization can therefore be replaced with a relatively simple frequency domain combining. Normally an inverse Fast Fourier Transform (IFFT) block is used in the transmitter to modulate user data onto the subcarriers, and an FFT block is used in the receiver to demodulate the data so as to achieve fast computation. Frequency domain diversity can be easily achieved in multicarrier CDMA systems by means of frequency diversity combining schemes [9]. Fast implementation and simple receiver design are especially important in wideband applications, where the data rate and consequently the processing burden are very high. However, sinusoid waveforms which are used as the subcarriers in the conventional multicarrier CDMA are not well localized in the time domain. Thus, time diversity within one chip duration is difficult to achieve. Therefore, in practice a cyclic prefix is inserted between consecutive symbols to eliminate residual Inter Symbol Interference (ISI) due to multipath. The length of the cyclic prefix is equal to or longer than the maximum channel delay spread. This method needs transmitting extra cyclic prefix, which introduces overhead and thus decreases bandwidth efficiency and data rate. A few blind methods have been proposed to eliminate such guard intervals for single user OFDM systems and MC-CDMA systems [10]-[12]. In the approach of [10] an overlapped pulse-shaping filter is used to change the transmitted signal from stationary to cyclostationary so that a second order method can be derived. Although the authors did not mention or realize it, the basic idea behind this approach is introducing some kind of time localization, which can be achieved naturally in our wavelet packet based system discussed later. The works of [11] and [12] use subspace based methods in the detection, therefore requiring much higher computational complexity. This is contrary to the basic philosophy of MC-CDMA which is developed to reduce computational complexity.

All the above works investigate system performances under time-invariant channel conditions. A number of works have been performed on the channel estimation and detection of MC-CDMA systems with time-varying channels. A tracking algorithm has been presented for the MMSE detector in multicarrier CDMA systems by Miller et al [13], where a recursive approach is used to estimate the

channel under the assumption that the channel parameters are constant over a window of several bits. Kalofonos et al [14] investigated the adaptive MMSE detectors with explicit channel estimation based on the LMS and RLS algorithms for MC-CDMA systems in fast fading channel condition. It has been shown that this approach can achieve better performance than the adaptive detection without explicit channel estimation. Linnartz [15] modeled the Doppler spread of time-varying channels and evaluated its effect on the MC-CDMA system performance. A simple channel estimation method is also proposed and proved efficient in [15]. A number of other works on multicarrier CDMA applications can be found in [16]-[21].

On the other hand, wavelet packets have good orthogonality properties and have found a number of applications in the CDMA communication systems. The wavelet packet transform can be implemented efficiently using a tree structure to achieve fast computation [22]. Hetling *et al* [23] first proposed user signature waveform designs using wavelet packets for improving cross-correlation properties over pseudo random codes. Learned et al [24] investigated a CDMA system using wavelet packet waveforms as spreading codes and designed an optimal joint detector that achieved a lower complexity compared with the conventional CDMA optimal receiver designs. Wong et al [25] investigated the timing error effect in a wavelet packet division multiplexing system. An algorithm to optimize the wavelet packet design has been derived to achieve a lower error probability. The multiple access in the work of [25] is achieved by assigning each user to a particular wavelet packet waveform, but not the CDMA concept where each user uses all wavelet packet waveforms through a distinct user code. All of these works make use of wavelet packets as some kind of non-binary spreading code and the systems they investigated can be looked at as a compromise between the CDMA and the FDMA. Wavelet packet based modulation can be used to provide multirate communications [26], multipath channel identification [27], and power spectrum shaping [28]. Newlin has given an overview of the early applications of wavelets in communications systems [29]. Wornell [30] has thoroughly reviewed three different approaches of using wavelets in communications. These designs apply to different communication channel conditions. It has been pointed out that the over-lapping of wavelet waveforms in time provides better ability to combat time-varying channel fading. Also, lower side-lobe of the wavelets performs better in rejecting narrowband interferences in multicarrier communication systems. However, [30] paid little attention to wavelet packets and the detection or receiver design issues. Other wavelet and wavelet packet based applications have been discussed in [31]-[39].

Wang *et al* [40] introduced the idea of using wavelet packets as subcarriers in the MC-CDMA system and analyzed the performance. They have cooperated error control coding to enhance the system performance. However, they have simply used wavelet packets as the modulation waveforms instead of sinusoid waveforms by replacing the FFT block with a DWPT block. There is no consideration of diversity combining in their work.

Wavelet packets have the important property of localization in both frequency and time domains, and can approach the optimum time-frequency localization measure [41]. The utilization of this property in the wavelet packet based system and detection algorithm design can provide time domain or frequency domain diversity of the multipath signals. However, this has not been thoroughly investigated in previous works. In this report we will present new detection algorithms working in the time domain and the wavelet packet domain, respectively. These detection algorithms utilize the orthogonality and time-frequency localization properties of wavelet packets to achieve time and/or frequency diversity. In these system designs a set of wavelet packets are used as the modulation waveforms in a multicarrier CDMA system. The need for cyclic prefix is eliminated in the system design and the received signals are combined in either the time domain or the wavelet packet domain to combat multipath interferences. Better bit error rate performance is achieved by utilizing the saved cyclic prefix overhead for error correction coding.

Fourier transform plays a significant role in today's signal processing and communications field. By converting both signals and systems (or communication channels) into a common "*frequency*" domain using the Fourier transform, usually a much faster implementation can be designed based on the FFT algorithm. However, although a number of different algorithms of using wavelet packets in communications have been proposed and investigated, no work has been done on modeling communication channels using wavelet packets. To fully utilize the advantages that wavelets or wavelet packets have to offer in digital communications, it is desirable to have both the transmitted signal and the communications channel represented in the same domain, for example, the wavelet packet domain.

We have therefore developed a wavelet packet based time-varying channel model [42], [43]. This channel model converts the time-varying channel impulse responses to a set of wavelet packet coefficients. These coefficients exactly represent the channel and have been used to develop a novel wavelet packet domain detection algorithm. This new detection algorithm achieved a very low computational complexity since all the signal processing is in a single wavelet packet domain.

For the time-varying channel condition, we have used a channel prediction/estimation method in the detection. A recursive least squares (RLS) algorithm is used to predict the upcoming channel coefficients, either directly in the time domain or in the wavelet packet domain. A decision feedback algorithm is used to estimate or update the current channel coefficients, which again will be used to predict future channels. Simulation examples using statistical and field measured time-varying channels validate the theoretical analysis of the new channel model, the time domain detection algorithm, and the wavelet packet domain detection algorithm. They will be presented and discussed throughout this report.

This report is organized as follows. In Section 2 the background information on multicarrier CDMA communications and wavelet packets are given followed by a brief discussion of previous work of wavelet packets in communications. A doubly orthogonal waveform based on wavelet packets that can be used as CDMA spreading waveform will be introduced in Section 3. The wavelet packet based time-varying channel model will be presented in Section 4. Section 5 discusses the system design of wavelet packet based multicarrier CDMA system and the time domain combining detection algorithm. The wavelet packet domain detection algorithm and its performance will be analyzed in Section 6. Finally, a conclusion of this work will be given in Section 7. The papers that we have published based on this work are listed in Section 8.

2. Background and Related Works

The framework of this research has been built up from two concepts, i.e., multicarrier CDMA communications and wavelet packets. We have combined the wavelet packet based signal processing theory with the well-established multicarrier modulation technology and developed a new system design based on wavelet packet multicarrier modulation. We have also proposed and evaluated two categories of detection algorithms: time domain detection and wavelet packet domain detection. In this section, an introduction of multicarrier CDMA communications and wavelet packets will be presented first. Then some previous work on the application of wavelet packets to communications, especially to CDMA and multicarrier modulations, will be introduced.

2.1 Multicarrier CDMA Communications

Multicarrier CDMA (Code Division Multiuser Access) communication is a combination of the multicarrier modulation scheme and the CDMA concept. Multicarrier transmission in the single user case is called orthogonal frequency division multiplexing (OFDM). OFDM has the advantage of low complexity because a frequency selective fading channel is divided into a number of narrow band flat fading channels by extending the symbol duration. The desired data rate is achieved by modulating the user data parallelly in a number of such subcarriers created via the Discrete Fourier Transform (DFT) and implemented by FFT. In practical implementation, a guard interval is inserted between consecutive symbols to eliminate residual ISI (Inter Symbol Interference) due to the multipath transmission of the signal. The length of the guard interval is equal to or longer than the maximum channel delay spread. In the guard interval a copy of the end part of the data symbol block is transmitted. This block is then taken out at the receiver and the linear convolution of the signal with the channel is converted into a circular convolution. Due to the convolution property of the DFT, the effect of the multipath channel is converted into a single complex channel coefficient in each subcarrier. Therefore, simpler frequency combining methods can be used to replace usually computationally complex time domain equalization algorithms. However, this method needs transmitting extra guard interval signals that introduces overhead and thus decreases efficiency and data rate. And the fixed length of the guard interval will not work well for the time-varying channel when the channel delay spread varies. If the channel spread is

shorter than the guard interval the spectral resources are wasted, while in the case the channel spread is longer than the guard interval the ISI will then not be completely eliminated.

On the other hand, CDMA provides a good way to support multiuser applications and is achieving broad applications such as in the second and third generation of cellular systems. Combining the CDMA with the OFDM results in a system that is suitable for multiuser applications and, in the mean time, keeps a possible simple implementation. Frequency domain diversity can still be easily achieved in multicarrier CDMA systems.

The combination of multicarrier transmission and CDMA can be achieved in different ways. Consequently, the multicarrier CDMA designs fall in two categories, time domain spreading and frequency domain spreading.

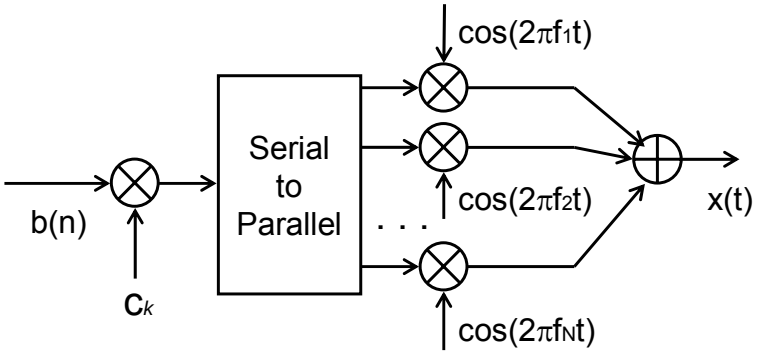

Figure 2.1 MC-CDMA transmitter

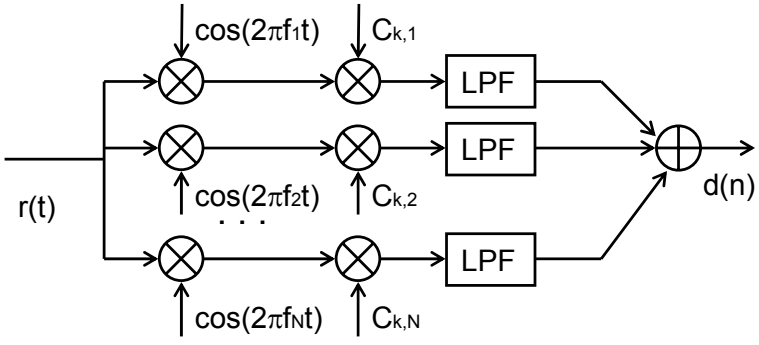

Figure 2.2 MC-CDMA receiver

2.1.1 MC-CDMA (Frequency Domain Spreading)

MC-CDMA [2]-[4] combines the multicarrier transmission with the frequency domain spreading, i.e., the original data stream from a user is spread with this user's specific spreading code in the frequency domain but not in the time domain. In other words, each symbol is transmitted simultaneously in a number of subcarriers, but multiplied by corresponding chips of the spreading code for every subcarrier. *Figures 2.1* and *2.2* give the transmitter and receiver structures of an MC-CDMA. It can be seen that the data rate for each subcarrier is only *1/N* as that of a single carrier DS-CDMA system. This means that the chip duration is *N* times longer. Therefore, the channel delay spread is comparatively shorter. If it is much shorter than the extended chip duration, the original frequency selective fading channel is divided into a number of flat fading channels. Thus, the complicated time domain equalization can be replaced by a simple gain combining in the frequency domain.

In the basic one chip per carrier MC-CDMA system, the number of subcarriers N_c is equal to the length of the spreading code N. The nth data symbol for user k, $b_k(n)$, is spread by user k's corresponding spreading code vector $\mathbf{c}_k$, each of the N subcarriers is modulated by a single chip. All the modulated subcarriers are added up to form the baseband signal as

$$x_k(t) = \sum_{m=0}^{N-1} b_k(n) c_k(m) \exp(j\omega_m t), \qquad (n-1)T_c \le t \le nT_c \tag{2.1}$$

where T_c=T_s is the chip duration which equals to the symbol duration. The frequencies for the subcarriers are usually chosen to be orthogonal to each other, that is

$$\int_0^{T_c} \cos(\omega_i t + \theta_i)\cos(\omega_j t + \theta_j)dt = 0, \qquad i \ne j \tag{2.2}$$

where ω_i and ω_j are the ith and jth carrier frequencies, and θ_i and θ_j are arbitrary carrier phases, respectively. The orthogonality condition ensures that a signal in the ith subcarrier does not cause interference to the jth subcarrier signal. However, this orthogonality might be lost because of multipath propagation or asynchronous transmission.

The combined signal for all K users, in the synchronized downlink direction, is

$$x(t) = \sum_{k=1}^{K} \sum_{m=0}^{N-1} b_k(n) c_k(m) \exp(j\omega_m t), \qquad (n-1)T_c \le t \le nT_c \tag{2.3}$$

If the channel delay spread is shorter than the guard interval inserted between the symbols, the resulting channel effect is a complex channel coefficient for each subcarrier. The equivalent received signal $r(t)$ is

$$r(t) = \sum_{k=1}^{K} \sum_{m=0}^{N-1} h(m) b_k(n) c_k(m) \exp(j\omega_m t) + n(t), \qquad (n-1)T_c \le t \le nT_c \tag{2.4}$$

where $n(t)$ is the additive white Gaussian noise, and $h(m)= \rho_m e^{j\theta_m}$ is the complex channel coefficient of the mth subcarrier. Thus, the signals from different subcarriers are subject to different amplitude and phase distortions, and the orthogonality among users is not maintained. The orthogonality among users can be restored perfectly by dividing the signals from each subcarrier with the corresponding channel coefficient of that subcarrier $h(m)$. This combination strategy (frequency domain equalization) is called Orthogonality Restoring Combining (ORC) or Zero-Forcing Combining. However, in this approach low-level subcarriers tend to be multiplied by high gains. Thus the noise in these subcarriers is enhanced which degrades the system performance. Other combining schemes such as Equal Gain Combining (EGC), Maximum Ratio Combining (MRC), Controlled Equalization (CE), and Minimum Mean Square Error Combining (MMSEC) are proposed for applications in different environments. Different multiuser detection algorithms using these combining schemes are possible to achieve further performance improvement [17-19].

It can be seen from *Figure 2.2* that the received signals from all the subcarriers are combined to generate the decision variables. Frequency diversity is explicitly achieved in MC-CDMA scheme. However, this scheme has no time diversity at all. Thus, coding and interleaving are needed prior to the modulation to combat the channel fading. Other implementation issues also need to be considered. For example, in very high data rate applications the number of subcarriers N_c needs to be very large to ensure the flat fading condition. This may increase the system complexity dramatically. Special measures need to be taken to cope with such problems.

2.1.2 MC-DS-CDMA (Time Domain Spreading)

Another way of combining multicarrier modulation with CDMA is the MC-DS-CDMA scheme that spreads the original user data stream in the time domain [6]. As shown in *Figure 2.3*, the user data stream is first serial to parallel converted into N_c (the number of subcarriers) substreams, each of which is time-spread and transmitted in an individual subcarrier. In other words, a block of N_c symbols are transmitted simultaneously. The value of N_c can be chosen according to the system design requirement. However, it is commonly assumed to be equal to the length of spreading code N which will also make the comparison with MC-CDMA easier. All these symbols are spread in the time domain using the same

spreading code for a particular user. The baseband signal for the *i*th block of data symbols for user *k*, $b_k(iN_c+m)$, $m=0,1,...,N_c-1$, is therefore

$$x_k(t) = \sum_{n=0}^{N-1} \sum_{m=0}^{N_c-1} b_k(iN_c + m) c_k(n) p_c(t - iN_c T_c - nT_c) \exp(j\omega_m t) \qquad (2.5)$$

where $p_c(t)=1$ for $0<t<T_c$ and $p_c(t) = 0$ otherwise.

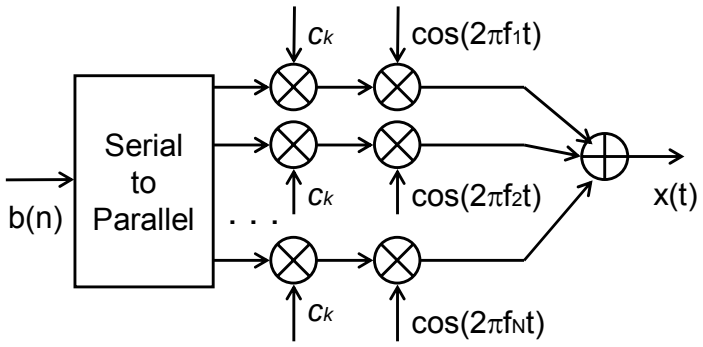

Figure 2.3 MC-DS-CDMA transmitter

It is clear that this scheme achieves time domain diversity but no frequency domain diversity for each individual data symbol. The subcarriers satisfy the same orthogonality condition as that of MC-CDMA. This scheme is suitable for uplink transmission since it is easy for the establishment of quasi-synchronization between different users. *Figure 2.4* gives the basic structure of the receiver of the MC-DS-CDMA system where each branch equals to a single CDMA signal detector. Several variations of this basic MC-DS-CDMA scheme are proposed to achieve either frequency domain diversity [7] or narrow band interference suppression [8].

Another time domain spreading multicarrier CDMA scheme called MT-CDMA scheme uses much longer spreading codes so that the bandwidth for each subcarrier signal is about the same as the original DS-CDMA signal. The signals for different subcarriers overlap heavily and do not satisfy orthogonality condition, but longer spreading codes help to eliminate the multiuser interference [5].

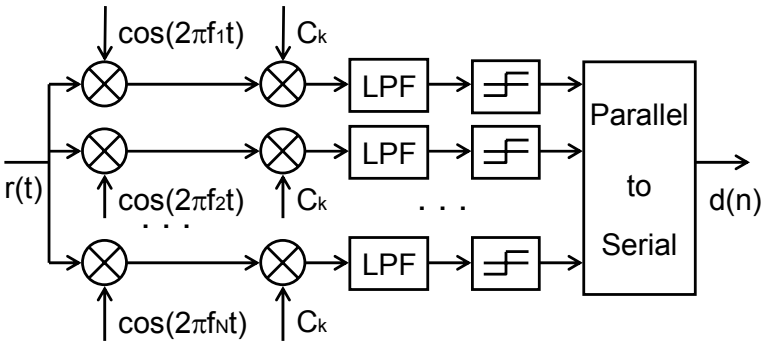

Figure 2.4 MC-DS-CDMA receiver

2.2 Wavelet Packets and Their Properties

As a generalization of wavelets, wavelet packets were introduced first for data analysis and compression. They are functions well localized in both time and frequency domains. The construction of a wavelet packet basis starts from a pair of quadrature mirror filters (QMF), g_1 and g_0, satisfying the following conditions,

$$\sum_{n=-\infty}^{\infty} g_1(n) = 2 \tag{2.6}$$

$$\sum_{n=-\infty}^{\infty} g_1(n) g_1(n-2k) = 2\delta(k) \tag{2.7}$$

$$g_0(n) = (-1)^n g_1(L-n-1) \tag{2.8}$$

The sequence of functions $\varphi_n(x)$, called wavelet packets, are recursively defined by the QMF $g_1(n)$ and $g_0(n)$ as

$$\varphi_{2n}(x) = \sum_{k \in Z} g_1(k) \varphi_n(2x-k) \tag{2.9}$$

$$\varphi_{2n+1}(x) = \sum_{k \in Z} g_0(k) \varphi_n(2x-k) \tag{2.10}$$

The first two functions of this sequence $\varphi_0(x)$ and $\varphi_1(x)$ are exactly the scaling function and its corresponding wavelet function from a Multiresolution Analysis (MRA) [22]. Since the two functions

$\varphi_{2n}(x)$ and $\varphi_{2n+1}(x)$ are generated from the same function $\varphi_n(x)$, they are called the "children" functions of the "parent" $\varphi_n(x)$. Wavelet packets have the following orthogonality properties

$$\langle \varphi_n(x-j), \varphi_n(x-k) \rangle = \delta(j-k) \tag{2.11}$$

$$\langle \varphi_{2n}(x-j), \varphi_{2n+1}(x-k) \rangle = 0 \tag{2.12}$$

Equation (2.11) indicates that each individual wavelet packet is orthogonal to its nonzero integral shifted version. Equation (2.12) means that any pair of "children" wavelet packets coming from the same "parent" function are orthogonal at all nonzero integral shifts.

Two operators, also known as filtering-downsampling processes using the QMF $g_1(n)$ and $g_0(n)$, are defined as

$$G_1\{x\}(2n) = \sum_{k \in Z} x(k) g_1(k-2n) \tag{2.13}$$

$$G_0\{x\}(2n) = \sum_{k \in Z} x(k) g_0(k-2n) \tag{2.14}$$

These two operators can be used to decompose (analyze) any discrete function x(n) on the space $\ell_2(Z)$ into two orthogonal subspaces $\ell_2(2Z)$. In each step the resulting two coefficient vectors have a length half of the input vector so that the total data length remains unchanged. The process can continue and stop at any desired step. For the deepest decomposition the output coefficient vectors become scalars. This decomposition process is called Discrete Wavelet Packet Transform (DWPT). The DWPT transform is orthogonal and the original signal x(n) can be recovered from the coefficients by the inverse transform, which is defined as a series of upsampling-filtering processes using the reversed filters $g_1(-n)$ and $g_0(-n)$. The wavelet packet function set defined in (2.9) and (2.10) can also be constructed using the Inverse DWPT (IDWPT) with the dual operators of (2.13) and (2.14) defined as,

$$G_1^{-1}\{x\}(n) = \sum_{k \in Z} x(k) g_1(n-2k) \tag{2.15}$$

$$G_0^{-1}\{x\}(n) = \sum_{k \in Z} x(k) g_0(n-2k) \tag{2.16}$$

The process of constructing a wavelet packet function set can be more clearly seen via the wavelet packet construction tree shown in Figure 2.5. Each wavelet packet function is constructed by starting from a leaf of this binary tree with an impulse δ(n), going up node by node until reaching the root of the tree. The operator from one node to an upper layer node is one of the above operators G_1^{-1} and G_0^{-1}

depending on the left/right direction. The set of functions constructed starting with all possible shifts of the impulse δ(n), from all the leafs of an admissible tree[1] form a complete orthonormal function set for the space V_1 spanned by the scaling function $\varphi_0(x)$ and its shifts, i.e., a wavelet packet basis. A large number of wavelet packet bases are available to be chosen from by different pruning of the binary wavelet packet tree for a given maximum level L.

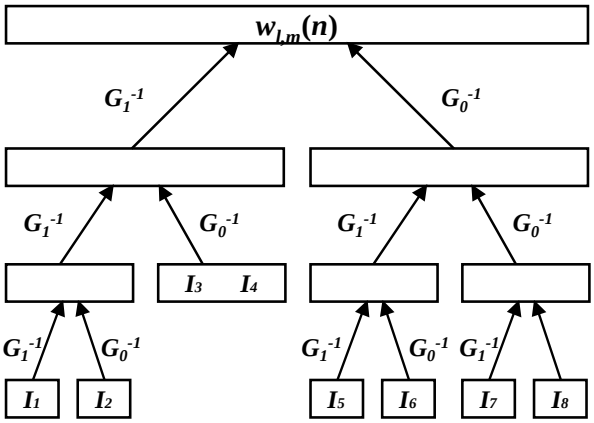

Figure 2.5 wavelet packet construction tree

Wavelet packets have the following remarkable features that make them useful in communications:

A. Flexibility-- To decompose a discrete signal with length N, there exist as many as $2^{N/2}$ to $2^{5N/8}$ wavelet packet bases, by different pruning of the binary wavelet construction tree [22]. This feature provides great flexibility for the use of wavelet packets in communications. A pruning configuration that best matches the communication channel characteristics can be chosen and adaptively modified to follow the varying communication channels in practice.

B. Time and frequency localization-- Wavelet packets are well localized in both time and frequency domains. This feature, together with the orthogonality, relaxes the requirement of frequency/time guard between different user signals because the orthogonality is maintained for overlapped (in both time and frequency domains) wavelet packets. This is also an advantage of using wavelet packets to model many communication channels that are characterized by not only frequency selectivity but also time variation.

[1] A binary tree where each node has either 0 or 2 children nodes is called an admissible tree.

C. Orthonormal basis-- An orthonormal and complete wavelet packet set, i.e., an orthonormal basis set can be constructed efficiently. This provides perfect spreading codes that have zero cross-correlations, thereby eliminating multiple access interference in the absence of synchronization error.

D. Multirate ability—An orthonormal wavelet packet basis generated from a certain configuration of a wavelet packet tree divides the frequency axis into (overlapped) bands of various sizes. The functions in the basis occupy different intervals in the time domain. This feature naturally enables multirate communications.

E. Low complexity-- A discrete signal can be decomposed into a wavelet packet basis with fast filter bank algorithms whose complexity is in the order of Nlog2N. Therefore, wavelet packet based methods have the advantage of low computation complexity.

Figure 2.6 is an example of wavelet packets generated using Daubechies 10 wavelet filter. They are listed according to the order of frequency band they occupy. Unlike the sinusoid waveforms, wavelet packets are localized in the time domain and often have a limited support. This can be seen clearly in the figure. Figure 2.7 gives the same wavelet packets but in the frequency domain (magnitude only). It is clear that wavelet packets are also well localized in the frequency domain.

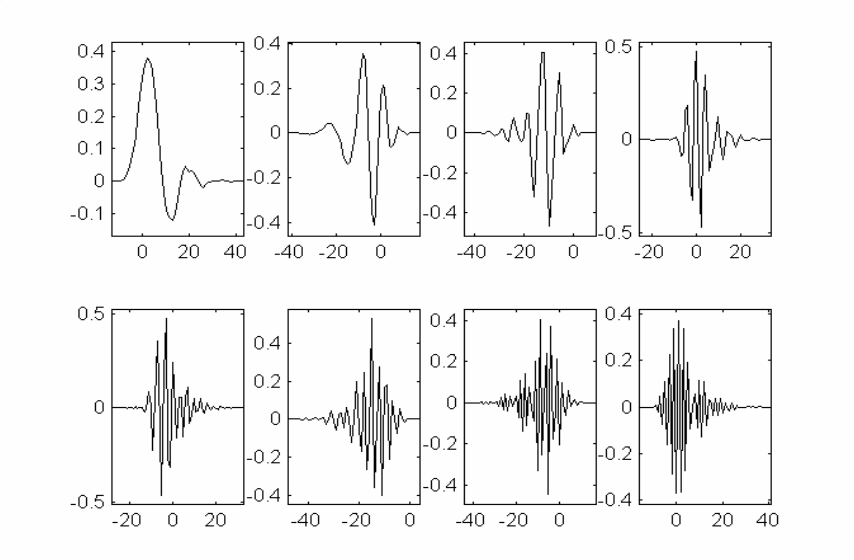

Figure 2.6 Wavelet packets generated using Daubechies 10 filter

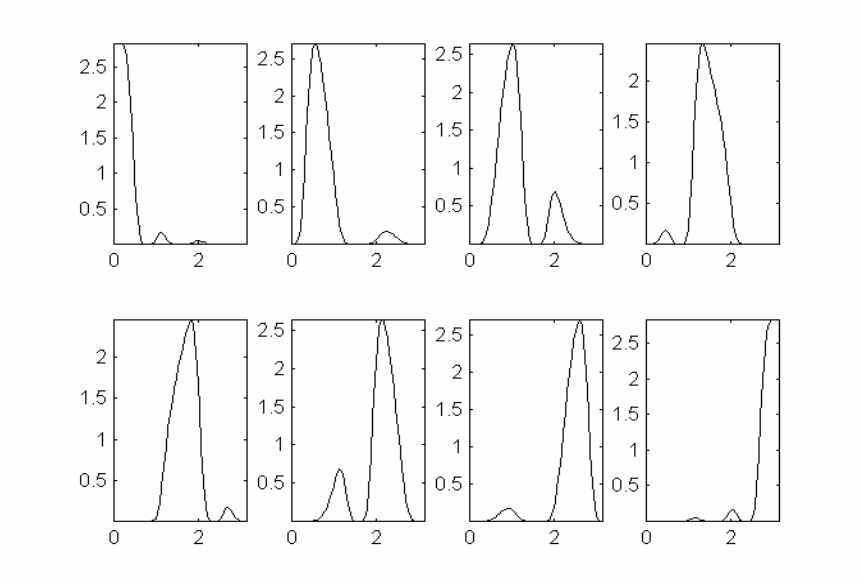

Figure 2.7 Wavelet packets in the frequency domain

2.3 Applications of Wavelet Packets in Communications

Investigations have provided promising results on the usage of wavelet packets in CDMA communications. Hetling *et al* [23] have proposed and evaluated the use of wavelet packets as spreading codes in CDMA systems. Learned *et al* [24] derived an optimal joint detector for the wavelet packet based CDMA communications. The receiver design achieved low complexity detection compared with the conventional CDMA optimal receiver designs. Lindsey [31] found that by prudent choices of the WP basis sets, wider selection of time-frequency tilings could achieve much better match of the transmission signal with the channel. Based on this observation, a method called wavelet packet modulation (WPM) was proposed and proved to achieve significant improvement of communication performance over Quardrature Amplitude Modulation (QAM). Gracias and Reddy [33] present a single user equalization algorithm for wavelet packet based modulation schemes. Wornell [30] has pointed out that the over-lapping of wavelet waveforms in time provides better ability to combat time-varying channel fading. Also, lower side-lobe of the wavelets and wavelet packets helps in rejecting narrowband interferences in multicarrier communication systems.

The approaches in the literature using wavelet packets as spreading user waveforms differ from the conventional CDMA systems in the following ways. First, they are more like FDMA or TDMA than

CDMA. Since wavelet packet basis functions have the property of localization in both time and frequency domains, each user using one particular wavelet packet as its spreading code mainly occupies relatively a small portion of the total available bandwidth, and/or transmit mainly in a small portion of the symbol duration. Thus, compared with the conventional CDMA system, this kind of multiple accesses may suffer from narrow band or impulsive interference if there is no information about the interference available at hand. Second, the orthogonality among the wavelet packet waveforms requires good, if not perfect, synchronization. However, the narrow band wavelet packet waveforms tend to behave like periodic functions, i.e., their autocorrelations have more than one major peaks. This makes the synchronization task difficult in the receiver.

Obviously, timing error cannot be ignored in many cases such as in the uplink communication in a cellular system. Wong *et al* [25] investigated the timing error effect and derived an algorithm to optimize the wavelet packet design in a wavelet packet division multiplexing system. It has been shown that a lower error probability can be achieved using the optimum design than commonly used wavelet packets. Other researchers also discussed the interference in such a spread spectrum system [37]-[38]. Most of these works propose alternative wavelet packet filter designs to reduce the multiuser interference.

Although many works using wavelet packets as user waveforms have given promising results as discussed above, many issues concerning multiple access communications remain unsolved or even untouched. In addition to the shortcomings discussed above, none of these works considered time-varying multipath channels that are common in a wireless communication environment, especially for the wideband applications in a CDMA system due to the larger bandwidth the signals occupy. Furthermore, no work has been done on the wavelet packet based channel modeling and integration of this model in the receiver design.

Multicarrier CDMA has shown promising results in wide band applications, especially its simple implementation and high efficiency due to the use of fast Fourier transform. However, the Fourier transform based system has the drawback that the subcarriers have high sidelobes in their spectrum. Therefore, interference from neighboring subcarriers is relatively strong if the channel effect is not completely compensated, because of the overlap of frequency bands among the subcarriers. Other transforms, e.g., the wavelet transform and the wavelet packet transform, may better serve as candidates

to create the subcarriers. In other words, other basis functions may have better properties suitable for multicarrier CDMA systems.

Chang *et al* [35] analyzed the MC-CDMA system based on wavelets. It has been shown that by using wavelet waveforms as the pulse-shaping filter in the MC-CDMA modulation, higher bandwidth efficiency can be achieved at the same BER level. Muayyadi and Abu-Rgheff [36] have shown in their work that an M-band wavelet based multicarrier system yields lower interchannel interference, and is more robust against multipath fading and narrow band interference. Madhukumar *et al* [37] proposed and analyzed the performance of a wavelet packet based multicarrier DS-CDMA system, with the use of a multistage interference cancellation scheme to enhance the system performance. They also used over-sampling to achieve better timing error for path resolving. However, they assumed a delay spread longer than the symbol duration, and the time localization property of wavelet packets has not been utilized to achieve intra-symbol path diversity. Bouwel *et al* [44] discussed the implementation issues of using wavelet packet transform in multicarrier modulation. It was shown that, due to the complicated frequency behavior of the wavelets, optimization of time-frequency tiling was an unrealistic task. But for a wavelet packet based multicarrier CDMA system optimization of time-frequency tiling is not the main objective. The main objective of using wavelet packets in multicarrier CDMA system is to provide time or frequency domain diversity ability and therefore improve anti-interference performance. Others have also investigated different issues of wavelet packet based multicarrier CDMA systems. Zhang and Dill [39] gave a comparison of the equalization techniques in a wavelet packet based multicarrier modulation DS-CDMA system. Wang *et al* [40] analyzed the coded wavelet packet based multicarrier CDMA system, where Reed-Muller code is used to achieve better BER performance.

Although the basic idea of using wavelet packets in multicarrier CDMA systems has been proposed and analyzed in the above works, the detection algorithms in these works are mostly a simple copy of DFT based multicarrier CDMA system receivers, with the IFFT block replaced by an IDWPT block. None of them has utilized the time and frequency localization property of wavelet packets to achieve additional time/frequency diversity in the multicarrier CDMA system.

In the following sections we will first develop wavelet packet based doubly orthogonal signature waveforms for DS-CDMA. This waveform set has much better auto- and cross-correlation properties than the conventional wavelet packets. Then time-invariant and time-varying channels will be modeled by wavelet packets as basis functions. We will then introduce two different detection algorithms that

make use of the time/frequency localization property and the orthogonality property of wavelet packets to achieve better time and frequency diversity. These new algorithms work in the multicarrier CDMA scenarios and are able to eliminate the need for cyclic prefix due to the better anti-interference ability of wavelet packet waveforms than sinusoid waveforms. They are also suitable for time-varying channels by using the time-varying channel models based on wavelet packets.

3. Wavelet Packets for Doubly Orthogonal CDMA Waveforms

As described in the previous sections, wavelet packets have good properties that make them promising candidates for communication applications. One obvious approach of using wavelet packets in CDMA communication is using them as signature waveforms, or non-binary spreading codes [23], [24]. In the case of directly using wavelet packets as non-binary spreading codes in a DS-CDMA system, the waveforms are usually chosen from an orthonormal basis such as wavelet packets so that there will be no interference between different users. However, timing errors may cause these signature waveforms to loose orthogonality to each other [25].

In this section we present new doubly orthogonal signature waveforms based on wavelet packets. This new doubly orthogonal wavelet packet based signature waveform set utilizes the orthogonality of both wavelet packets and the Walsh code. This design achieves better correlation properties than wavelet packets and is less sensitive to timing error than the ordinary wavelet packets. The double orthogonal signature design also enables easy implementation in low complexity receiver design.

3.1 Background on CDMA Using Wavelet Packets as Signature Waveforms

When applied to CDMA communications, wavelet packets are normally used as non-binary orthogonal spreading codes or signature waveforms. By arbitrary pruning of a binary wavelet packet construction tree, an orthonormal and complete wavelet packet set as an orthonormal basis can be constructed efficiently. This provides perfect spreading codes which have zero cross-correlations between any two spreading codes so that multiple-access interference is eliminated provided that no synchronization error exists. Wavelet packet based methods also have the advantage of naturally enabling multirate communication. Much work was devoted to user signature waveform designs using wavelet packets due to their potentially better cross correlation properties than the pseudorandom codes [23]-[26]. However, the approaches in the literature using wavelet packets as spreading user waveforms differ from the conventional CDMA systems in the following ways. First, they are more like FDMA or TDMA systems. Each user mainly occupies relatively a small portion of the available bandwidth, or transmits mainly in a small portion of the symbol duration. Thus, compared with the conventional CDMA system, this kind of multiple access may suffer from narrow band or impulsive interference if there is no information about

the interference available at hand. In addition, the narrow band waveforms tend to behave like periodic functions, i.e., their autocorrelations have more than one peak. This makes the synchronization task difficult in the receiver. Second, since the waveform set is generated from the nodes of the lowest level (beginning with a length 1 signal) and some higher levels of a binary wavelet packet tree, some of the waveforms are simply shifted versions of one another. Thus, this approach requires good, if not perfect, synchronization.

However, timing error cannot be ignored in some cases, such as in reverse link communication in a cellular system. Wong *et al* [25] investigated the timing error effect and derived an algorithm to optimize the wavelet packet design in a wavelet packet division multiplexing system. It has been shown that a lower error probability than commonly used wavelet packets can be achieved using the optimum design. Hetling *et al* [32] investigated the possible interference from another user waveform for asynchronous communication channel. Sesay *et al* [34] also investigated the multiuser interference from the perspective of auto- and cross-correlation functions and error probability in a waveform division multiple access system. Other researchers also discussed the interference in such a spread spectrum system [28][61]. Most of these works propose alternative wavelet packet filter designs to reduce the multiuser interference.

In the following, we describe and investigate a doubly orthogonal wavelet packet set, which utilizes double orthogonality based on both wavelet packets and binary Walsh codes. This double orthogonality produces much better auto- and cross-correlations and performs better than the ordinary wavelet packet sets, especially in the case of not accurate timing estimation. The double orthogonality may also enable low complexity receiver design. Computer simulation results confirm the effectiveness of this new waveform design.

3.2 Doubly Orthogonal Signature Waveforms

We propose a set of user waveforms as a candidate of spreading codes for a CDMA system. The code waveforms should have good autocorrelation and cross correlation properties. The autocorrelation functions should have only one narrow peak. This ensures the initial acquisition and the following tracking of synchronization. The cross correlation between any pair of waveforms in the set should be small, and the shifted cross correlations should be also small enough so that the multiple access interference due to other users can be maintained at minimum. The proposed doubly orthogonal wavelet packet waveforms have the desired correlation properties.

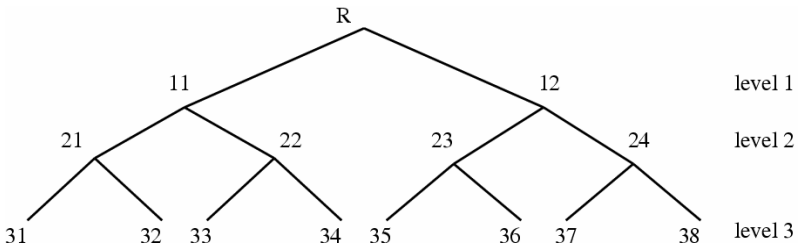

Figure 3.1 Binary wavelet packet tree structure

As discussed in Section 2, wavelet packet waveforms are generated by up-sampling and filtering impulses from certain nodes of the binary wavelet packet tree. *Figure 3.1* shows one example of the binary wavelet packet tree structure. To generate wavelet packet waveforms, we begin from a certain node and go up to the root of the tree by up-sampling and filtering an impulse signal. The level and position of the node determine how many times of the up-sampling and filtering process are taken and types of the filter, usually a low-pass or high-pass quardrature mirror filter. As shown in *Figure 3.1*, from eight level-3 nodes of the tree, we can generate eight wavelet packet waveforms. The length of the generated waveforms is determined by the length of the input impulse signals. The shortest waveform can be generated from a level-3 node is length 8, if the input impulse has a length of 1. However, the filtering process will make the generated waveforms to fold several times. Higher filter level results in more folding. As a consequence, some of the waveforms from different nodes become just shifted versions of each other, and may not be used in an asynchronous system.

Now consider the proposed doubly orthogonal wavelet packet waveforms. Without loss of generality, we consider a 64-user CDMA system. Instead of generating all 64 waveforms from 64 level-6 nodes, we divide the users into 8 groups, named A through H, each containing eight users. We also chop each symbol into 8 chips in the time domain. Each group of 8 users associates with one length 8 Walsh code as the chip code for each symbol interval. Due to the orthogonality of Walsh code, we will soon find these 8 groups of users have waveforms orthogonal to each other. The 8 users in one group are assigned orthogonal waveforms based on wavelet packets. If we generate the wavelet packet waveforms from all the eight level-3 nodes of a wavelet packet tree, we can generate 8 orthogonal wavelet packet waveforms. We name these wavelet packet waveforms from 1 to 8. The proposed doubly orthogonal waveforms are thus generated by mapping the 8 wavelet packet waveforms to each of the 8 chips of the Walsh code. Eight different ordering possibilities of the mapping enable us to fit 8 users in one Walsh

code. Thus totally we can generate 64 different user waveforms. The mapping is simply done by multiplying the wavelet packet waveforms with the Walsh code chip value, i.e., 1 or -1.

Figure 3.2 is an example of the mapping matrix which defines the 8 different orders of mapping wavelet packet waveforms to Walsh code chips of all '1's, i.e., user group A. The numbers shown in the 8×8 matrix is the wavelet packet waveform indexes (1 to 8). Each column in the mapping matrix corresponds to one Walsh code chip, or one time slot. Each row in the matrix corresponds to one possible order of mapping 8 wavelet packet waveforms to 8 chips. This defines a unique user waveform. Eight rows define eight user waveforms in one user group. For example, the third row specifies that the waveform for user 3 in the group is generated by concatenating wavelet packet waveforms 3, 7, 4, 5, 8, 2, 6, and 1. This particular order makes the waveform unique. Other users have different mapping orders so that the generated waveforms differ from that of user 3. Note that in each time slot the 8 users have been mapped with 8 different wavelet packet waveforms. This ensures that the 8 user waveforms in the same user group are orthogonal to each other. Since all of the rows define mappings of all the 8 wavelet packet waveforms to the Walsh chips, all user waveforms will occupy the entire frequency bandwidth as well as all the time slots.

chipslots	*1*	*2*	*3*	*4*	*5*	*6*	*7*	*8*
*user*1	1	2	3	4	5	6	7	8
*user*2	2	1	6	8	4	3	5	7
*user*3	3	7	4	5	8	2	6	1
*user*4	4	8	7	2	6	1	3	5
*user*5	5	4	2	7	3	8	1	6
*user*6	6	5	8	1	2	7	4	3
*user*7	7	6	5	3	1	4	8	2
*user*8	8	3	1	6	7	5	2	4

Figure 3.2 Chip wavelet packet indexes of 8 group A users

Since different users occupy distinct wavelet packet waveforms in any of the time slots, it is desirable to represent the signal using permutation notations. Using the above example, the eight rows or eight columns in the mapping matrix are different permutations of $X_8 = \{1,2,3,4,5,6,7,8\}$. Note that absence of repetition of the eight wavelet packet waveforms in each column is important to ensure

orthogonality, whereas such absence in each row is not essential, although desirable. The constructed signal set of group A users using the above example is

$$s_{A,k}(n) = \sum_{i=1}^{8} P_{3,\sigma_i(k)}(n-8(i-1)), \qquad k = 1,...,8 \tag{3.1}$$

where $\sigma_i(k)(i = 1,...,8)$ are eight permutations of X_8 for the k*th* user, and $P_{3,l}(l = 1,...,8)$ are eight wavelet packet waveforms each with length 8.

For user Group B, the Walsh code is, e.g., 1,1,1,1,-1,-1,-1,-1. Then the mapping matrix should be the same as *Figure 3.2*, except that in the last four columns all wavelet packet waveforms need to be multiplied by -1. Other user groups follow *Figure 3.2* and the corresponding Walsh codes in a similar way. Thus the constructed signal set of the k*th* user in the j*th* group is

$$\begin{aligned} &s_{j,k}(n) = \sum_{i=1}^{8} O_j(i) P_{3,\sigma_i(k)}(n-8(i-1)) \\ &j = A, B, ..., H, \qquad k = 1, 2, ..., 8 \end{aligned} \tag{3.2}$$

where $O_j(i),(i = 1,2,...,8)$ is the j*th* length 8 Walsh code. Since the Walsh codes form an orthogonal basis, user waveforms with same wavelet packet mapping orders but in different groups are also orthogonal to each other. For example, user 1 in group A and B have the same wavelet packet mapping order, but because the wavelet packet waveforms are multiplied by two orthogonal Walsh codes, these two waveforms are orthogonal to each other. It is easy to see that user waveforms in different groups and with different mapping orders are also orthogonal to each other. Thus, the 64 user waveforms form an orthogonal set.

This algorithm can be generalized to achieve a tradeoff between the autocorrelation and cross correlation properties of the waveforms. If the desired length of the waveforms is $N = 2^{j+k}$, we can divide the users into $M = 2^j$ groups, and generate length of $L = 2^k$ wavelet packet waveforms. An orthogonal waveform set can be formed by combining the wavelet packet waveforms according to the above algorithm. The number of waveforms in the set is $N = L \times M$. A tradeoff between the autocorrelation and cross correlation properties can be achieved with different combinations of *L* and *M*. In general, a smaller *M* and a larger *L* results in better cross correlation but poorer autocorrelation, and vise versa.

3.3 Correlation Properties of The Waveforms

Now, we investigate the autocorrelation and cross-correlation properties of the waveforms proposed in the last section. As an example, we choose the Daubechies 4 wavelet as the mother wavelet from which a wavelet packet tree is constructed. The reason is that the order of the filter is lower than other wavelets because Daubechies wavelets have minimum size of support. The correlation functions we are to investigate are discrete periodic auto- and cross-correlation functions defined as

$$R_i(k) = \frac{1}{N}\sum_{n=0}^{N-1} s_i(n)s_i(n+k) \tag{3.3}$$

and

$$C_{ij}(k) = \frac{1}{N}\sum_{n=0}^{N-1} s_i(n)s_j(n+k) \tag{3.4}$$

where N is the waveform length. We have also investigated the averaged cross-correlation functions defined as

$$\overline{C}_i(k) = \frac{1}{N-1}\sum_{j=1,\, j\neq i}^{N} C_{ij}(k) \tag{3.5}$$

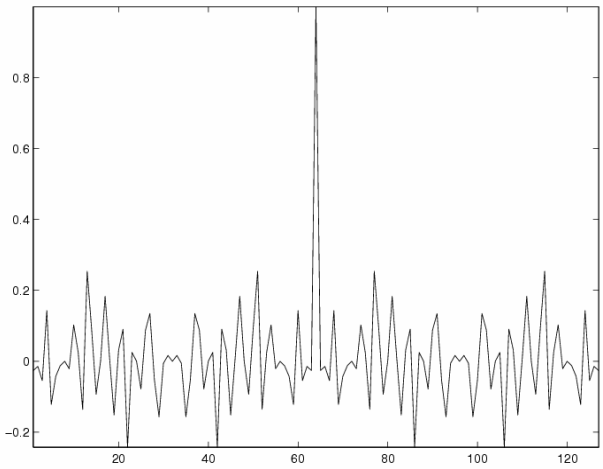

Figure 3.3 Autocorrelation of a DOWP waveform

Figure 3.3 gives an example of the autocorrelation function of a length-64 doubly orthogonal wavelet packet waveform. We can see that this autocorrelation has a single narrow peak. This is similar to the

autocorrelation function of the length-63 Gold code given in *Figure 3.4*. *Figure 3.5* gives an example of the autocorrelation function of a length-64 wavelet packet waveform, which is much worse.

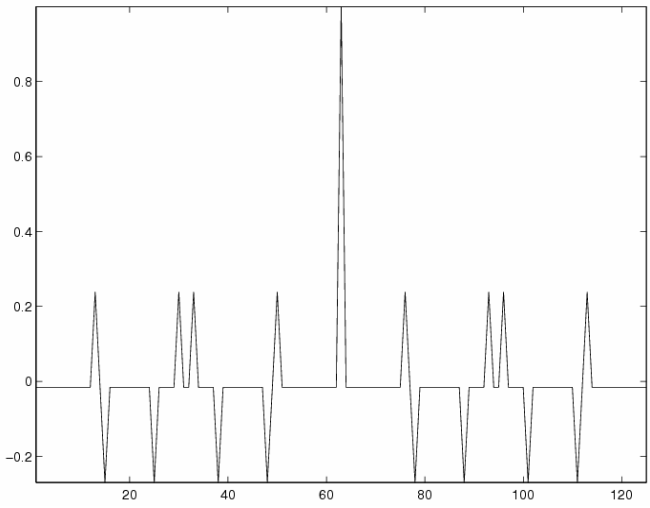

Figure 3.4 Autocorrelation of a length-63 Gold code

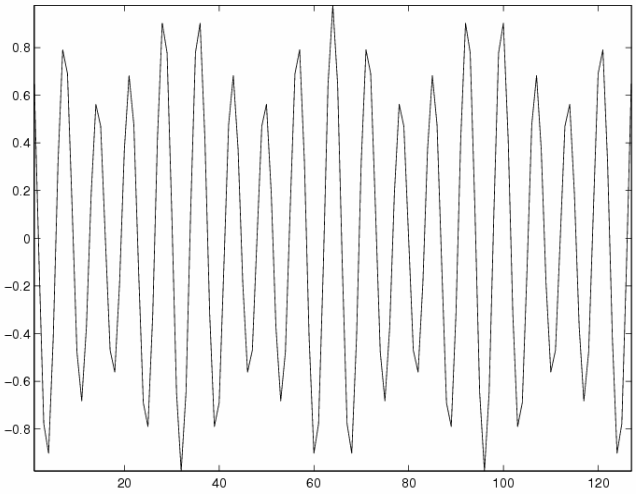

Figure 3.5 Autocorrelation of a WP waveform

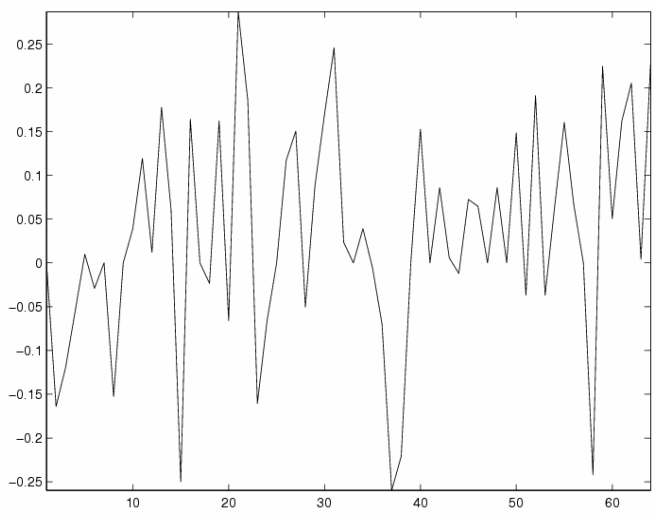

Figure 3.6 Cross-correlation of a pair of DOWP waveforms

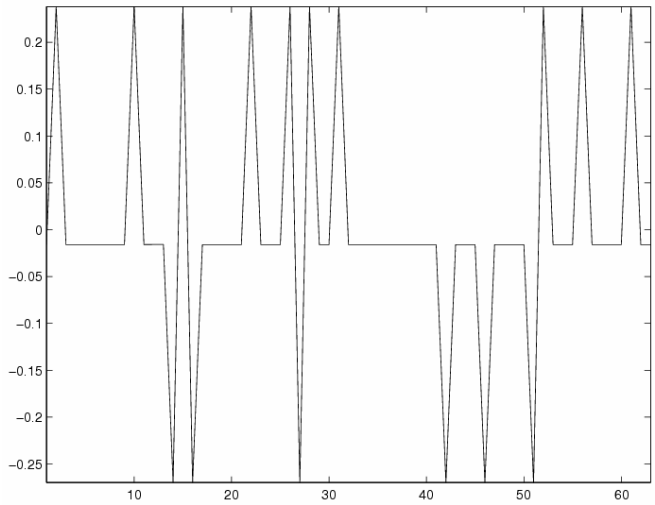

Figure 3.7 Cross-correlation between a pair of Gold codes

Figure 3.6 gives an example of the cross-correlation function between a pair of doubly orthogonal wavelet packet waveforms. Note that the cross-correlation is zero when the relative shift of the two waveforms is zero. Compared with the cross-correlation function of Gold codes given in *Figure 3.7*, we can find that the cross-correlation of the proposed waveforms is in the same level with that of Gold codes, but not as regularly distributed. For the conventional wavelet packets, the cross-correlation is much better than Gold codes on the average [23]. However, in the wavelet packet set many waveforms are the shifted versions of one another, which gives poor cross-correlation. *Figure 3.8* gives such an example of the cross-correlation function between a pair of length-64 wavelet packet waveforms. Since

these two waveforms are shifted versions of each other, the cross-correlation not only has large values but also has value '1' for some relative shifts. This is not the case for the doubly orthogonal wavelet packet waveforms.

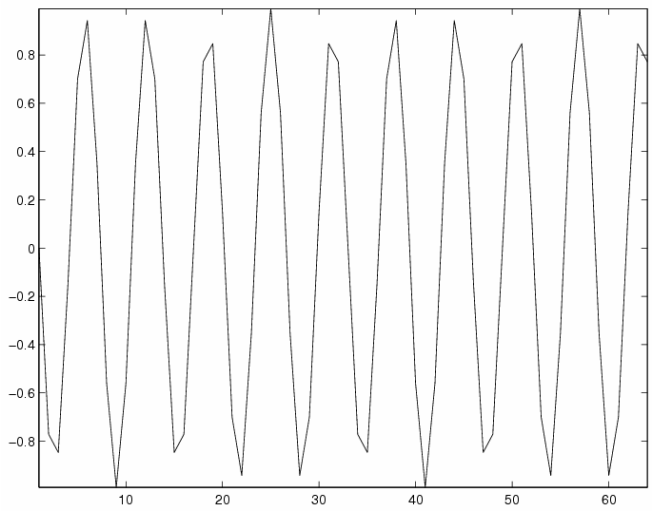

Figure 3.8 Cross-correlation between a pair of WP waveforms

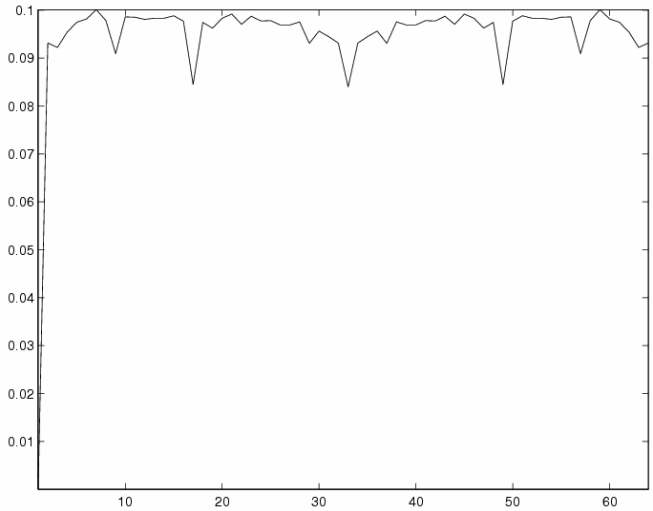

Figure 3.9 Averaged cross-correlation of a DOWP waveform

Figure 3.9 gives an example of the averaged cross-correlation function of one doubly orthogonal wavelet packet waveform. Compared with the averaged cross-correlation function of Gold code given in *Figure 3.10*, we can find the proposed waveforms are at a similar level. *Figure 3.11* gives the averaged

cross-correlation function of a length-64 wavelet packet waveform. We can see that the cross-correlation of the doubly orthogonal wavelet packet waveform is higher than that of a conventional wavelet packet waveform. However, the proposed waveforms do not have any large cross-correlation values as the conventional wavelet packet waveforms in *Figure 3.8*.

These figures have shown that the doubly orthogonal signature waveforms have much better auto- and cross-correlations than the ordinary wavelet packet sets. This will improve the ability of interference rejection, especially in the case when accurate timing estimation is not available. These signature waveforms have similar correlation property as that of Gold code. However, they enable low complexity receiver design and naturally support multirate applications.

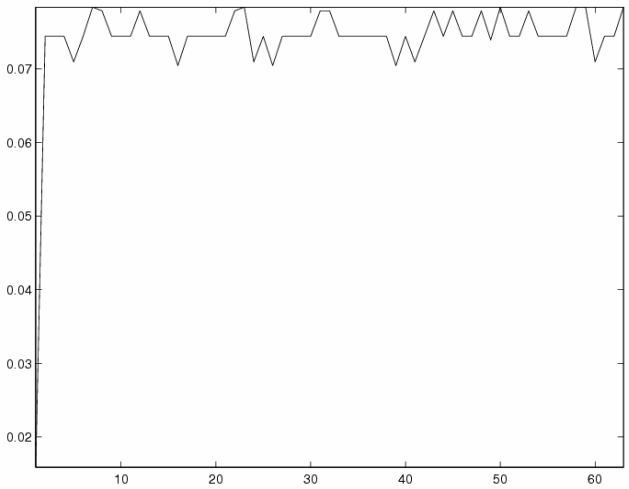

Figure 3.10 Averaged cross-correlation of a Gold code

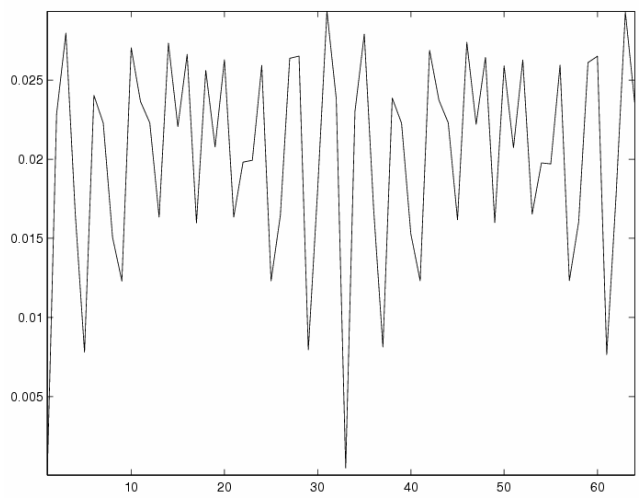

Figure 3.11 Averaged cross-correlation of a WP waveform

3.4 Over Loaded Waveform Design

In the previous sections, the design algorithm and performance evaluation of the doubly orthogonal signature waveform based on wavelet packets and Walsh code are presented. The designed waveform set has desired auto- and cross-correlation properties as shown in Section 3.3. It is not possible to add more waveforms into this basic waveform set while keeping the orthogonality because the dimension is limited by the waveform length. Yet, it is possible to add more waveforms if the orthogonality requirement is relaxed. This relaxation is reasonable in asynchronous systems because timing error makes perfect orthogonality impossible. However, it is still desired that the cross-correlation between any pair of the waveforms be kept at a low level.

In the following, another set of orthogonal waveforms is constructed as a complementary waveform set to the basic set described above. Any waveform in this supplementary set has at most one common chip waveform with any one in the basic waveform set. As to the 64-user waveform basic set example, an example of mapping matrix for constructing the supplementary waveform set is depicted in *Figure 3.12*. The number of available waveforms in the supplementary set is limited by two factors. First, it is not allowed to have more than one common chip waveform at the same chip intervals between the basic set and the supplementary set of waveforms. Second, the desired low level cross-correlation requires as few shifted common chip waveforms as possible between these two sets.

The example supplementary mapping matrix in *Figure 3.12* adds 16 waveforms to the basic set so that a total number of 80 waveforms are constructed, each having only length 64. Note that once the orthogonality requirement is relaxed, one can add more user waveforms in much the same way in those systems that use the pseudo-random binary waveforms or the conventional wavelet packets. However, our particular design using the doubly orthogonal wavelet packets ensures minimum overlap of chip waveforms with those in the basic set. This in turn results in lower cross-correlation of the enlarged set than the conventional wavelet packets, as will be shown in the following.

$$\begin{array}{lc} \textit{chipslots} & \begin{matrix} 1 & 2 & 3 & 4 & 5 & 6 & 7 & 8 \end{matrix} \\ \textit{user}9 & \begin{bmatrix} 1 & 4 & 8 & 6 & 7 & 5 & 2 & 3 \end{bmatrix} \\ \textit{user}10 & \begin{bmatrix} 3 & 8 & 5 & 2 & 4 & 1 & 7 & 6 \end{bmatrix} \end{array}$$

Figure 3.12 Chip wavelet packet indexes in the supplementary waveform set

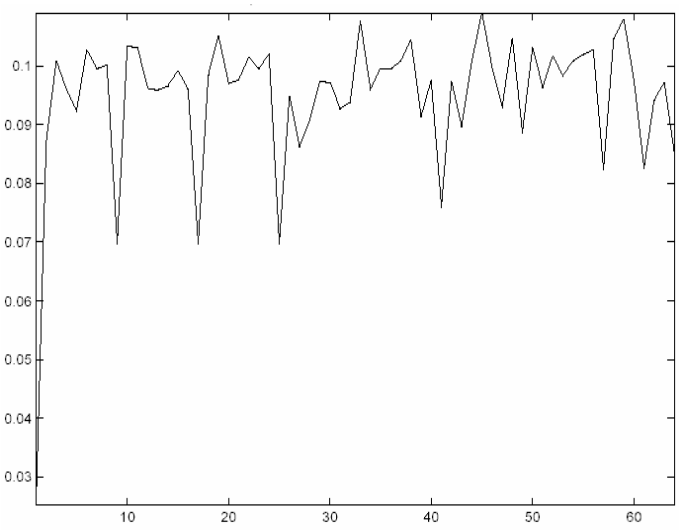

Figure 3.13 Averaged cross-correlation of a over-loaded DOWP waveform

The autocorrelation property for the waveforms in the supplementary set is the same with that of the basic waveform set. However, adding the two sets together raises the cross-correlation to a slightly higher level, as illustrated in *Figure 3.13*. As a comparison, *Figure 3.14* gives the cross-correlation between a pair of over-loaded wavelet packet waveforms proposed in [24]. It can be seen that it has not only a high level of cross-correlation, but also a non-zero cross-correlation for the unshifted waveform pair. *Figure 3.15* gives the averaged cross-correlation of a length-63 pseudo-random binary sequence in

the large Kasami set of 520 sequences. It can be seen that the proposed waveform set has about the same level of cross-correlation with the Kasami sequence set. However, they have the advantage of low computational complexity receiver design and naturally support multirate applications.

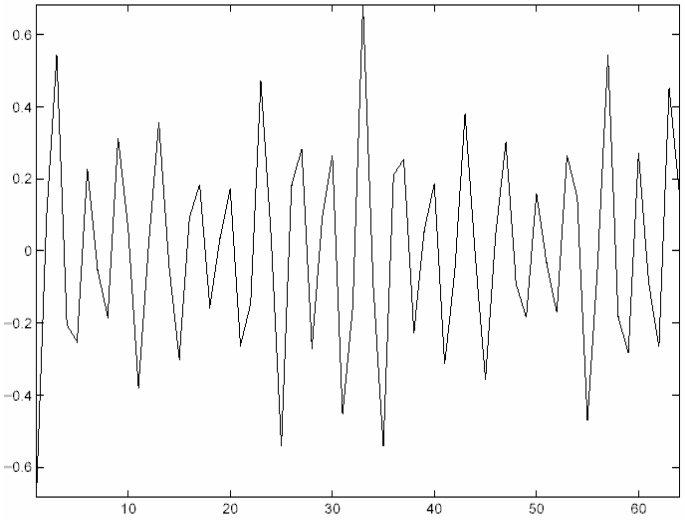

Figure 3.14 Cross-correlation between a pair of over-loaded WP waveforms

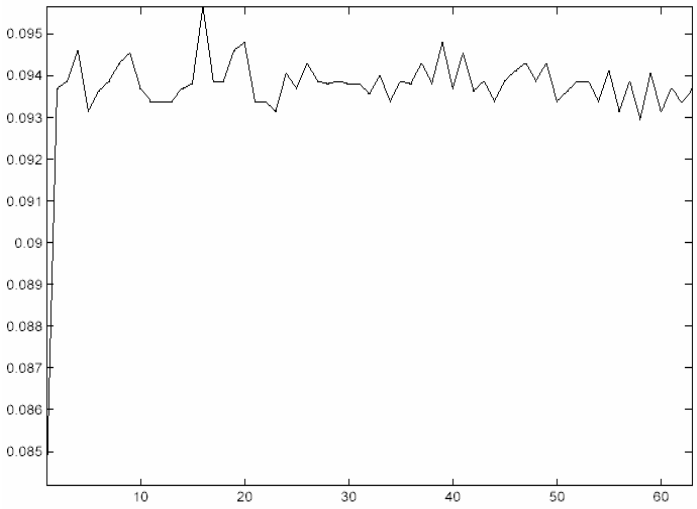

Figure 3.15 Averaged cross-correlation of a large Kasami code

4. Wavelet Packet Based Time-Varying Channel Modeling

Wireless communication systems encounter time-varying multipath fading channels that introduce distortion to signals. A wavelet packet based approach to study such time-varying channel effects seems appropriate, especially when the signals are modulated using the wavelet packet basis functions. It can be expected that a receiver design can utilize this kind of channel modeling to achieve better performance or simpler implementations, similar to what has been done in the "*Fourier kingdom*". However, no report has been found in modeling wireless channels using wavelet packets, although there are a number of works on wavelet packet based modulation.

The well-established Fourier transform is suitable for time-invariant analysis since it is based on time-unlimited sinusoid basis. However, it is not an efficient analysis tool for time-varying channel modeling. A few methods have been studied for time-varying channel modeling. For example, time-varying channels have been modeled using a time-Doppler representation [45]. However, the time-Doppler model can be considered only a special case of the much more general wavelet packet based model described here. In particular, wavelet packet based time-varying channel modeling can be more efficient in that fewer coefficients may be needed compared to the time-Doppler model. In addition, the flexible time-frequency tiling property of wavelet packets may enable a wavelet packet channel model to more efficiently represent certain types of wireless channels. Both these aspects become more prominent when modeling wideband channels.

Doroslovacki and Fan [46] proposed an algorithm to model time-varying systems by discrete time wavelets. They proved that a time-varying system could be represented by two sets of wavelets and a constant coefficient matrix.

Wavelet packets provide more flexible representation of signals and channels than wavelets. This is due to the flexible wavelet packet binary analysis/synthesis tree structure. Based on this idea, the wavelet-based system model [47] is extended to wavelet packets for time-varying channel modeling. This section presents the wavelet packet based channel modeling. This modeling algorithm has been evaluated for time-invariant channels, statistical model of indoor channels, and field measured time-varying wireless channels.

When wavelet packets are used as modulation waveforms in a CDMA or multicarrier CDMA system, the baseband version of the transmitted signal is a combination of shifted wavelet packets. If the time-varying channel itself can be well represented by means of a wavelet packet basis, it is then possible to utilize the remarkable orthonormality and flexible tree-structure of the wavelet packet basis to achieve efficient channel equalization and multiuser detection. In this section, we study such modeling issue, starting with modeling time-invariant channels, then progress onto modeling time-varying channels. The utilization of this channel model in the signal detection of wavelet packet based multicarrier CDMA systems will be addressed in the following sections.

4.1 Time-Invariant Channel Model

A time-invariant wireless communication channel can be fully described by its impulse response. In the following the channel and the wavelet packets are represented in their continues-time form. The discrete-time form remains valid in a similar way. A time-invariant channel impulse response $h(t)$ can be represented by a set of wavelet packets $\varphi_j(t)$, j=1,2,…,N, as

$$h(t) = \sum_{j=1}^{N} \alpha_j \varphi_j(t) \qquad (4.1)$$

The set of wavelet packet coefficients α_j are unique since the wavelet packets form a complete basis. They can be obtained from the inner product of $h(t)$ and the wavelet packets as

$$\alpha_j = \left\langle h(t), \varphi_j(t) \right\rangle \qquad j = 1, 2, ..., N \qquad (4.2)$$

This wavelet packet domain representation is accurate and can be seen from the following simulation. In the simulation the wavelet packet based channel representation in (4.1) is used to model time-invariant channels from field measured data obtained from a Rice University website, and one example is shown in *Figure 4.1*. The channel length is 512. As to the wavelet packet basis, we choose Daubechies 10 wavelet as the mother wavelet from which a wavelet packet tree is constructed. The reason for choosing Daubechies wavelet packets is that they have a compact support of minimum size for a given vanishing moment. This minimum support is helpful for the system and receiver design because the computational complexity of the system is highly dependent upon the length of the used Quardrature Mirror Filters.

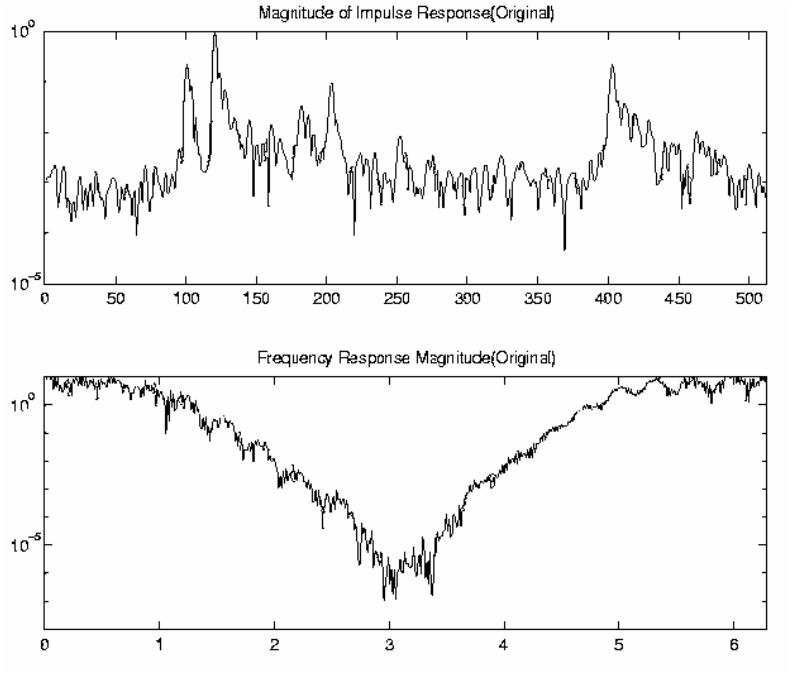

Figure 4.1 A time-invariant channel example

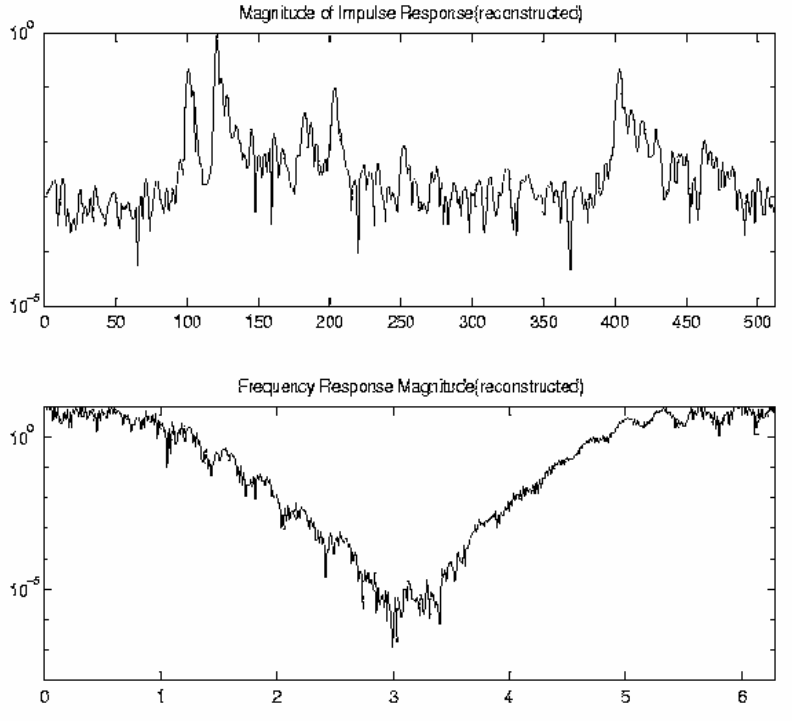

Figure 4.2 Reconstructed channel from 67% wavelet packet coefficients

The reconstructed channel using (4.1) is given in *Figure 4.2*. It is clear that the channel is well represented although only the most significant 67% of the WP coefficients are kept in the reconstruction. To see the advantage of this wavelet packet based channel model more clearly, *Figure 4.3* gives plots of wavelet packet coefficients for different levels of the binary wavelet packet tree. Each subplot in the figure corresponds to one level in the wavelet packet tree. The binary pruning method of [47] is used in the modeling. It can be easily seen that the coefficients are fairly sparse. This means that the channel energy is concentrated in a few wavelet packets. Therefore, only the most significant part of the coefficients are needed in the reconstruction of the channel while desired modeling accuracy can be maintained as *Figure 4.2* has shown.

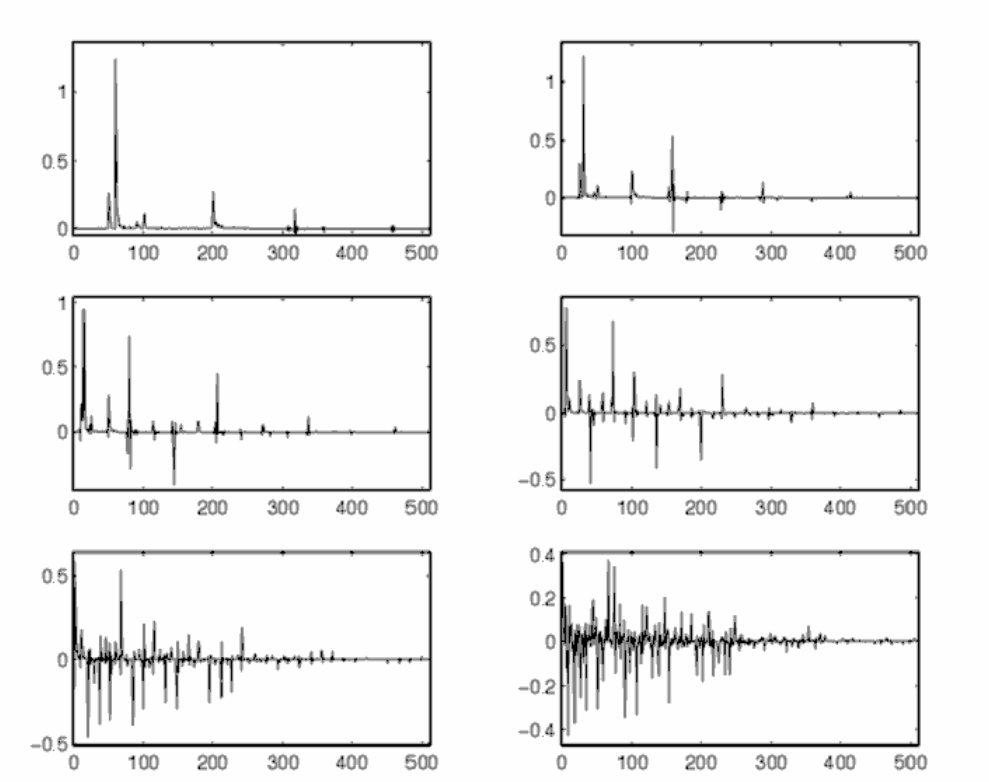

Figure 4.3 The wavelet packet coefficients of the channel model

4.2 Time-Varying Channel Model

A time-varying channel $h(t,\tau)$ can be modeled by two sets of wavelet packets as

$$h(t,\tau) = \sum_{j=1}^{N_i} \sum_{k=1}^{N_o} \alpha_{j,k} \varphi_j(\tau) \phi_k(t) \qquad (4.3)$$

where φ and ϕ are two (possibly different) sets of wavelet packet bases, N_i and N_o are number of packets in the two wavelet packet sets. From (4.3) it can be seen that a time-varying channel can be characterized by the $N_i \times N_o$ constant matrix **A** whose elements $\alpha_{j,k}$ are called channel coefficients. *Figure 4.4* is a block diagram of the wavelet packet channel model. The wavelet packet set φ are capable of performing frequency selection while the wavelet packet set ϕ performs time selection so that the time-varying channel can be represented. Based on careful choices of appropriate mother wavelets and wavelet packet tree pruning, the two sets of wavelet packets can be constructed more frequency selective and more time selective, respectively or simultaneously. Thus, the model will have good properties in representing frequency-selective fading and time-varying channels. Due to the orthonormality property of the wavelet packet bases, this representation is accurate for channels with limited delay spread. The length of the wavelet packets is chosen according to the length of the channel. The size of the wavelet packet bases is therefore determined. With this model the channel output with an input $x(t)$ can be written as

$$y(t) = \sum_{k=1}^{N_o} \phi_k(t) \sum_{j=1}^{N_i} \alpha_{j,k} (\varphi_j * x)(t) \qquad (4.4)$$

where * means convolution operation. The detection algorithm for a wavelet packet based multicarrier CDMA system described in Section 6 will be based on this channel representation.

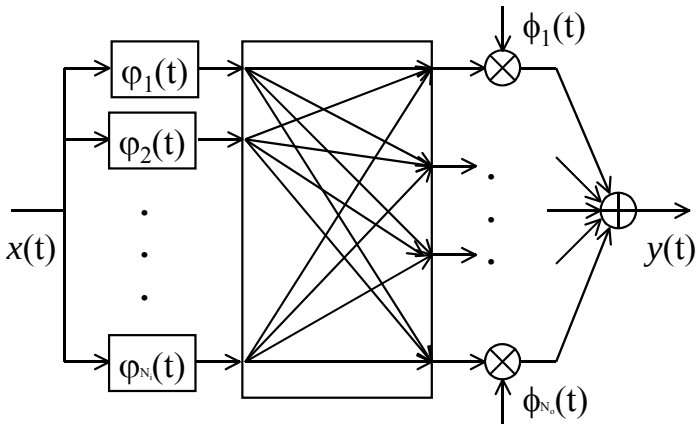

Figure 4.4 WP modeling of time-varying channels

A complex channel can be modeled with two wavelet packet channel models; each of them deals with the real part or the imaginary part of the channel impulse responses, respectively. This gives

$$\begin{aligned} h(t,\tau) &= \sum_{j=1}^{N_i}\sum_{k=1}^{N_o}\alpha_{j,k}\varphi_j(\tau)\phi_k(t) \\ &= \sum_{j=1}^{N_i}\sum_{k=1}^{N_o}\alpha_{j,k}^{R}\varphi_j(\tau)\phi_k(t) + i\sum_{j=1}^{N_i}\sum_{k=1}^{N_o}\alpha_{j,k}^{I}\varphi_j(\tau)\phi_k(t) \end{aligned} \tag{4.5}$$

where the matrix $\mathbf{A}$ is now complex and is separated into the real and imaginary parts as $\mathbf{A} = \mathbf{A}^R + i\mathbf{A}^I$, and i is the square root of minus one.

Generally, the wavelet packets used to model the real and imaginary parts of the channel can be chosen to be different if these two parts of the channel impulse responses have different properties. However, due to the fact that the phase of the channel impulse responses can be well characterized as uniformly distributed in [0, 2π], these two parts generally have the same features. Thus two identical sets of wavelet packets can be used to model a complex channel $h(t,\tau)$. As a result, *Figure 4.4* and Equations (4.3) and (4.4) are both unchanged. We only need to make the matrix $\mathbf{A}$ complex.

The wavelet packet based channel modeling concept described above has been used to model time-varying channels generated according to the statistical indoor channel model of [48]. An example of such statistical channels is shown in *Figure 4.5*. A series of impulse responses are generated with predefined correlation as if a mobile is moving. Therefore the generated channel resembles real time-

varying indoor wireless channels. In the simulation we have enlarged the number of impulse responses to 64 so that we can test our model in a longer time period. However, the time and space correlations are kept the same as that of [48]-[50]. The magnitude channel impulse responses shown in *Figure 4.5* are based on the Line-of-Sight channel model.

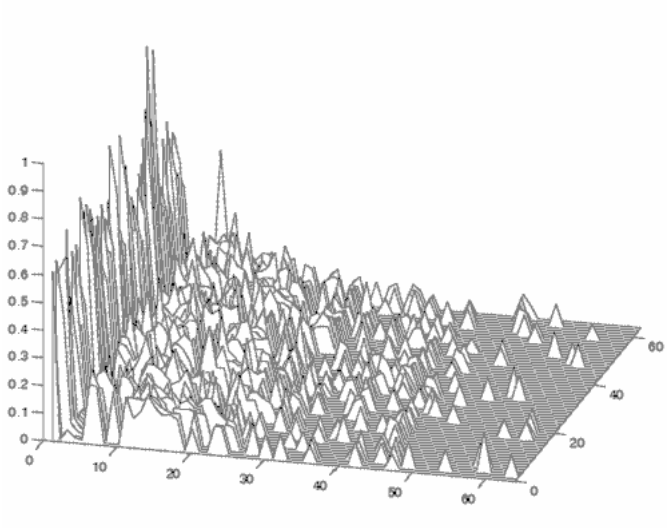

Figure 4.5 Magnitude impulse responses of a statistical time-varying channel

Figure 4.6 gives the reconstructed channel impulse responses. In the reconstruction of the channel impulse responses, only the significant 50% of the wavelet packet coefficients are used. The effectiveness of our model is clear. The modeling accuracy can be measured by the mean square error between the reconstructed channel and the original channel. *Figure 4.7* gives the MSE performance when we keep only most significant part of the WP coefficients. It can be seen from the figure that when only half of the coefficients in the matrix **A** are kept, the reconstructed channel has only about 1% MSE and can still well represent the original channel. A comparison of one impulse response snapshot of the reconstructed and the original channel is given in *Figure 4.8* where 1/3, 1/2, 2/3 and 3/4 of the WP coefficients in the channel coefficient matrix **A** are kept, respectively.

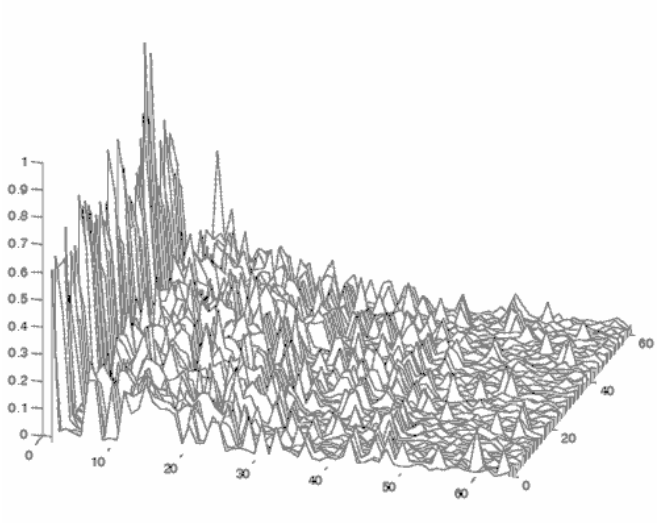

Figure 4.6 The reconstructed time-varying channel

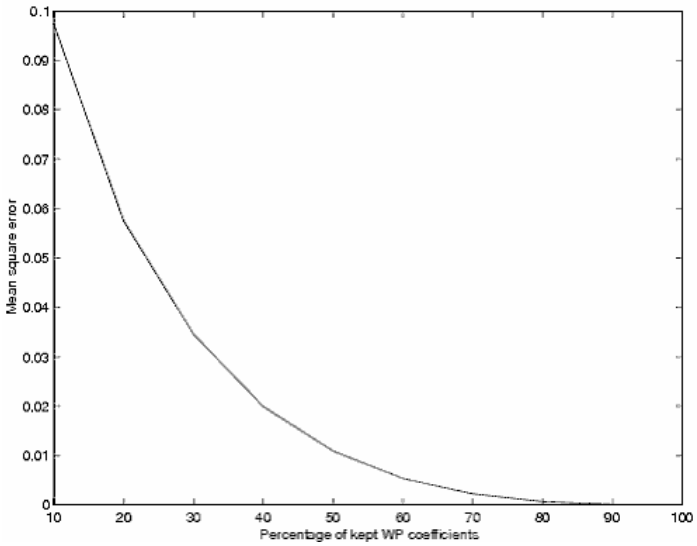

Figure 4.7 Error performance of the WP based channel model

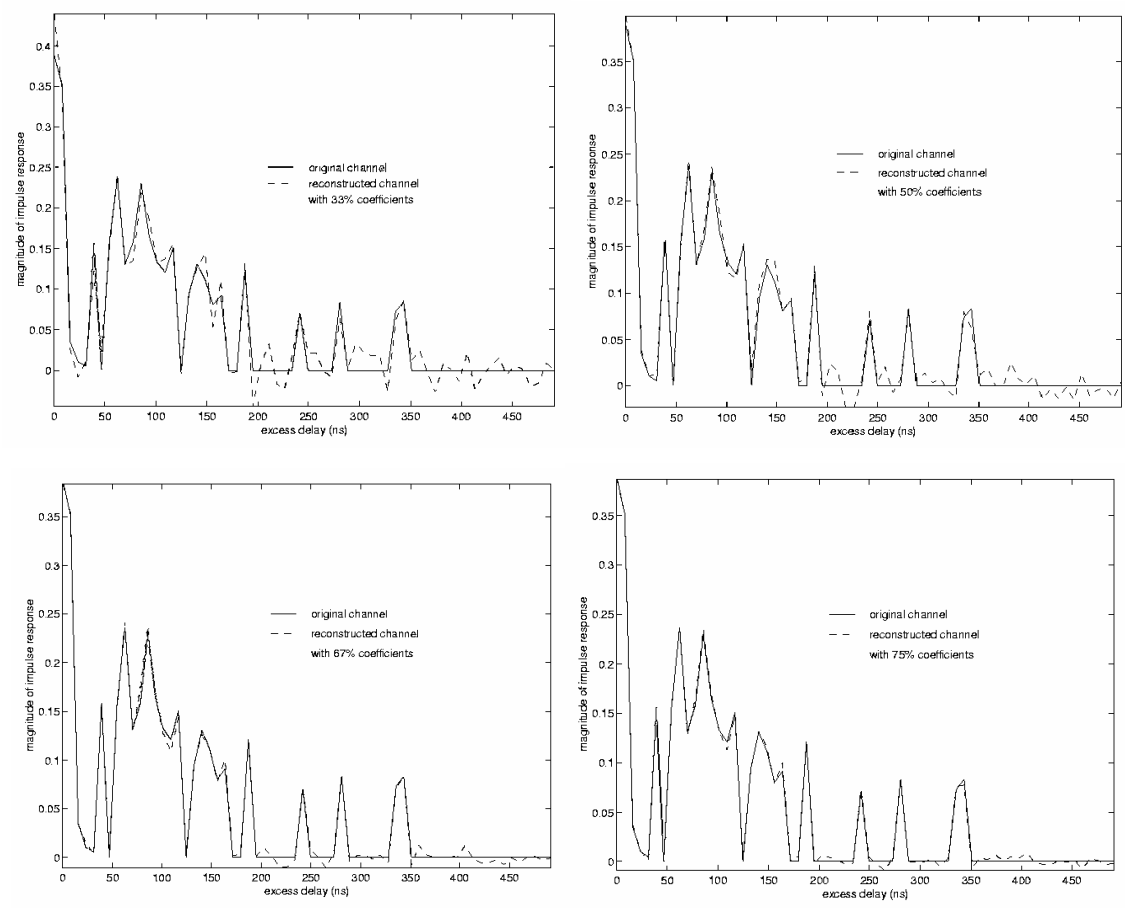

Figure 4.8 Snapshot comparison between original and reconstructed time-varying channel

Note that no pruning has been performed in the simulation for the sake of simplicity. The full binary wavelet packet tree is used, thus the lowest level WP coefficients are used in the modeling and reconstruction of the channels. If binary pruning had been performed, better results would be expected with the same number of coefficients. Nevertheless, it is clear from above examples that both time-invariant and time-varying channels can be well represented by the wavelet packet model.

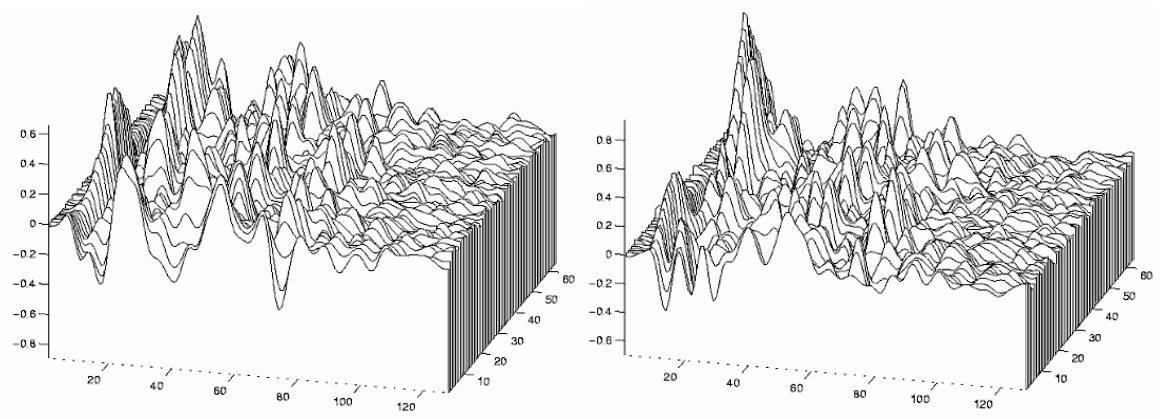

(a) Real part ***(b) Imaginary part***

Figure 4.9 The impulse responses of an urban channel

The model has also been applied to model the complex channel impulse responses obtained from field measurement data. The time-varying channel data are obtained from the Institute for Telecommunication Sciences [51]. The data contains blocks of a series (64 in each block) of complex channel impulse responses. The time delay between two adjacent impulse responses is 4.6 ms. We truncate the measured channel to a length of 128 samples, which corresponds to a time span of 3.2μs at the sampling interval of 25 ns. *Figure 4.9*(a) and (b) give the real part and the imaginary part of a typical urban wireless channel impulse response. *Figure 4.10*(a) and (b) show the wavelet packet model coefficients of the real part and the imaginary part, respectively. These figures illustrate clearly how well the channel energies are concentrated in mostly low-frequency wavelet packets.

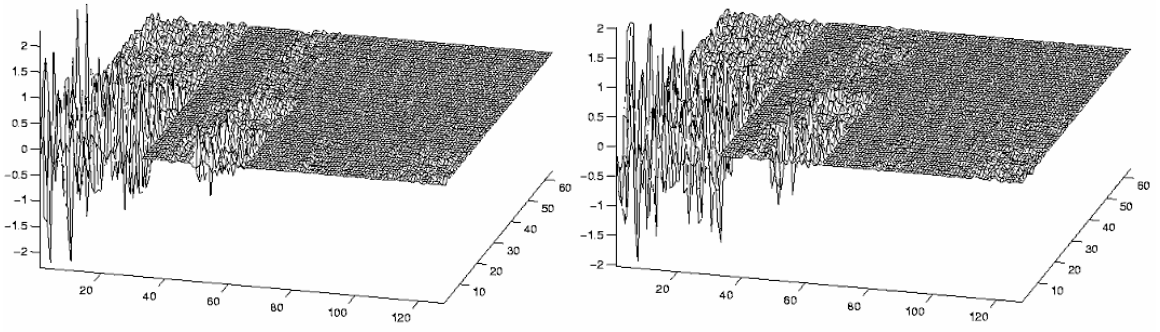

Figure 4.10 The wavelet packet model coefficients of the urban channel

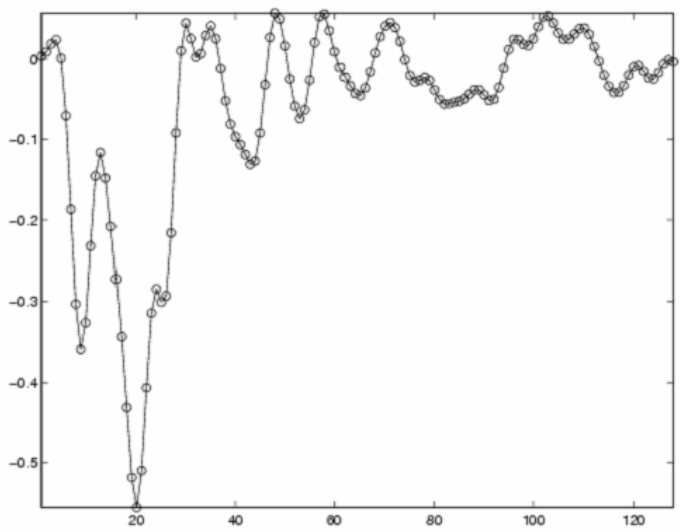

Figure 4.11 One snap-shot of the real part of the urban channel

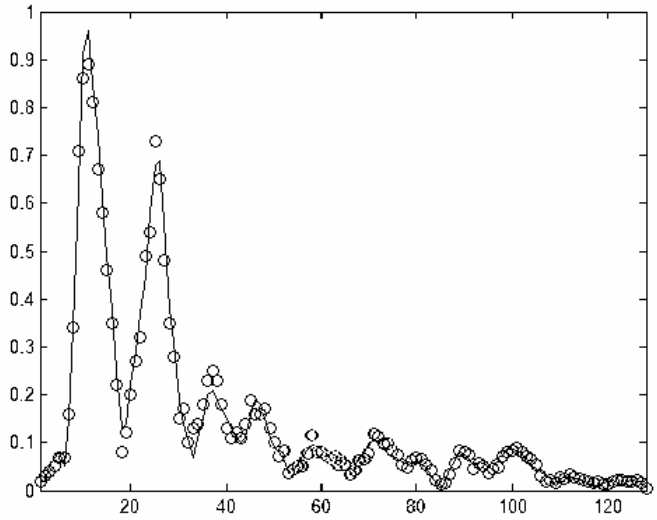

Figure 4.12 One snap-shot of the urban channel when ¼ coefficients are kept

Figure 4.11 gives one snap-shot of the real part of the channel and the reconstructed one. The solid line shows the original channel data, while the circles show the reconstructed channel using the wavelet packet model coefficients. In fact, the reconstructed channel impulse responses are almost identical to that of the data for all snapshots. It is clear that the channel is represented accurately. *Figure 4.12* presents one snap-shot of the reconstructed channel when only ¼ most significant coefficients are kept

in the reconstruction. It can be seen that the reconstructed channel well represents the original one even most of the coefficients are set to zero.

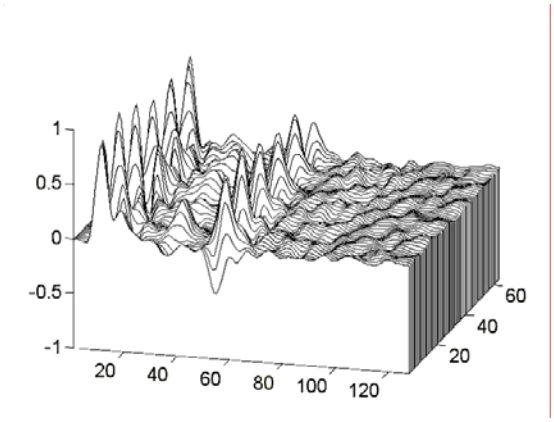

Figure 4.13 The real part of the impulse responses of a suburban channel

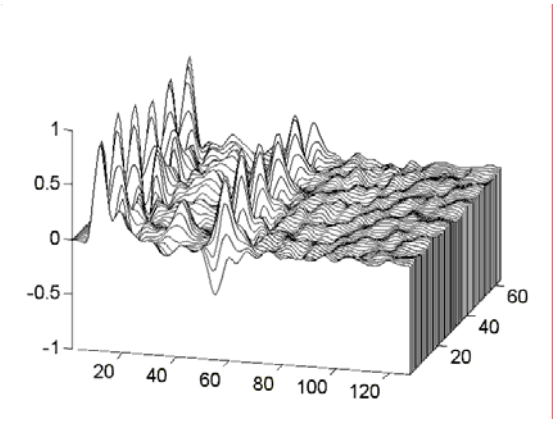

Figure 4.14 The reconstructed suburban channel with 50% WP coefficients kept

Figures 4.13 and *4.14* give a suburban wireless channel impulse response and the reconstructed channel with half of the wavelet packet coefficients kept. To save space we give only the results for the real part of the channel. It can be seen that the reconstructed impulse response is almost indistinguishable from the original one. The corresponding wavelet packet model coefficients are shown in *Figure 4.15.* More than half of the coefficients have values very close to zero. This explains why the reconstructed channel is almost indistinguishable from the original one.

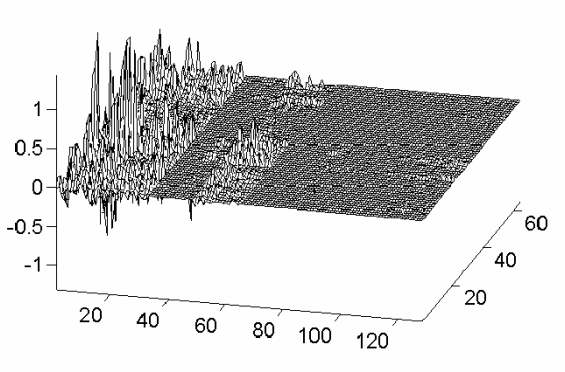

Figure 4.15 The model coefficients of the real part of the suburban channel

Figure 4.16 and *4.17* give an example of a slowly time-varying wireless channel and the wavelet packet model coefficients of this channel. It can be found that in this case the wavelet packet coefficients are more concentrated in the lower frequency part.

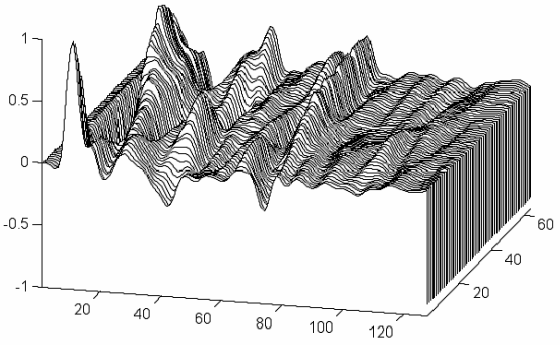

Figure 4.16 A slowly time-varying channel impulse responses

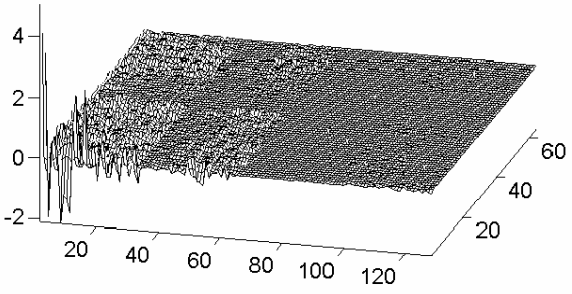

Figure 4.17 The wavelet packet model coefficients of the channel shown in Fig 16

Figure 4.18 gives a suburban channel and model coefficients using different wavelet packet bases. It can be seen that the concentration of the model coefficients does not differ too much, but Daubechies 10 seems to be among the best. Searching for a best wavelet packet basis to model a particular type of channel seems helpful in the system and receiver design, although in practice this requires more computation. Thus it is not included in this work and is left for further study.

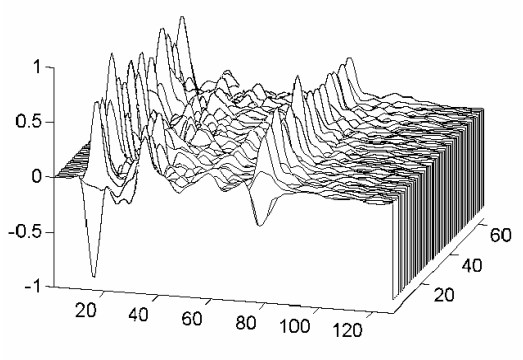

(a) Real part of a suburban channel impulse responses

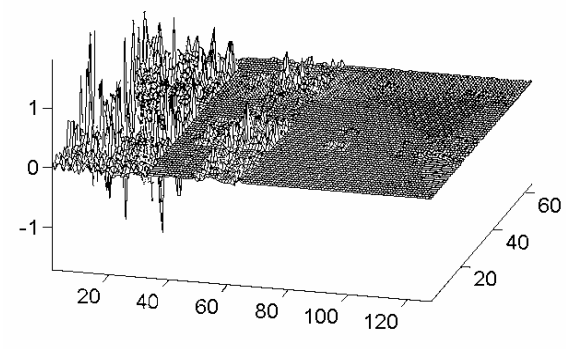

(b) Daubechies 10 WP coefficients

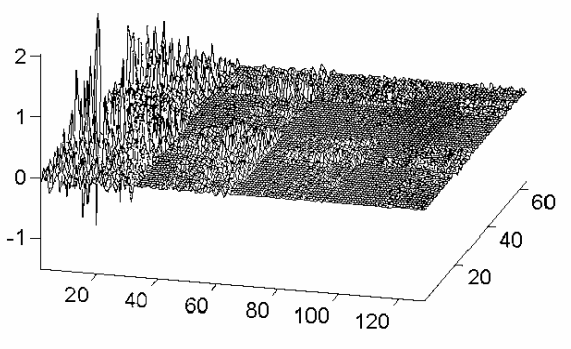

(c) Daubechies 4 WP coefficients

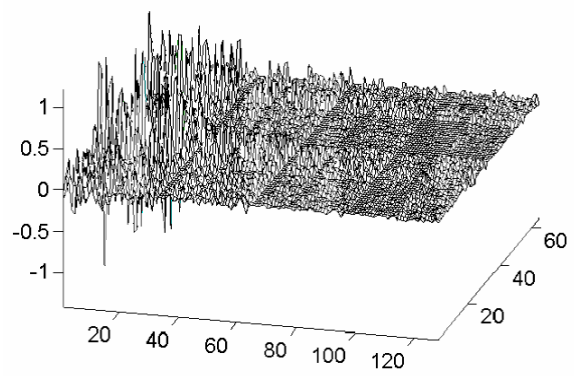

(d) Haar WP coefficients

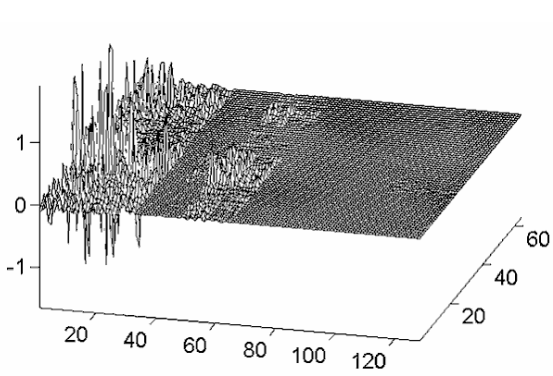

(e) Symmlet 10 WP coefficients

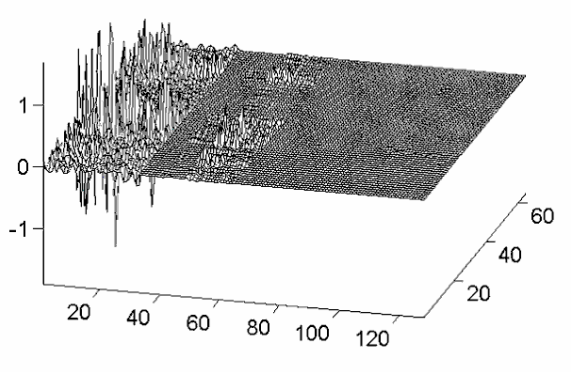

(f) Coiflet 4 WP coefficients

Figure 4.18 Real part of a suburb channel impulse responses and wavelet packet coefficients using different wavelet bases

5. WP-MC-CDMA System and A Time Domain Detection Algorithm

Although a number of different schemes have been proposed in the literature, the multicarrier CDMA schemes can be categorized mainly into two groups. One group spreads the user symbols in the frequency domain and the other spreads user symbols in the time domain. Accordingly, the detection algorithms for these two different multicarrier CDMA systems also fall into time domain and frequency domain signal processing. As illustrated in the previous sections, wavelet packets have the property of both time and frequency localization. Therefore, it is possible to make utilization of this property in two different ways. In this section we will describe a wavelet packet based multicarrier CDMA (WP_MC_CDMA) system and a time domain detection algorithm. To achieve time domain diversity, the system considered in this section will take the similar form of MC-DS-CDMA system architecture. This is because such an approach is able to sense relative time delay and thus multipath signals can be discriminated and then combined. Note that there is a need of one RAKE combiner for each sub-carrier in an ordinary MC-DS-CDMA system, the complexity of the receiver depends highly on the number of sub-carriers and limits the number of frequency bins. In the wavelet packet based multicarrier CDMA system, only one time domain RAKE combiner is needed in the detector, because the wavelet packet transform is used to combine signals from all sub-carriers prior to the time domain RAKE combiner. Therefore, there is no strict limit to the number of sub-carriers.

This section is organized as follows. The wavelet packet based multicarrier CDMA system and the basic time domain detection algorithm will be introduced in Section 5.1. Performance analysis of the detector in synchronous transmission systems and asynchronous systems will be addressed in Sections 5.2 and 5.3. Some simulation results will be illustrated in Section 5.4. The system performance in time-varying channel environment will be analyzed along with some simulation results in Section 5.5.

5.1 The WP-MC-CDMA System and Time Domain Detector

To utilize the time localization property of the wavelet packets by means of a time domain detection algorithm, it is desirable to have the spreading process implemented in the time domain, too. Therefore we consider a similar system structure to that of MC-DS-CDMA.

5.1.1 WP-MC-CDMA System Model

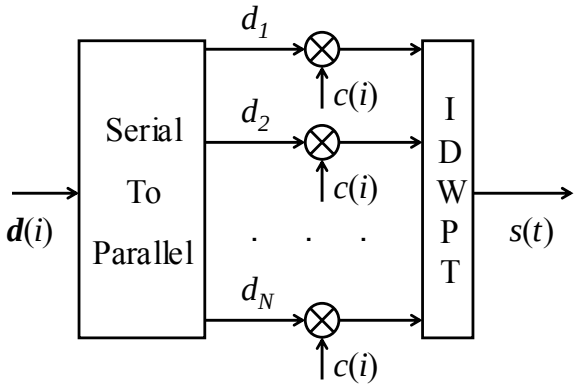

Figure 5.1 Transmitter of the WP-MC-CDMA system

The transmitter structure of this system design is shown in *Figure 5.1*. In this transmitter design a block of *N* user symbols are first converted from serial to parallel to decrease symbol rate by a factor of *N* that is equal to the number of sub-carriers. Then the parallel blocks of symbols are spread individually by the same spreading code assigned to the user. The spread chips are then modulated to different subcarriers through an IDWPT (Inverse Digital Wavelet Packet Transform) block. This modulation/mapping is equivalent to the Inverse Digital Fourier Transform block in the conventional sinusoid waveform based multicarrier system. Frequency domain diversity is also possible by simultaneously transmitting the same user symbol in a subset of the available subcarriers although it is not considered hereafter.

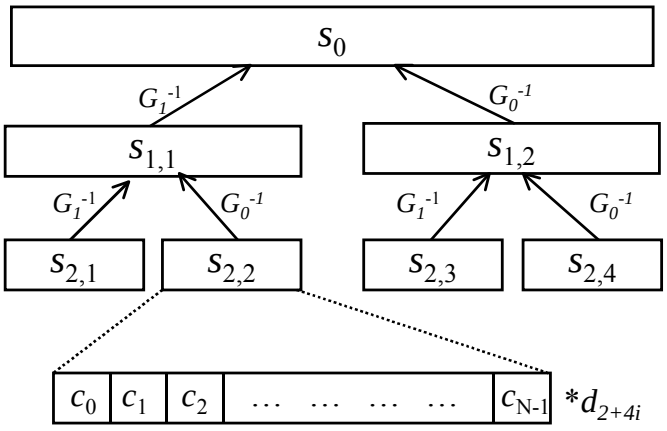

Figure 5.2 The IDWPT block in the WP-MC-CDMA transmitter

The exact structure of the inverse digital wavelet packet transform depends on the selected wavelet packet tree. To achieve better performance in different situations, different wavelet packet tree structures can be used, as discussed by Lindsey [52] and Jones [53]. An example diagram of the IDWPT block is shown in *Figure 5.2*, where G_1^{-1} and G_0^{-1} are two up-sampling-filtering operators defined as

$$G_1^{-1}\{x\}(n) = \sum_{k \in Z} x(k) g_1(n - 2k) \tag{5.1}$$

$$G_0^{-1}\{x\}(n) = \sum_{k \in Z} x(k) g_0(n - 2k) \tag{5.2}$$

where g_1 and g_0 are a pair of Quardrature Mirror Filters (QMF). In *Figure 5.2*, *4* layer-2 nodes in the wavelet packet tree stand for *4* subcarriers (wavelet packet functions in different frequency bands). The spread chips, denoted by $s_{2,1}$ through $s_{2,4}$ are the inputs to the modulator, and s_0 is the modulated signal. Each of the chip signals consists of one spread data symbol, $d_i \left[c_0 \quad \cdots \quad c_{N-1} \right]$, as indicated in the figure. The length of the corresponding IDWPT waveform for each pulse-shaped chip is *4N*, resulting from *2* steps of an up-sampling process. However, the length of the IDWPT waveform for any single chip, e.g., c_0, is not *4*, but *4L* where *L* is the length of the wavelet packet filter. This is because the wavelet packet waveforms are generated from an impulse function $g(n)$ with a length equal to *L*. Thus, in this process the waveforms for subsequent chips are overlapped. However, the correlation property of wavelet packets guarantees the orthogonality between these overlapped waveforms.

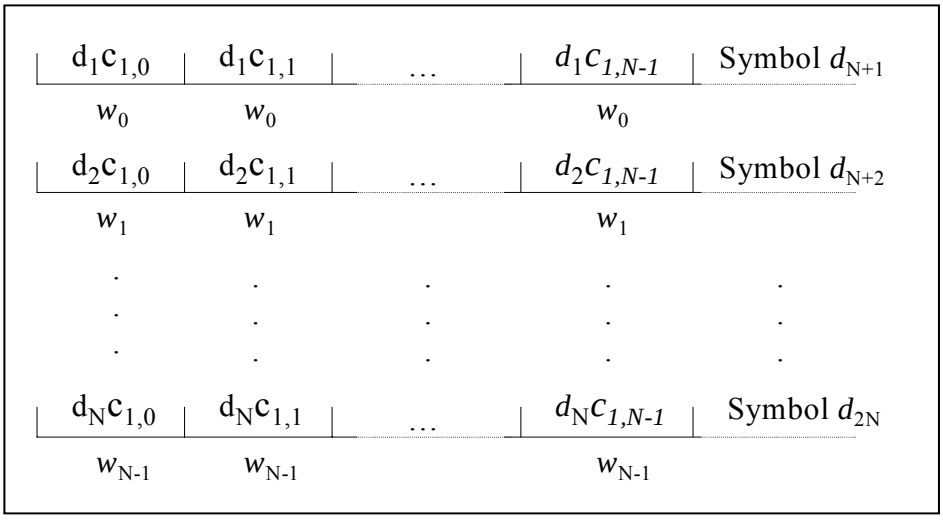

Figure 5.3 Signal timing diagram

To give a clear understanding of the signal structure, a signal timing diagram is given in *Figure 5.3* where d_l is the lth symbol, $c_{k,i}$ is the kth user's code at the ith chip, and w_l is the lth wavelet packet waveform. The set of the wavelet packet waveforms w_0 to w_{N-1} are generated with a full binary wavelet packet tree using a specific pair of QMF $g_1(n)$ and $g_0(n)$, e.g., Daubechies 4 wavelet filters. The $d_l c_{k,i}$ in each chip interval is modulated onto w_{l-1} that is completely contained in that chip interval. The transmitted signal is the sum along the vertical direction.

An example is given in the following to show how the modulation is done in *Figure 5.2*. Daubechies 4 QMF $\mathbf{g}_0 = \begin{bmatrix} 0.483 & 0.837 & 0.224 & -0.129 \end{bmatrix}^T$ (Low-pass filter) and $\mathbf{g}_1 = \begin{bmatrix} 0.129 & 0.224 & -0.837 & 0.483 \end{bmatrix}^T$ (High-pass filter) are used in the example, where bold face letters denote signal (impulse response, or code) sample vectors.

Let's assume a 4-carrier modulation, and the spreading code $\mathbf{c}_1 = \begin{bmatrix} 1 & -1 & -1 & 1 \end{bmatrix}^T$ is assigned to the first user. In any given time interval four symbols, e.g., $\mathbf{d}^1 = \begin{bmatrix} 1 & 1 & -1 & -1 \end{bmatrix}^T$ can be modulated into the four sub-carriers. After spreading we have four spreaded signals $\mathbf{s}_{2,1} = d_1 c = \begin{bmatrix} 1 & -1 & -1 & 1 \end{bmatrix}^T$, $\mathbf{s}_{2,2} = d_3 c = \begin{bmatrix} 1 & -1 & -1 & 1 \end{bmatrix}^T$, $\mathbf{s}_{2,3} = d_2 c = \begin{bmatrix} -1 & 1 & 1 & -1 \end{bmatrix}^T$, and $\mathbf{s}_{2,4} = d_4 c = \begin{bmatrix} -1 & 1 & 1 & -1 \end{bmatrix}^T$. Each of them corresponds to one symbol multiplied by the spreading code. These four signals are the inputs to the four lowest level nodes in *Figure 5.2*. For $\mathbf{s}_{2,3}$, for example, the first step of up-sampling gives $\begin{bmatrix} -1 & 0 & 1 & 0 & 1 & 0 & -1 & 0 \end{bmatrix}^T$. Filtering with the high-pass filter $\mathbf{g}_1$ gives $\begin{bmatrix} 0.966 & -0.259 & -0.707 & 0.707 & -0.966 & 0.259 & 0.707 & -0.707 \end{bmatrix}^T$. After another up-sampling and low-pass filtering with filter $\mathbf{g}_0$ we get the modulated signal $\mathbf{s}_3$. Other signals are processed in the same way so that we can get the final modulated signal sample vector $\mathbf{s}_0 = \mathbf{s}_1 + \mathbf{s}_2 + \mathbf{s}_3 + \mathbf{s}_4$. This final summing step is the same as summing vertically in *Figure 5.3.*

The transmitted signal in the ith chip interval from user k is therefore

$$x_k^i(n) = c_{k,i} \sum_{l=0}^{N-1} d_{l+1}^k w_l(n), n = 0,1,...,N-1 \qquad (5.3)$$

where $c_{k,i}$ is the *i*th chip of the *k*th spreading code, d_l^k is the *l*th symbol for the *k*th user, and $w_l(n)$ is the *n*th sample of the *l*th wavelet packet waveform. Note that the spreading codes in all the subcarriers are the same for one particular user and this equation specifies only one out of *N* chips for all the symbols. Putting all *N* samples of the wavelet packet waveform in the vector form, we have

$$\mathbf{x}_k^i = \begin{bmatrix} x_k^i(0) \\ \vdots \\ x_k^i(N-1) \end{bmatrix} = \begin{bmatrix} w_0(0) & \cdots & w_{N-1}(0) \\ \vdots & \ddots & \vdots \\ w_0(N-1) & \cdots & w_{N-1}(N-1) \end{bmatrix} \begin{bmatrix} d_0^k \\ \vdots \\ d_{N-1}^k \end{bmatrix} c_{k,i} = \mathbf{W}\mathbf{d}^k c_{k,i} \tag{5.4}$$

where $\mathbf{W}$ is an $N \times N$ orthogonal wavelet packet matrix, with each column vector $\begin{bmatrix} w_i(0) & \cdots & w_i(N-1) \end{bmatrix}^T$ being a wavelet packet waveform. It can be seen from this equation that the spreading process is carried out in the time domain. Assuming synchronous downlink transmission, the combined signal for *N* WP samples of the *i*th chip and from all *K* users is

$$\mathbf{x}^i = \begin{bmatrix} x^i(0) \\ \vdots \\ x^i(N-1) \end{bmatrix} = \sum_{k=1}^{K} \mathbf{x}_k^i = \mathbf{W} \begin{bmatrix} \mathbf{d}^1 & \cdots & \mathbf{d}^K \end{bmatrix} \begin{bmatrix} c_{1,i} \\ \vdots \\ c_{K,i} \end{bmatrix} = \mathbf{W}\mathbf{D}\mathbf{c}^i \tag{5.5}$$

where the vector $\mathbf{c}^i$ is the *i*th column of the spread code matrix $\mathbf{C}$ which is defined as

$$\mathbf{C} = \begin{bmatrix} c_{1,0} & c_{1,1} & \cdots & c_{1,N-1} \\ c_{2,0} & \ddots & & \vdots \\ \vdots & & \ddots & \vdots \\ c_{K,0} & \cdots & \cdots & c_{K,N-1} \end{bmatrix} = \begin{bmatrix} \mathbf{c}^0 & \mathbf{c}^1 & \cdots & \mathbf{c}^{N-1} \end{bmatrix} = \begin{bmatrix} \mathbf{c}_1^T \\ \mathbf{c}_2^T \\ \vdots \\ \mathbf{c}_K^T \end{bmatrix}. \tag{5.6}$$

In (5.6) the code matrix $\mathbf{C}$ is also partitioned by the row vectors $\mathbf{c}_1^T, \mathbf{c}_2^T, ..., \mathbf{c}_K^T$ which correspond to the spreading codes for users *1* to *K*. These row vectors will be used in the following analysis.

5.1.2 The Time Domain Detection Algorithm

The receiver with multipath combining ability is shown in *Figure 5.4* where a series of delayed versions of the received signal are detected by single path detectors. In each single path detector, a DWPT (Digital Wavelet Packet Transform) block is used for demodulation of the signal for the corresponding resolved path. The multiuser interference can be effectively eliminated if the desired user spreading code is known, which is assumed true in the following. The DWPT demodulated signal is forwarded to

the despreading part to obtain a detected decision variable for this resolved path. The results of these detectors are combined in the RAKE combiner. The maximum ratio combining is used in the following analysis. Therefore, the combining weights $\eta_j = \hat{h}^*(j)$ where $\hat{h}(j), j = 1,...,L$ are estimated path strengths. It is the time localization property of the WP that makes this time diversity combining possible. This multipath receiver can effectively eliminate the inter-symbol interference from the multipath transmission of the desired signal as well as the interference due to the multipath transmission of other user's signals. Without loss of generality, user *1* is assumed as the desired user in the following.

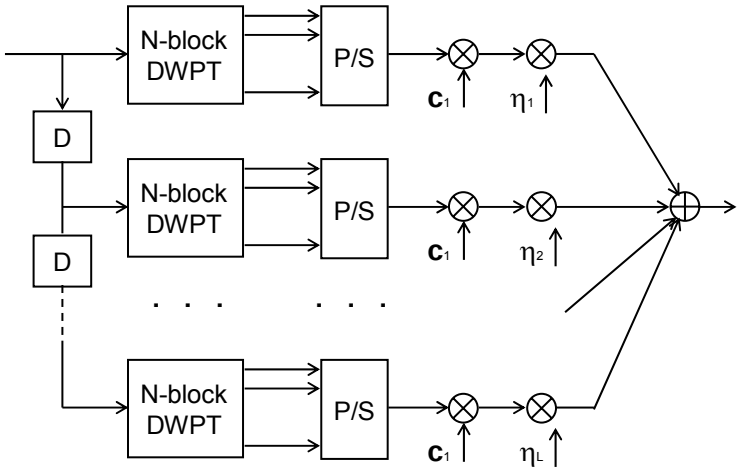

Figure 5.4 Multipath receiver of wavelet packet MC-CDMA system

Implementation of the corresponding DWPT and the despreading block in the demodulator is shown in *Figure 5.5*, where G_1 and G_0 are the two operators corresponding to filtering and down-sampling by the highpass filter $\mathbf{g}_1(-n)$ and the lowpass filter $\mathbf{g}_0(-n)$, respectively. This wavelet packet demodulation is a dual process of the modulation process shown in *Figure 5.2* and the original signal can be recovered in a single path channel condition. The demodulated signals from the nodes of the lowest level are despread using the corresponding spreading code $\mathbf{c}_1 = [c_{1,0}, c_{1,1}, \cdots, c_{1,N-1}]^T$.

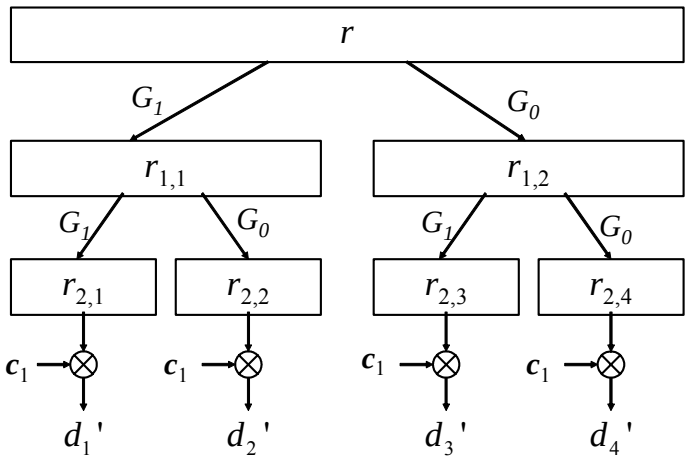

Figure 5.5 The wavelet packet based multicarrier demodulator

5.2 Performance in Synchronous Transmission Conditions

In a synchronous transmission condition such as the downlink transmission in cellular systems all user signals are aligned in time. More importantly in this kind of scenarios all user signals go through the same channel.

5.2.1 Interference Analysis

The received signal of the *i*th block of chips is then

$$\mathbf{r}^i(0) = \mathbf{H}\begin{bmatrix}\mathbf{x}^{i-1}\\ \mathbf{x}^i\end{bmatrix} + \mathbf{n}^i(0) \tag{5.7}$$

where $\mathbf{r}^i(0) = [r^i(0), r^i(1), \cdots, r^i(N-1)]^T$ and $\mathbf{n}^i(0) = [n^i(0), n^i(1), \cdots, n^i(N-1)]^T$ denotes the additive white Gaussian noise at the *i*th block, and the N×2N matrix

$$\mathbf{H} = \begin{bmatrix} O & h(L-1) & \cdots & h(0) & 0 & & & O \\ & \ddots & \ddots & \ddots & \ddots & \ddots & & \\ & & \ddots & h(L-1) & \cdots & h(0) & \ddots & \\ O & & & \ddots & \ddots & \ddots & \ddots & 0 \\ & & & & 0 & h(L-1) & \cdots & h(0) \end{bmatrix} \tag{5.8}$$

$h(n)$ is the channel impulse response and the channel length L is assumed smaller than N so that most of the elements of **H** are zeros, O stands for zero elements other than those specified. The left part of **H** reflects the interference from the previous symbol while the right part of **H** reflects the multipath effect within the current symbol. In the following it is assumed that the channel has normally distributed path strengths. Since the performance of the receiver for a given SNR depends only on the relative strength of the paths, this assumption will not affect the analytical result. The delayed (by j samples) version of $\mathbf{r}^i(0)$ which appear at the inputs of *Figure 5.4* can be written as

$$\mathbf{r}^i(j) = \mathbf{H}\mathbf{L}_j \begin{bmatrix} \mathbf{x}^{i-1} \\ \mathbf{x}^i \\ \mathbf{x}^{i+1} \end{bmatrix} + \mathbf{n}^i(j), \qquad j = 0,1,...,L-1 \tag{5.9}$$

where $\mathbf{L}_j$ is a $2N \times 3N$ matrix whose (l,m)th elements are ones when $m - l = j$, and all other elements are zeros. Those "1"s in the right N columns of $\mathbf{L}_j$ reflect interference from symbol $\mathbf{x}^{i+1}$ due to the delay.

Each single path detector in *Figure 5.4* first demodulates the multicarrier signal using DWPT. For the jth detector, this yields,

$$\mathbf{y}^i(j) = \mathbf{W}^T\mathbf{r}^i(j) = \mathbf{W}^T\mathbf{H}\mathbf{L}_j \begin{bmatrix} \mathbf{W}\mathbf{D}\mathbf{c}^{i-1} \\ \mathbf{W}\mathbf{D}\mathbf{c}^i \\ \mathbf{W}\mathbf{D}\mathbf{c}^{i+1} \end{bmatrix} + \mathbf{W}^T\mathbf{n}^i(j) \tag{5.10}$$

where $\mathbf{W}^T$ is the transposition of **W**. The column vectors of (5.10) can be grouped together into a matrix as

$$\begin{aligned} \mathbf{Y}(j) &= \left[\mathbf{y}^0(j) \quad \cdots \quad \mathbf{y}^{N-1}(j)\right] \\ &= \mathbf{W}^T\mathbf{H}\mathbf{L}_j \begin{bmatrix} \mathbf{W}\mathbf{D}\left[\mathbf{c}^{N-1} \quad \mathbf{c}^0 \quad \cdots \quad \mathbf{c}^{N-2}\right] \\ \mathbf{W}\mathbf{D}\left[\mathbf{c}^0 \quad \mathbf{c}^1 \quad \cdots \quad \mathbf{c}^{N-1}\right] \\ \mathbf{W}\mathbf{D}\left[\mathbf{c}^1 \quad \cdots \quad \mathbf{c}^{N-1} \quad \mathbf{c}^0\right] \end{bmatrix} + \mathbf{W}^T\mathbf{N}(j) = \mathbf{W}^T\mathbf{H}\mathbf{L}_j \begin{bmatrix} \mathbf{W}\mathbf{D}\mathbf{C}_{-1} \\ \mathbf{W}\mathbf{D}\mathbf{C} \\ \mathbf{W}\mathbf{D}\mathbf{C}_1 \end{bmatrix} + \mathbf{W}^T\mathbf{N}(j) \end{aligned} \tag{5.11}$$

where the AWGN matrix is denoted as $\mathbf{N}(j) = [\mathbf{n}^0(j), \mathbf{n}^1(j), \cdots, \mathbf{n}^{N-1}(j)]$. The jth single path detector output for the desired user *1* is obtained by despreading **Y***(j)* with the spreading code $\mathbf{c}_1 = [c_{1,0}, c_{1,1}, ..., c_{1,N-1}]^T$ as

$$\mathbf{z}(j)=\mathbf{Y}(j)\begin{bmatrix} c_{1,0} \\ \vdots \\ c_{1,N-1} \end{bmatrix}=\mathbf{W}^T\mathbf{H}\mathbf{L}_j\begin{bmatrix} \mathbf{W}\mathbf{D}\mathbf{C}_{-1}\mathbf{c}_1 \\ \mathbf{W}\mathbf{D}\mathbf{C}\mathbf{c}_1 \\ \mathbf{W}\mathbf{D}\mathbf{C}_1\mathbf{c}_1 \end{bmatrix}+\mathbf{W}^T\mathbf{N}(j)\mathbf{c}_1=\mathbf{W}^T\mathbf{H}\mathbf{L}_j\begin{bmatrix} \mathbf{W}\mathbf{e}_{-1} \\ \mathbf{W}\mathbf{D}\mathbf{C}\mathbf{c}_1 \\ \mathbf{W}\mathbf{e}_1 \end{bmatrix}+\mathbf{W}^T\mathbf{N}(j)\mathbf{c}_1 \qquad (5.12)$$

where $\mathbf{e}_{-1}$ and $\mathbf{e}_1$ correspond to the interference from the previous symbol and the next symbol, respectively. Due to the structures of $\mathbf{C}$, $\mathbf{c}_1$, and the correlation properties of the spreading codes, it is clear that $\mathbf{C}\mathbf{c}_1=\begin{bmatrix}1 & 0 & \cdots & 0\end{bmatrix}^T$ for orthogonal spreading codes. For non-orthogonal codes such as Gold code a small error exists, so that

$$\mathbf{D}\mathbf{C}\mathbf{c}_1=\mathbf{d}^1+\mathbf{e}_0 \qquad (5.13)$$

where $\mathbf{d}^1$ is the first user's symbol vector defined in (5.4), and $\|\mathbf{e}_0\|<<1$. $\mathbf{e}_{-1}$ and $\mathbf{e}_1$ are also small due to the auto- and cross-correlation properties of the spreading codes. Partitioning $\mathbf{L}_j$ into three *2N* by *N* sub matrices as $\mathbf{L}_j=\begin{bmatrix}\mathbf{L}_{j,-1} & \mathbf{L}_{j,0} & \mathbf{L}_{j,1}\end{bmatrix}$, $\mathbf{z}(j)$ can be written as

$$\begin{aligned}\mathbf{z}(j)&=\mathbf{W}^T\mathbf{H}\mathbf{L}_{j,0}\mathbf{W}\mathbf{d}^1+\mathbf{W}^T\mathbf{H}\mathbf{L}_{j,0}\mathbf{W}\mathbf{e}_0\\&\quad+\mathbf{W}^T\mathbf{H}\mathbf{L}_{j,-1}\mathbf{W}\mathbf{e}_{-1}+\mathbf{W}^T\mathbf{H}\mathbf{L}_{j,1}\mathbf{W}\mathbf{e}_1+\mathbf{W}^T\mathbf{N}(j)\mathbf{c}_1\\&=\mathbf{W}^T\mathbf{H}\mathbf{L}_{j,0}\mathbf{W}\mathbf{d}^1+\mathbf{I}_{j,0}+\mathbf{I}_{j,-1}+\mathbf{I}_{j,1}+\mathbf{W}^T\mathbf{N}(j)\mathbf{c}_1\\&=\mathbf{W}^T\mathbf{H}\mathbf{L}_{j,0}\mathbf{W}\mathbf{d}^1+\mathbf{I}_{j,sc}+\mathbf{W}^T\mathbf{N}(j)\mathbf{c}_1\end{aligned} \qquad (5.14)$$

where $\mathbf{I}_{j,0}$, $\mathbf{I}_{j,-1}$ and $\mathbf{I}_{j,1}$ correspond to the interferences from $\mathbf{e}_0$, $\mathbf{e}_{-1}$ and $\mathbf{e}_1$ respectively. Since all $\mathbf{e}$'s have small norms, the interference term $\mathbf{I}_{j,sc}$ in (5.14) is small. The modified channel matrix $\mathbf{H}\mathbf{L}_{j,0}$ in the first term can be shown to be

$$\mathbf{H}\mathbf{L}_{j,0}=\begin{bmatrix} h(j) & \cdots & h(0) & & & O \\ \vdots & \ddots & & \ddots & & \\ h(L-1) & & & & \ddots & \\ & \ddots & & & & h(0) \\ & & \ddots & & \ddots & \vdots \\ O & & & h(L-1) & \cdots & h(j) \end{bmatrix}=h(j)\mathbf{I}+\sum_{l=0,l\neq j}^{L-1}h(l)\mathbf{J}_{l-j} \qquad (5.15)$$

where $\mathbf{I}$ is an *N* by *N* identity matrix. Matrices $\mathbf{J}_{l-j}$ are all *N* by *N*, whose (*m*,*n*)th elements are ones for all *m* and *n* satisfying *m*-*n*=*l*-*j*, and all other elements are zeros. Therefore $\mathbf{z}(j)$ can be rewritten using (5.15) as

$$\begin{aligned}\mathbf{z}(j) &= h(j)\mathbf{d}^1 + \sum_{l=0,l\neq j}^{L-1} h(l)\mathbf{W}^T\mathbf{J}_{l-j}\mathbf{W}\mathbf{d}^1 + \mathbf{I}_{j,sc} + \mathbf{W}^T\mathbf{N}(j)\mathbf{c}_1 \\ &= h(j)\mathbf{d}^1 + \mathbf{I}_{j,wp} + \mathbf{I}_{j,sc} + \mathbf{W}^T\mathbf{N}(j)\mathbf{c}_1\end{aligned} \tag{5.16}$$

where $\mathbf{I}_{j,wp}$ stands for the interference due to the partial correlation of WP, while $\mathbf{I}_{j,sc}$ stands for the interference introduced by non-ideal correlation of the spreading codes.

It needs to be pointed out that, as stated before, the main advantage of the WP approach is the time localization property of WP waveforms. This can be clearly seen in (5.16), where the interference terms are expressed in terms of $\mathbf{W}^T\mathbf{J}_{l-j}\mathbf{W}$. This is the partial correlations[2] of the waveform samples in $\mathbf{W}$. Due to the time localization property of the WP waveforms, the WP system results in much smaller (in magnitude) partial correlations than the DFT based system, thus reduces the interference level.

If the channel is single path, then $\mathbf{HL}_{0,0} = h(0)\mathbf{I}$. Thus without considering the noise (5.14) or (5.16) becomes $\mathbf{z}(0) = h(0)\mathbf{d}^1 + \mathbf{I}_{0,0}$, i.e., the symbols $\mathbf{d}^1$ can be detected with a small error. However, this single path detector would suffer severe interference in a multipath channel without a strong line of sight path. This is because although the interference terms of (5.16) are small, the signal term $h(j)\mathbf{d}^1$ in (5.16) may not be significantly larger than the second term due to a potentially small $h(j)$. Our solution is to employ a RAKE combiner to achieve time diversity as in *Figure 5.4*. Each branch of the receiver deals with one path of the signal. The output of the RAKE combiner is then, using (5.16),

$$\mathbf{z} = \sum_{j=0}^{L_R-1}\eta_j\mathbf{z}(j) = \sum_{j=0}^{L_R-1}\eta_j h(j)\mathbf{d}^1 + \sum_{j=0}^{L_R-1}\eta_j\left(\mathbf{I}_{j,wp} + \mathbf{I}_{j,sc}\right) + \sum_{j=0}^{L_R-1}\eta_j\mathbf{W}^T\mathbf{N}(j)\mathbf{c}_1 \tag{5.17}$$

where L_R is the number of combined (strongest) paths. It is assumed L_R=L in the following for the sake of simplicity. If the path strength can be estimated accurately and maximum ratio combining is used, then $\eta_j = h^*(j)$. Equation (5.17) then becomes

[2] The structure of the matrix **J** determines that not all N entries in **W** are used in the calculation of each correlation. We thus call it partial correlation.

$$\begin{aligned}\mathbf{z} &= \left(\sum_{j=0}^{L-1} |\, h(j)\,|^2 \right) \mathbf{d}^1 + \sum_{j=0}^{L-1} h^*(j)\left(\mathbf{I}_{j,wp} + \mathbf{I}_{j,sc}\right) + \sum_{j=0}^{L-1} h^*(j)\mathbf{W}^T\mathbf{N}(j)\mathbf{c}_1 \\ &= \alpha\mathbf{d}^1 + \sum_{j=0}^{L-1} h^*(j)\left(\mathbf{I}_{j,wp} + \mathbf{I}_{j,sc}\right) + \sum_{j=0}^{L-1} h^*(j)\mathbf{W}^T\mathbf{N}(j)\mathbf{c}_1\end{aligned} \tag{5.18}$$

where $\alpha > 0$ is the channel energy. If the channel can be accurately estimated, (5.18) is near real. However, due to imperfect channel estimation and the additive noise, (5.18) is in general complex. The final decision variable is thus the real part of (5.18) since $\mathbf{d}^1$ is assumed real. From (5.18) it is seen that correct detection of $\mathbf{d}^1$ from $\mathbf{z}$ depends on the noise and interference level which consists of two different interferences $\mathbf{I}_{j,wp}$ and $\mathbf{I}_{j,sc}$. Once the WP waveforms and the user codes are chosen, the probability density function of the decision vector $\mathrm{Re}\{\mathbf{z}\}$ in (5.18) can be calculated, from which the expected bit error rate can be calculated. The interference terms can be written as

$$\begin{aligned}\mathbf{I}_{j,wp} &= \sum_{l=0,l\neq j}^{L-1} h(l)\mathbf{W}^T\mathbf{J}_{l-j}\mathbf{W}\mathbf{d}^1 = \sum_{l=0,l\neq j}^{L-1} h(l)\begin{bmatrix} a_{1,1}^{l-j}d_1 \\ \vdots \\ a_{N,N}^{l-j}d_N \end{bmatrix} + \sum_{l=0,l\neq j}^{L-1} h(l)\begin{bmatrix} b_1^{l-j} \\ \vdots \\ b_N^{l-j} \end{bmatrix} \\ \mathbf{I}_{j,sc} &= \mathbf{W}^T\mathbf{H}\mathbf{L}_{j,0}\mathbf{W}\mathbf{e}_0 + \mathbf{W}^T\mathbf{H}\mathbf{L}_{j,-1}\mathbf{W}\mathbf{e}_{-1} + \mathbf{W}^T\mathbf{H}\mathbf{L}_{j,1}\mathbf{W}\mathbf{e}_1 = \sum_{l=0}^{L-1} h(l)\begin{bmatrix} b_{sc,1}^{l-j} \\ \vdots \\ b_{sc,N}^{l-j} \end{bmatrix}\end{aligned} \tag{5.19}$$

where $a_{i,n}^{l-j}$ corresponds to the (i,n)th element of $\mathbf{W}^T\mathbf{J}_{l-j}\mathbf{W}$, the partial cross-correlation matrix of WP, and $b_n^{l-j} = \sum_{i=1,i\neq n}^{N} a_{i,n}^{l-j}d_i, \quad n = 1,...,N$. Thus the first sum of $\mathbf{I}_{j,wp}$ in (5.19) stands for the interference from the partial autocorrelations of WP waveforms, and the second sum of $\mathbf{I}_{j,wp}$ in (5.19) stands for the interference from the partial cross-correlations of WP. The $b_{sc,n}^{l-j}$'s in the interference term $\mathbf{I}_{j,sc}$ can be written as

$$\begin{aligned}b_{sc,n}^{l-j} &= u(l-j-1)\sum_{i=1}^{N} e_{-1,i} \sum_{m=j+1}^{l} w_n(l-m)w_i(N-l+j) \\ &\quad + u(j-l-1)\sum_{i=1}^{N} e_{1,i} \sum_{m=l}^{j-1} w_n(N-l+j)w_i(m-l) + \sum_{i=1}^{N} a_{i,n}^{l-j}e_{0,i}\end{aligned} \tag{5.20}$$

where $u(l)$ is the unit step function, 'w's are wavelet packet samples defined in (5.4), and $e_{k,i}$ are the elements of the error vectors that have been defined in (5.12) and (5.13) as $\mathbf{e}_0 = \mathbf{D}\mathbf{C}\mathbf{c}_1 - \mathbf{d}^1$,

$\mathbf{e}_{-1} = \mathbf{D}\mathbf{C}_{-1}\mathbf{c}_1$ and $\mathbf{e}_1 = \mathbf{D}\mathbf{C}_1\mathbf{c}_1$. Without loss of generality, the first bit d_1 of (5.18), which is assumed to be +1, is analyzed. Using (5.19), the decision variable, i.e., the real part of z_1 in (5.18), denoted as z, can be written as

$$\begin{aligned} z &= \mathrm{Re}\{z_1\} = \mathrm{Re}\{\alpha + \sum_{j=0}^{L-1} h^*(j)\left(I_{j,wp} + I_{j,sc} + \mathbf{w}_0^T\mathbf{N}(j)\mathbf{c}_1\right)\} \\ &= \alpha + \sum_{j=0}^{L-1} h^*(j) \sum_{l=0, l\neq j}^{L-1} h(l)\left(a_{1,1}^{l-j} + b_1^{l-j}\right) + \sum_{j=0}^{L-1} h^*(j)\sum_{l=0}^{L-1} h(l) b_{sc,1}^{l-j} + \mathrm{Re}\{\sum_{j=0}^{L-1} h^*(j)\mathbf{w}_0^T\mathbf{N}(j)\mathbf{c}_1\} \end{aligned} \tag{5.21}$$

where $\mathbf{w}_0^T = \begin{bmatrix} w_0(0) & w_0(1) & \cdots & w_0(N-1) \end{bmatrix}$ is the first column of the WP matrix **W**. For each fixed relative delay |*l*-*j*|, the correlation value $a_{1,1}^{l-j}$ has a deterministic value and can thus be computed. Conditioned on the data vector of all users $\mathbf{d}^i$, *i*=1, …, K, b_1^{l-j} and $b_{sc,1}^{l-j}$ can also be computed. The channel coefficients have been assumed zero-mean normal random variables, therefore *z* is a weighted summation of the product of two normal random variables, which can be analyzed using the method of [62] as follows.

5.2.2 Performance Evaluation

The decision variable z can be written in the following quadratic Hermitian form.

$$z = \mathbf{h}^H\mathbf{Q}_0\mathbf{h} + \frac{1}{2}\left(\mathbf{h}^H\mathbf{n} + \mathbf{n}^H\mathbf{h}\right) = \begin{bmatrix} \mathbf{h}^H & \mathbf{n}^H \end{bmatrix} \begin{bmatrix} \mathbf{Q}_0 & \frac{1}{2}\mathbf{I} \\ \frac{1}{2}\mathbf{I} & O \end{bmatrix} \begin{bmatrix} \mathbf{h} \\ \mathbf{n} \end{bmatrix} = \mathbf{g}^H\mathbf{Q}\mathbf{g} \tag{5.22}$$

where

$$\mathbf{Q}_0 = \begin{bmatrix} \alpha + b_{sc,1}^0 & a_{1,1}^{-1} + b_1^{-1} + b_{sc,1}^{-1} & \cdots & a_{1,1}^{1-L} + b_1^{1-L} + b_{sc,1}^{1-L} \\ a_{1,1}^1 + b_1^1 + b_{sc,1}^1 & \alpha + b_{sc,1}^0 & \ddots & \vdots \\ \vdots & \ddots & \ddots & a_{1,1}^{-1} + b_1^{-1} + b_{sc,1}^{-1} \\ a_{1,1}^{L-1} + b_1^{L-1} + b_{sc,1}^{L-1} & \cdots & a_{1,1}^1 + b_1^1 + b_{sc,1}^1 & \alpha + b_{sc,1}^0 \end{bmatrix} \tag{5.23}$$

I is L×L identity matrix and **O** is L×L all-zero matrix, and **g** is the extended channel vector. The equivalent noise for L RAKE fingers **n** is

$$\mathbf{n} = \begin{bmatrix} n_R(0) \\ \vdots \\ n_R(L-1) \end{bmatrix} = \begin{bmatrix} \mathbf{w}_0^T \mathbf{N}(0)\mathbf{c}_1 \\ \vdots \\ \mathbf{w}_0^T \mathbf{N}(L-1)\mathbf{c}_1 \end{bmatrix} \tag{5.24}$$

The characteristic function of z is [62]

$$\phi(\omega) \quad = \left|\mathbf{I} - j\omega\mathbf{VQ}\right|^{-1} \exp\left\{-\bar{\mathbf{g}}^H \mathbf{V}^{-1}[\mathbf{I} - \left(\mathbf{I} - j\omega\mathbf{VQ}\right)^{-1}]\bar{\mathbf{g}}\right\} \tag{5.25}$$

where $\mathbf{V}$ is the extended channel covariance matrix and $\bar{\mathbf{g}}$ is the mean of the extended channel vector. Due to the fact that the different paths of the channel are assumed independent, $\mathbf{V}$ satisfies

$$\mathbf{V} = E\left[(\mathbf{g}^H - \bar{\mathbf{g}}^H)(\mathbf{g} - \bar{\mathbf{g}})\right] = \begin{bmatrix} \sigma_0^2 \mathbf{I} & O \\ O & \mathbf{V}_n \end{bmatrix} \tag{5.26}$$

where σ_0^2 corresponds to the variance of channel path strengths, $\mathbf{V}_n$ is the covariance matrix of the noise. Since the noise terms for L fingers are linear combination of shifted AWGN terms, they are still Gaussian, but no longer white. Using (5.24) and the definition of $\mathbf{N}(j)$, the *l*-*k* entry of $\mathbf{V}_n$ can be calculated as

$$\begin{aligned}
&E\{n_R(l)n_R^*(k)\} = E\{\mathbf{w}_0^T \mathbf{N}(l)\mathbf{c}_1 (\mathbf{w}_0^T \mathbf{N}(k)\mathbf{c}_1)^H\} \\
&= E\{\mathbf{w}_0^T \sum_{i=0}^{N-1} \sum_{m=0}^{N-1} c_{1i} c_{1m}^* \mathbf{n}^i(l)\mathbf{n}^{mH}(k)\mathbf{w}_0\} \\
&= \mathbf{w}_0^T \sum_{i=0}^{N-1} \sum_{m=0}^{N-1} c_{1i} c_{1m}^* E\{\mathbf{n}^i(l)\mathbf{n}^{mH}(k)\}\mathbf{w}_0 \\
&= \mathbf{w}_0^T \sum_{i=0}^{N-1} [c_{1i} c_{1i}^* E\{\mathbf{n}^i(l)\mathbf{n}^{iH}(k)\} + c_{1i} c_{1,i+1}^* E\{\mathbf{n}^i(l)(\mathbf{n}^{i+1}(k))^H\} \\
&\qquad\qquad + c_{1i} c_{1,i-1}^* E\{\mathbf{n}^i(l)(\mathbf{n}^{i-1}(k))^H\}]\mathbf{w}_0 \\
&= \mathbf{w}_0^T \{\sum_{m=0}^{N-1} |c_{1i}|^2 \sigma_n^2 \mathbf{L}_{l-k} + \sum_{m=0}^{N-2} c_{1i} c_{1,i+1}^* \sigma_n^2 \mathbf{L}_{N+k-l} + \sum_{m=1}^{N-1} c_{1i} c_{1,i-1}^* \sigma_n^2 \mathbf{L}_{N+l-k}\}\mathbf{w}_0 \\
&= \mathbf{w}_0^T \{\sigma_n^2 \mathbf{L}_{l-k} \sum_{m=0}^{N-1} |c_{1i}|^2 + \sigma_n^2 \mathbf{L}_{N+k-l} \sum_{m=0}^{N-2} c_{1i} c_{1,i+1}^* + \sigma_n^2 \mathbf{L}_{N+l-k} \sum_{m=1}^{N-1} c_{1i} c_{1,i-1}^*\}\mathbf{w}_0
\end{aligned} \tag{5.27}$$

Due to the correlation properties of the pseudorandom codes, the first sum equals *N* whereas the second and the third sums are no more than 0.05*N* in magnitude (for length-63 Gold codes). Therefore, while the entire expression can still be computed once the WP waveforms and the pseudorandom codes are

chosen, it can also be approximated by the first term only without sacrificing much accuracy. Therefore we have

$$E[n_R(l)n_R^*(k)] \approx \mathbf{w}_0^T N\sigma_n^2 \mathbf{L}_{l-k}\mathbf{w}_0 = N\sigma_n^2 a_{1,1}^{l-k} \approx \sigma_1^2 a_{1,1}^{l-k} \tag{5.28}$$

where $a_{1,1}^1$ is the partial autocorrelation of first wavelet waveform $\mathbf{w}_0$. Therefore, the covariance matrix V_n becomes

$$\mathbf{V}_n \approx \sigma_1^2 \begin{bmatrix} 1 & a_{1,1}^1 & \cdots & a_{1,1}^{L-1} \\ a_{1,1}^1 & \ddots & & \vdots \\ \vdots & & \ddots & a_{1,1}^1 \\ a_{1,1}^{L-1} & \cdots & a_{1,1}^1 & 1 \end{bmatrix} \tag{5.29}$$

which can be easily computed.

Since both the channel impulse response and the AWGN noise are assumed zero-mean Gaussian, $\bar{\mathbf{g}} = \mathbf{0}$. Therefore, (5.25) is simplified to

$$\phi(\omega) \quad = \left|\mathbf{I} - j\omega\mathbf{VQ}\right|^{-1} = \prod_{l=0}^{2L-1}\left(1 - j\omega\lambda_l\right)^{-1} \tag{5.30}$$

where λ_l is the *l*th eigenvalue of

$$\mathbf{VQ} = \begin{bmatrix} \sigma_0^2\mathbf{I} & O \\ O & \mathbf{V}_n \end{bmatrix}\begin{bmatrix} \mathbf{Q}_0 & \frac{1}{2}\mathbf{I} \\ \frac{1}{2}\mathbf{I} & O \end{bmatrix} = \begin{bmatrix} \sigma_0^2\mathbf{Q}_0 & \frac{\sigma_0^2}{2}\mathbf{I} \\ \frac{1}{2}\mathbf{V}_n & O \end{bmatrix} \tag{5.31}$$

Due to the structure of **VQ**, it is non-singular, and thus there are *2L* non-zero eigenvalues. The probability distribution function of z conditioned on the data vector of all users $\mathbf{d}^i$, *i*=1, …, K, is

$$p(z \mid \mathbf{d}^1, \ldots \mathbf{d}^K) = \frac{1}{2\pi}\int_{-\infty}^{\infty}\phi(\omega)e^{-j\omega z}d\omega \tag{5.32}$$

which can be calculated by the residue theorem once the λ_l's are computed. Replace $j\omega$ by s, (5.32) becomes

$$p(z\,|\,\mathbf{d}^1,\ldots\mathbf{d}^K)=\frac{1}{2\pi j}\int_{0-j\infty}^{0+j\infty}\phi(s)e^{-sz}ds$$

$$=\frac{1}{2\pi j}\int_{0-j\infty}^{0+j\infty}\frac{e^{-sz}}{\prod_{0}^{L-1}(1-s\lambda_l)}ds=\frac{1}{2\pi j}\int_{0+j\infty}^{0-j\infty}\frac{-e^{-sz}}{\prod_{0}^{L-1}(1-s\lambda_l)}ds \tag{5.33}$$

According to the residue theorem,

$$p(z\,|\,\mathbf{d}^1,\ldots\mathbf{d}^K)=\begin{cases}\sum(\text{residues of poles on LHS}) & z\geq 0\\ -\sum(\text{residues of poles on RHS}) & z<0\end{cases} \tag{5.34}$$

The probability density function of z is

$$p(z)=\frac{1}{2^{63K}}\sum_{\mathbf{d}^i,i=1,\ldots K}p(z\,|\,\mathbf{d}^1,\ldots\mathbf{d}^K) \tag{5.35}$$

since the data symbols have 2^{63K} different combinations. It is impractical to do the calculation of (5.35). Observing that (5.35) resembles statistical average, it may be closely approximated by averaging fewer terms than 2^{63K}. In fact, our computation indicates that averaging over more than 500 such terms gives very little change in the overall pdf. We have therefore used 1000 randomly generated combinations of data symbols to obtain an approximation to (5.35).

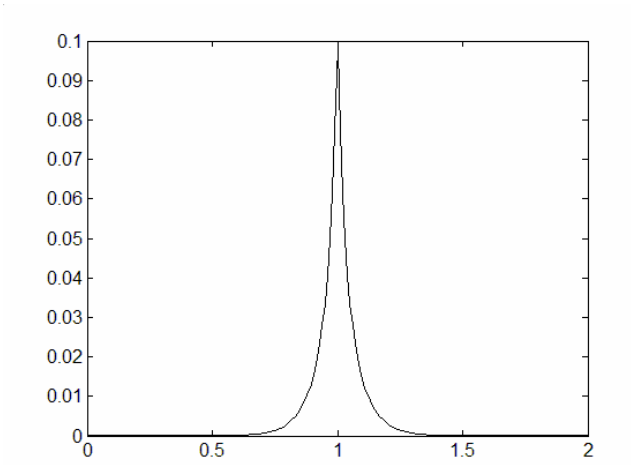

(a) WP waveforms

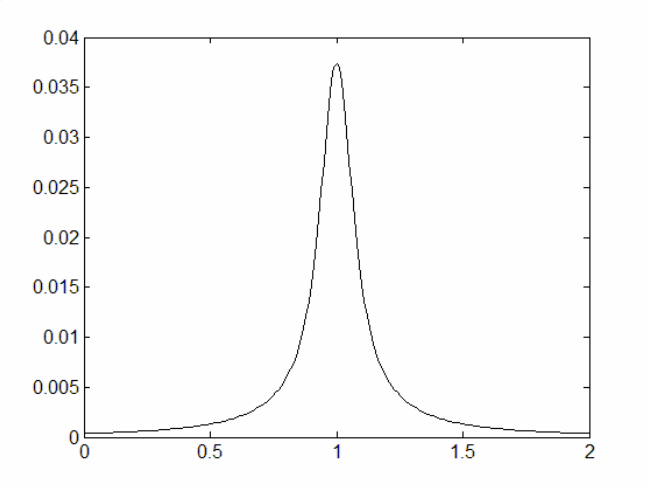

(b) sinusoid waveforms

Figure 5.6 pdf of z for WP and sinusoid waveforms, 5 path NLOS Channel

Figures 5.6 and *5.7* give plots of $p(z)$ for 5-path and 10-path NLOS channels when AWGN is not included in the calculation. In comparison, the figures also give the same density distribution function of z when sinusoid waveforms are used instead of wavelet packets. As indicated in previous sections, it is the time localization property of wavelet packets that make it possible to eliminate the need of guard intervals. This can be seen clearly from these figures that the wavelet packets result in a much smaller variance than sinusoid waveforms. This means that the WP based approach has a lower interference level and enables the elimination of guard intervals between symbols. It can also be seen that the decision variable has a distribution resembling product of Gaussian distribution due to the fact that the interference is the summation of a number of product of Gaussian variable terms. *Figure 5.8* gives another plot of p(z) for 5-path NLOS channel when AWGN is included in the calculation with Eb/No = 10 dB. The noise basically increases the variance of the decision variable and therefore the BER performance decreases accordingly. However, the WP based system still has a much narrower pdf than that of the DFT based system.

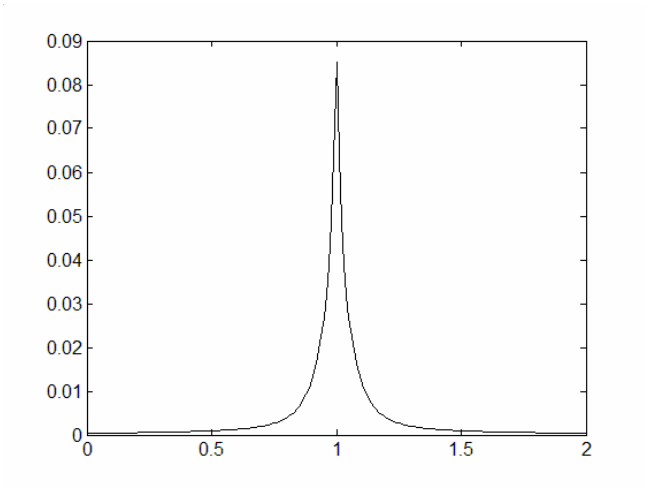

(a) WP waveforms

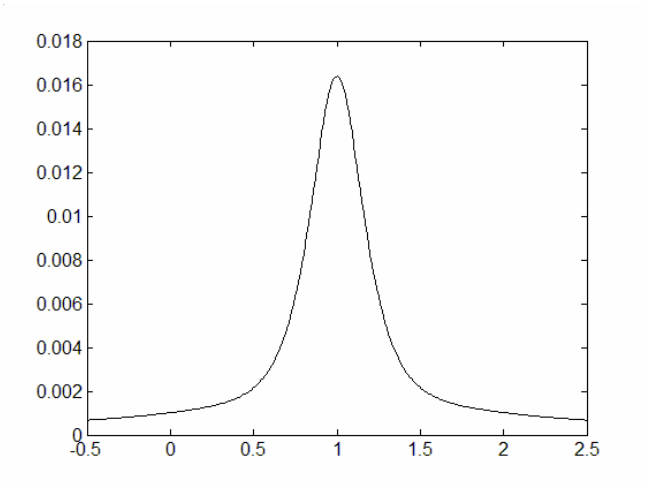

(b) sinusoid waveforms

Figure 5.7 pdf of z for WP and sinusoid waveforms, 10 path NLOS Channel

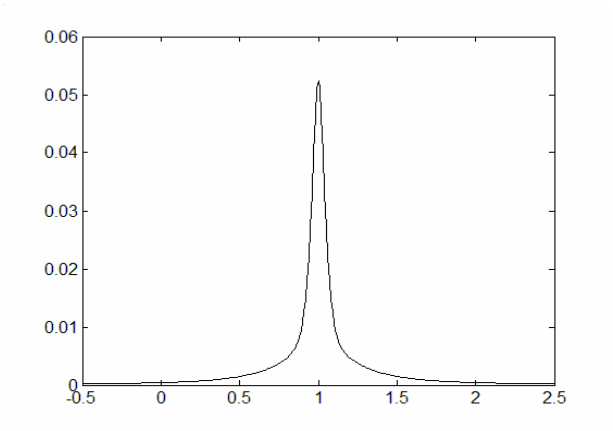

(a) WP waveforms

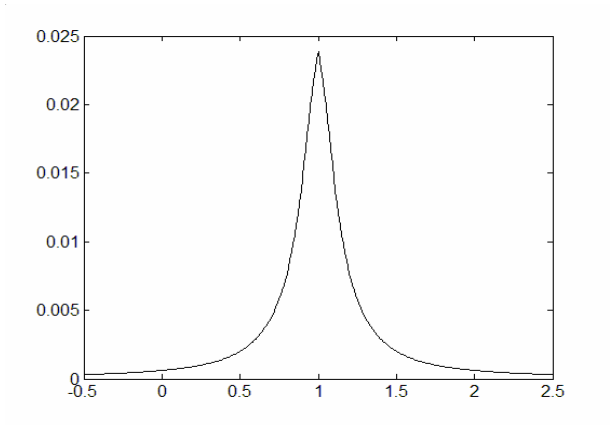

(b) sinusoid waveforms

Figure 5.8 pdf of z, 5 path NLOS Channel, Eb/No=10 dB

The bit error rate due to the interference can be determined by integrating the tail part of $p(z)$. The theoretical error probability from (5.35) has been used in the following for comparison purpose.

The path strength η_j can be estimated by chip/WP-correlation as

$$\eta_j = \begin{bmatrix} c_{1,0}\mathbf{w} & \cdots & c_{1,N-1}\mathbf{w} \end{bmatrix} \begin{bmatrix} \mathbf{r}^0(0) \\ \vdots \\ \mathbf{r}^{N-1}(0) \end{bmatrix} \tag{5.36}$$

where $\mathbf{w} = \sum_{l=0}^{N-1} \begin{bmatrix} w_l(0) & \cdots & w_l(N-1) \end{bmatrix}$. The channel coefficients η_j 's are thresholded, and the strongest paths are chosen to be the input to the combiner. This approach is based on time domain correlation and therefore similar to the time domain RAKE design of DS-CDMA or MC-DS-CDMA, but different from frequency domain channel estimation of MC-CDMA. The effect of channel estimation error of our system can be similar to those of DS-CDMA or MC-DS-CDMA but different from that of MC-CDMA due to the fact that the time domain combining utilizes only the strongest paths while the frequency domain equalization adjusts signals from all subcarriers. Analysis of the effect of estimation error of η_j is outside the scope of this work. Likewise, the effect of timing estimation error of our system can be similar to those of DS-CDMA or MC-DS-CDMA but different from that of MC-CDMA, and is also outside the scope of this work.

Note that this time diversity is afforded by the time localization of wavelet packets, which the DFT based waveforms do not have. In fact, if the DFT waveforms were used in the same approach, the correlation sequence (5.36) would have such poor resolution that one would not be able to identify any of the paths.

5.2.3 Computational Complexity

The computational complexity of this receiver depends on the complexity of DWPT. For a length *N* signal, the DWPT corresponding to the full binary tree needs $MN\log_2 N$ complex additions and multiplications [22], where *M* is the length of the wavelet filters. An *L* finger receiver needs $MNL\log_2 N$ multiplications and additions. Compared with the DFT based system, the computational complexity is about *ML* times higher. For a reduced binary tree, the computational complexity decreases. For example, if the binary tree is a wavelet tree, the total number of multiplications will be less than *2MN* so that the receiver needs only $2MNL$ multiplications and additions. In practice, the wavelet packet binary tree will be between these two extreme cases.

5.3 Performance in Asynchronous Transmission Conditions

In the asynchronous transmission environment, the *timing* and the *channels* for different users are now all different. Without loss of generality, the relative delays for all *K* users are assumed to satisfy the

condition $|\tau_k| \le N, k = 2,3,...,K$ and $\tau_1 = 0$, where τ_k is the relative delay for user *k*. This assumption implies that the relative delays between all *K* users are shorter than one chip duration. The case where the relative delays are longer than one-chip duration is discussed later in this section.

Direct application of the synchronous transceiving method of the last section to the asynchronous case results in higher BER that may not be acceptable. This is because the interference introduced from other users is higher than that in the synchronous case. To combat the higher interference level introduced by the asynchronous transmission, a modification similar to those introduced in MC-DS-CDMA systems can be applied to the WP based multicarrier CDMA system. In this modification, the number of subcarriers is *M* times as many as in the original system, so that each bit stream out from the serial-to-parallel conversion block is transmitted simultaneously on *M* different subcarriers. In the DFT based system this results in *M*-fold reduction in spectrum efficiency if the subcarriers were already minimally separated [7], [8]. In the WP based multicarrier CDMA system discussed in this section, the same data bit stream is also modulated simultaneously on *M* different WP waveforms. However, these WP waveforms are now generated from a higher level of the WP construction tree, so that each waveform occupies less frequency bandwidth and the total bandwidth for the system is kept unchanged while the symbol length is extended by *M* times (i.e., the same penalty as in the DFT based system but appears as *M* fold reduction in the data rate). Note that this results in a slightly different transmitter and receiver structures from that shown in *Figures 5.1* and *5.4,* and there are *M* parallel inputs to the IDWPT and DWPT blocks corresponding to one symbol.

The transmitted signal in the *i*th chip interval from user *k* is in the same form as (5.3) and (5.4) except that the $\mathbf{d}^k$ vector is repeated *M* times, and that the length and the number of WP waveforms are increased *M* times, corresponding to the $log_2 M$ higher level WP tree. That is, the vector $\mathbf{x}_k^i$ is now *M* times longer as shown below.

$$x_k^i(n) = c_{k,i} \sum_{m=0}^{M-1} \sum_{l=0}^{N-1} d_{mN+l+1}^k w_{mN+l}(n), n = 0,1,...,MN-1 \qquad (5.37)$$

$$\mathbf{x}_k^i = \begin{bmatrix} x_k^i(0) \\ \vdots \\ x_k^i(MN-1) \end{bmatrix} = \begin{bmatrix} w_0(0) & \cdots & w_{MN-1}(0) \\ \vdots & \ddots & \vdots \\ w_0(MN-1) & \cdots & w_{MN-1}(MN-1) \end{bmatrix} \begin{bmatrix} \mathbf{d}^k \\ \vdots \\ \mathbf{d}^k \end{bmatrix} c_{k,i} = \mathbf{W}\mathbf{d}_M^k c_{k,i} \qquad (5.38)$$

The data vector $\mathbf{d}_M^k$ in (5.38) is the *M* times repeated version of $\mathbf{d}^k$ and has a dimension of *MN*. That is

$$\mathbf{d}_M^k = \begin{bmatrix} d_1^k & \cdots & d_N^k & \cdots & d_1^k & \cdots & d_N^k \end{bmatrix}^T = \underbrace{\begin{bmatrix} \mathbf{d}^{k^T} & \cdots & \mathbf{d}^{k^T} \end{bmatrix}^T}_{M \quad blocks} \tag{5.39}$$

The received signal from user *k* can then be written as

$$\mathbf{r}_k^i(0) = \mathbf{H}_k \mathbf{L}_k \begin{bmatrix} \mathbf{x}_k^{i-1} \\ \mathbf{x}_k^i \\ \mathbf{x}_k^{i+1} \end{bmatrix} + \mathbf{n}^i(0) \tag{5.40}$$

In (5.40) $\mathbf{H}_k$ stands for the *MN*×*2MN* channel matrix for the *k*th user, and is defined as

$$\mathbf{H}_k = \begin{bmatrix} O & h_k(L-1) & \cdots & h_k(0) & 0 & & & O \\ & & \ddots & \ddots & \ddots & \ddots & & \\ & & & h_k(L-1) & \cdots & h_k(0) & \ddots & \\ O & & & & \ddots & \ddots & \ddots & 0 \\ & & & & & h_k(L-1) & \cdots & h_k(0) \end{bmatrix} \tag{5.41}$$

$\mathbf{L}_k$ is a 2MN×3MN matrix whose (*l*,*m*)th elements are ones when $m - l = \tau_k$, and all other elements are zeros.

The combined signal from all *K* users is

$$\mathbf{r}^i(0) = \sum_{k=1}^{K} \mathbf{r}_k^i(0) = \sum_{k=1}^{K} \mathbf{H}_k \mathbf{L}_k \begin{bmatrix} \mathbf{x}_k^{i-1} \\ \mathbf{x}_k^i \\ \mathbf{x}_k^{i+1} \end{bmatrix} + \mathbf{n}^i(0) \tag{5.42}$$

The detector has the same structure as that of *Figure 5.4*. The DWPT demodulated signal is

$$\mathbf{y}^i(0) = \mathbf{W}^T \mathbf{r}^i(0) = \sum_{k=1}^{K} \mathbf{W}^T \mathbf{H}_k \mathbf{L}_k \begin{bmatrix} \mathbf{x}_k^{i-1} \\ \mathbf{x}_k^i \\ \mathbf{x}_k^{i+1} \end{bmatrix} + \mathbf{W}^T \mathbf{n}^i(0) = \sum_{k=1}^{K} \mathbf{W}^T \mathbf{H}_k \mathbf{L}_k \begin{bmatrix} \mathbf{W}\mathbf{d}_M^k c_{k,i-1} \\ \mathbf{W}\mathbf{d}_M^k c_{k,i} \\ \mathbf{W}\mathbf{d}_M^k c_{k,i+1} \end{bmatrix} + \mathbf{W}^T \mathbf{n}^i(0) \tag{5.43}$$

Grouping the signals for one data symbol (*N* chips) together, a matrix can be formed as

$$
\begin{aligned}
\mathbf{Y}(0) &= \left[\mathbf{y}^0(0) \quad \cdots \quad \mathbf{y}^{N-1}(0)\right] \\
&= \sum_{k=1}^{K} \mathbf{W}^T \mathbf{H}_k \mathbf{L}_k \begin{bmatrix} \mathbf{W}\mathbf{d}_M^k \begin{bmatrix} c_{k,N-1} & c_{k,0} & \cdots & c_{k,N-2} \end{bmatrix} \\ \mathbf{W}\mathbf{d}_M^k \begin{bmatrix} c_{k,0} & c_{k,1} & \cdots & c_{k,N-1} \end{bmatrix} \\ \mathbf{W}\mathbf{d}_M^k \begin{bmatrix} c_{k,1} & \cdots & c_{k,N-1} & c_{k,0} \end{bmatrix} \end{bmatrix} + \mathbf{W}^T \mathbf{N}(0) \\
&= \sum_{k=1}^{K} \mathbf{W}^T \mathbf{H}_k \mathbf{L}_k \begin{bmatrix} \mathbf{W}\mathbf{d}_M^k \mathbf{c}_{k,-1}^T \\ \mathbf{W}\mathbf{d}_M^k \mathbf{c}_k^T \\ \mathbf{W}\mathbf{d}_M^k \mathbf{c}_{k,1}^T \end{bmatrix} + \mathbf{W}^T \mathbf{N}(0)
\end{aligned}
\tag{5.44}
$$

This signal is despread using the corresponding spreading code of the first user. The output is then

$$
\begin{aligned}
\mathbf{z}(0) = \mathbf{Y}(0)\mathbf{c}_1 &= \sum_{k=1}^{K} \mathbf{W}^T \mathbf{H}_k \mathbf{L}_k \begin{bmatrix} \mathbf{W}\mathbf{d}_M^k \mathbf{c}_{k,-1}^T \\ \mathbf{W}\mathbf{d}_M^k \mathbf{c}_k^T \\ \mathbf{W}\mathbf{d}_M^k \mathbf{c}_{k,+1}^T \end{bmatrix} \mathbf{c}_1 + \mathbf{W}^T \mathbf{N}(0)\mathbf{c}_1 \\
&= \mathbf{W}^T \mathbf{H}_1 \begin{bmatrix} \mathbf{W}\mathbf{d}_M^1 \mathbf{c}_{1,-1}^T \\ \mathbf{W}\mathbf{d}_M^1 \mathbf{c}_1^T \end{bmatrix} \mathbf{c}_1 + \sum_{k=2}^{K} \mathbf{W}^T \mathbf{H}_k \mathbf{L}_k \begin{bmatrix} \mathbf{W}\mathbf{d}_M^k \mathbf{c}_{k,-1}^T \\ \mathbf{W}\mathbf{d}_M^k \mathbf{c}_k^T \\ \mathbf{W}\mathbf{d}_M^k \mathbf{c}_{k,+1}^T \end{bmatrix} \mathbf{c}_1 + \mathbf{W}^T \mathbf{N}(0)\mathbf{c}_1
\end{aligned}
\tag{5.45}
$$

The second term in (5.45) corresponds to the multiuser interference and can be termed as $\mathbf{I}_{0,\text{mu}}$. The correlation properties of the spreading codes ensure that this term has a small norm, at about the same level as that of synchronous transmission case. Note that in case the asynchronous delay $|\tau_k| > N, k \neq 1$, there will be other blocks $\mathbf{x}_k^{i\pm m}, m > 1$ in (5.42). These other blocks will result in, in the blocks of the second term of (5.45), additional blocks in the form of $\mathbf{W}\mathbf{d}_M^k \mathbf{c}_{k,\pm m}^T$. Thus, additional inner product $\mathbf{c}_{k,\pm m}^T \mathbf{c}_1, k \neq 1$ is formed. However, since the cross-correlations of the spreading code such as Gold code are at the same level for zero-shifted (*m=0*) codes and non-zero-shifted (*m≠0*) codes, relative delay of small integer number of chips will not affect the system performance dramatically.

The first term of (5.45) corresponds to the signal from the first user, and can be further divided into two parts, the desired signal and the multipath interference. Thus (5.45) can be rewritten as

$$
\begin{aligned}
\mathbf{z}(0) &= \mathbf{W}^T \mathbf{H}_1 \begin{bmatrix} \mathbf{W}\mathbf{d}_M^1 \mathbf{c}_{1,-1}^T \\ \mathbf{W}\mathbf{d}_M^1 \mathbf{c}_1^T \end{bmatrix} \mathbf{c}_1 + \mathbf{I}_{0,mu} + \mathbf{W}^T \mathbf{N}(0)\mathbf{c}_1 \\
&= \mathbf{W}^T \mathbf{H}_1^R \mathbf{W}\mathbf{d}_M^1 + \mathbf{W}^T \mathbf{H}_1^L \mathbf{W}\mathbf{d}_M^1 \mathbf{c}_{1,-1}^T \mathbf{c}_1 + \mathbf{I}_{0,mu} + \mathbf{W}^T \mathbf{N}(0)\mathbf{c}_1 \\
&= \mathbf{W}^T \mathbf{H}_1^R \mathbf{W}\mathbf{d}_M^1 + \mathbf{I}_{0,-1} + \mathbf{I}_{0,mu} + \mathbf{W}^T \mathbf{N}(0)\mathbf{c}_1
\end{aligned}
\tag{5.46}
$$

where $\mathbf{H}_1^L$ and $\mathbf{H}_1^R$ are the left and right half of the channel matrix $\mathbf{H}$. $\mathbf{I}_{0,-1}$ in (5.46) corresponds to the interference from shifted autocorrelation of the spreading code $\mathbf{c}_1$, and thus has a small norm.

The demodulated signal $\mathbf{z}(j)$ from the delayed versions of the received signal $\mathbf{r}(j)$ can be formulated similarly as

$$\mathbf{z}(j) = \mathbf{W}^T \mathbf{H}_1 \mathbf{L}_j \mathbf{W} \mathbf{d}_M^1 + \mathbf{I}_{j,-1} + \mathbf{I}_{j,1} + \mathbf{I}_{j,mu} + \mathbf{W}^T \mathbf{N}(j) \mathbf{c}_1 \tag{5.47}$$

where $\mathbf{H}_1 \mathbf{L}_j$ has the same structure as that of (5.15). Following the procedure from (5.15) to (5.18), a vector $\mathbf{z}$ that mainly consists of $\hat{\mathbf{d}}_M^1$ can be formed by time combining the demodulated results from the strongest paths. However, since the asynchronous delay τ_k could be much larger than the channel delay spread in the synchronous case, the amount of shift caused by $\mathbf{L}_j$ now is much more. This results in a higher interference level in the first three terms of (5.47). Recall from (5.39) that the vector $\mathbf{d}_M^1$ consists M replicas of N useful data bits so that a frequency combing can be used to lower this interference level. Since the combining elements come from the same user, pass through the same channel, and have the same bit energy, the equal gain combing, which is equivalent to the maximum ratio combing in this case, can be performed by

$$\hat{\mathbf{d}}^1 = \underbrace{\left[\mathbf{I} \quad \cdots \quad \mathbf{I}\right]}_{M \text{ 'I's}} \hat{\mathbf{d}}_M^1 = \underbrace{\left[\mathbf{I} \quad \cdots \quad \mathbf{I}\right]}_{M \text{ 'I's}} \mathbf{z} \tag{5.48}$$

where $\mathbf{I}$ is the $N \times N$ identity matrix. This combining is equivalent to raising the desired signal level M times. The resulting decision vector $\hat{\mathbf{d}}^1$ is the desired data vector plus a normally distributed random variable vector with a small variance. Thus the receiver can detect user data with a small bit error rate.

From (5.17) and (5.48) it can be seen that both the frequency combining and the path combining are linear operations, and are therefore exchangeable. Thus, in practice the frequency combining is usually done first.

5.4 Simulation Results of the Detection Algorithm

The proposed time domain RAKE combining detection algorithm has been evaluated by means of simulations for both synchronous and asynchronous transmission cases. In the simulation, the number of subcarriers is set to 64. The channel is assumed multipath plus Gaussian noise, time-invariant within the

simulation length. The bit error rate is calculated by running the simulation for 1,000,000 symbols. The delay spread of the channel is assumed within ¼ of the symbol length. Two types of the channel impulse responses are considered. In the first one, the channel response for each path is a normal random variable (Non-Line-of-Sight or NLOS). For the second one the channel response for each path is a normal random variable except the first path, which is assumed a Line-of-Sight (LOS) path contributing 2/3 of the total energy. In the receiver, the strongest paths with 80% or more of the total energy are combined to form the decision variable.

First, a comparison of the analytical results (Section 5.2, Equation 5.35) and the simulation results for 5-path NLOS and 5-path LOS channel has been given in *Figure 5.9*. The system performance is measured by Bit Error Rate (BER) against the bit-energy to noise ratio. In the simulation, 80% energy combining is used, which in most cases combines the strongest two or three paths. It is seen from Fig. 5.9 that the simulation results well follow the curves of the analysis.

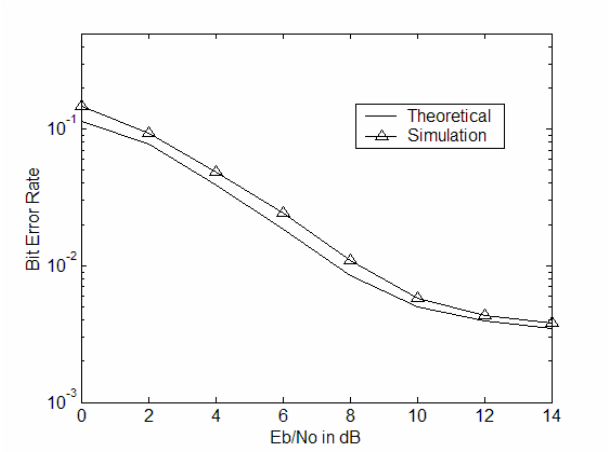

(a) 5-path NLOS channel

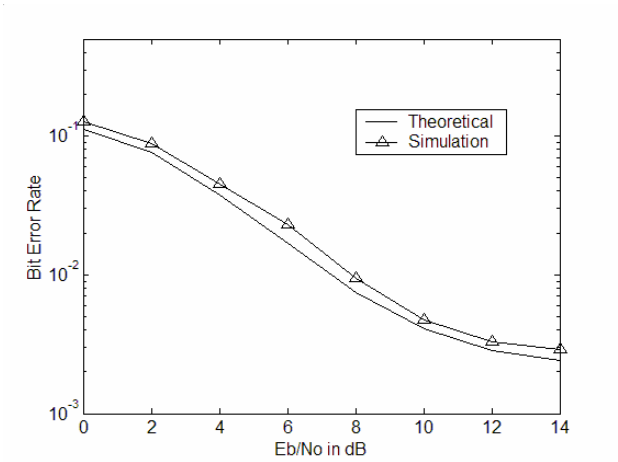

(b) 5-path LOS channel

Figure 5.9 Comparison of analytical and simulation results

30 synchronous users in 5-path channels

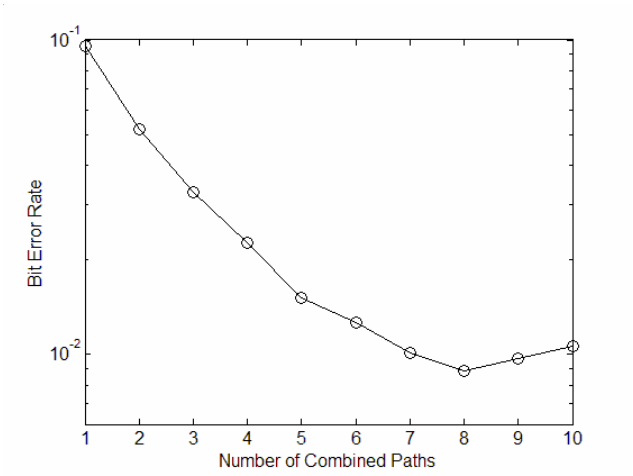

Figure 5.10 Performance for different number of combined paths, 40 synchronous users in 10-path NLOS channels, Eb/No=14 dB, ensemble average of 200 channels

Note that combining more paths is not always desirable and may raise the interference level. This is because the strongest paths contribute most of the combined energy of the signal, and when a weak path is combined a higher interference is introduced without raising the signal energy level significantly. However, in other conditions, especially for the asynchronous transmission case and NLOS channel case, combining more signal energy generally raises the signal to interference ratio. This can be seen in *Figure 5.10*, where the BER against the number of combined paths is given for 10-path NLOS channels

at Eb/No=14 dB. It can be seen that the BER becomes lower as the number of combined paths is increased, although not significantly for more than six combined paths and actually increases very slightly for more than eight paths. Thus in actual applications the number of combined paths should not be fixed, but chosen according to the channel condition. Generally, it is found that combining paths with about 80% total signal energy for LOS channels and 90% for NLOS channels gives good compromise between BER performance and system complexity.

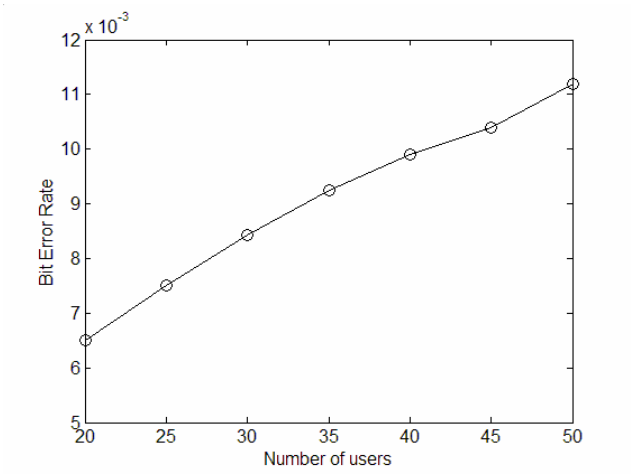

Figure 5.11 BER vs number of active users, 5-path NLOS channel

The number of users that can be active simultaneously in a system is also a very important measure of system performance. *Figure 5.11* gives the BER vs the number of active users for the WP based MC-DS-CDMA system, in the case of 5-path NLOS channel. It can be seen, for example, that the system can support about 40 users at the BER level of 0.01.

The proposed WP based multicarrier CDMA system has also been compared with the DFT based system. Since the length of the channel is set to be ¼ of one symbol duration, in the DFT based system the data rate is 80% of the original data rate due to the cyclic prefix. To compare the performance of these two systems with the same data rate, BCH coding [54] is applied to both of the systems, only with different code rate so that the resulted transmission rates for these two systems are the same. The code rates used in the simulation are (45,63) and (36,63) for the DFT based system and WP based system, respectively.

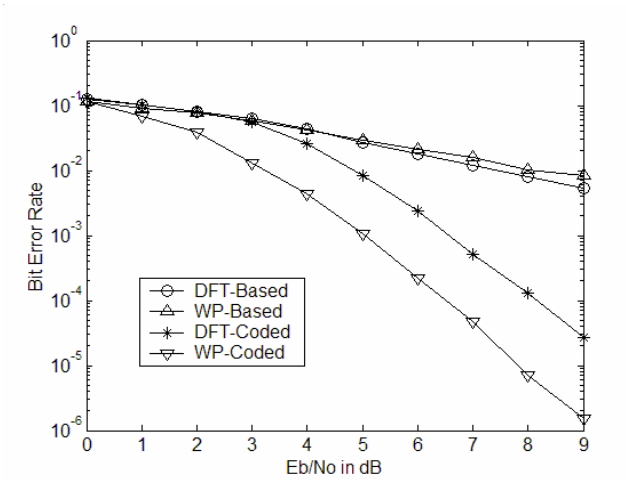

Figure 5.12 Performance comparison in the case of 30 active users, 5-path LOS channel

Figure 5.12 gives the performance comparison of the proposed WP-MC-DS-CDMA system with the conventional DFT based multicarrier CDMA system. The channel is 5-path Line-of Sight (LOS) channel. For the uncoded case, it can be seen that the WP based system achieves just a slightly higher BER but with 25% higher data rate than the DFT based system. For the coded case, however, the higher coding power of the WP-MC-DS-CDMA system that is afforded by the saved bandwidth enables it to achieve a much better BER performance (almost 20 dB) than the DFT based system with the same data rate.

Figure 5.13 illustrates the similar performance comparison in a different condition. The channel is now5-path Non-Line-of Sight (NLOS) channel, while the number of users is 30. In this case it can be seen that the WP based system still outperforms the DFT based system, although it encounters higher interference level per interfering user since the NLOS channel makes it more difficult to achieve precise path match. However, the total interference level is lower due to the fewer number of users.

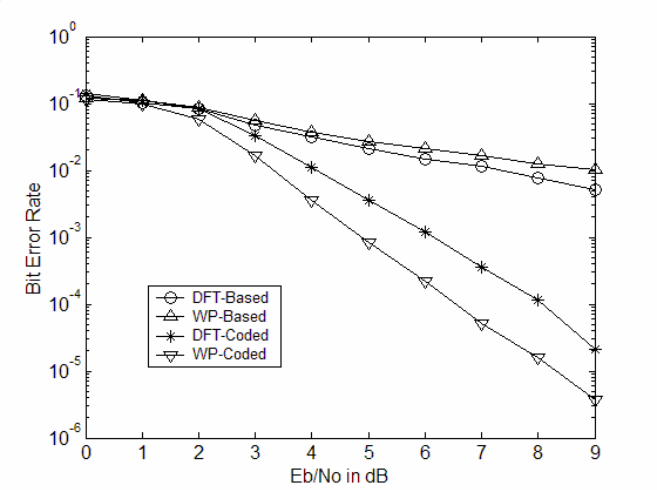

Figure 5.13 Performance comparison in the case of 30 active users, 5-path NLOS channel

The performance of the system in the asynchronous transmission condition has also been evaluated by simulation. In the simulation the relative delays between different users are uniformly distributed in [*0*, *T*], where *T* is the symbol length. However, the channel is still a multipath channel plus additive Gaussian white noise. The channel delay spread is still ¼ of the chip duration as in the synchronous case. Each data bit is transmitted simultaneously in *M=4* subcarriers.

Figure 5.14 gives the performance comparison between the WP-based and the DFT-based systems. Frequency combining (equal gain) is employed for both methods. It is seen that in the asynchronous transmission scenario WP-based system performs better than the DFT-based system even with a higher data rate. This is due to the fact that the former has the ability to distinguish different paths even when relative delays between the paths are shorter than the chip duration. But since the DFT-based system can only resolve multipath signals with relative delays larger than the chip duration, the multipath signals in this case are not resolvable by the DFT based method.

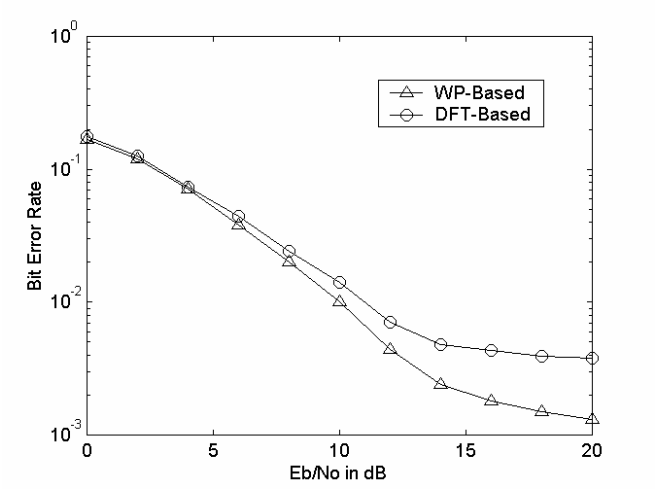

(a) 5-path NLOS channel

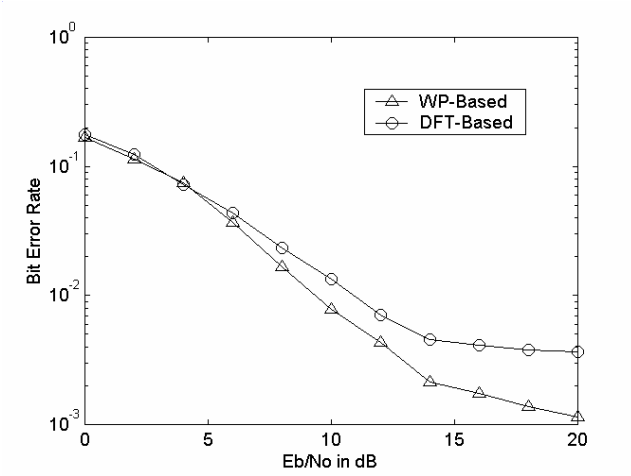

(b) 5-path LOS channel

Figure 5.14 BER vs Eb/No for asynchronous transmission, 40 active users

One way to overcome this problem in the DFT-based MC-DS-CDMA system is to employ fewer subcarriers compared with the MC-CDMA system, resulting in larger subcarrier bandwidths and thus relatively larger channel delay spread. And time domain methods such as the RAKE receiver rather than the frequency domain equalization, are usually used in the MC-DS-CDMA system. This requires, however, one RAKE combiner for each subcarrier, so that the number of subcarriers is limited by the system complexity. On the other hand, the WP-based system as proposed here needs only *one* RAKE combiner for all the subcarriers. Thus the number of subcarriers can be as large as desired, and the fast wavelet packet transform can still be utilized to achieve a moderate computational complexity.

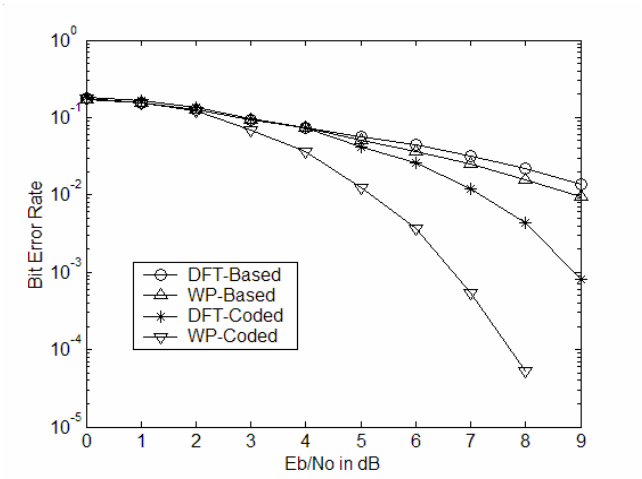

(a) 5-path NLOS channel

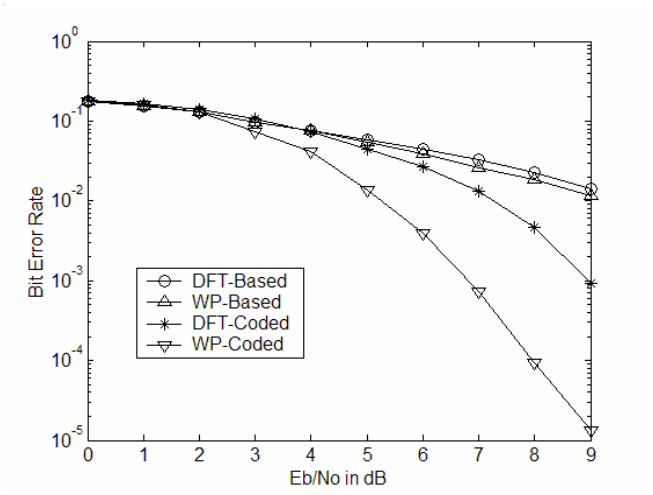

(b) 5-path LOS channel

Figure 5.15 Performance for asynchronous transmission with coding

The performance of these two systems in other channel conditions with different number of paths has also been investigated, and it has been seen that they perform in the same way as that of *Figure 5.14*. However, the figures are not shown here since they are similar to *Figure 5.14*.

Figure *5.15* gives the performance comparison when the same coding scheme as that in the synchronous case is introduced so that the two systems have the same data rate. It is clear the WP based system significantly outperforms the DFT based system even up to 40 dB. This is mainly due to the degradation of the DFT based system under the asynchronous case, whereas the WP based system preserves much the same level of performance as that in the synchronous case.

5.5 Time-Varying Channel Prediction and Estimation

In a time-invariant channel condition the channel can be estimated by training beforehand. In practice, the estimated channel is used for a certain time period and the channel estimation is repeated every such period. This approach assumes a slow time-varying channel, and will not work well for fast time-varying channels. In this section linear prediction is used for a relatively fast time-varying channel condition. *Figure 5.16* gives the receiver structure that combines the multipath receiver (as shown in *Figure 5.4*) with channel prediction and estimation.

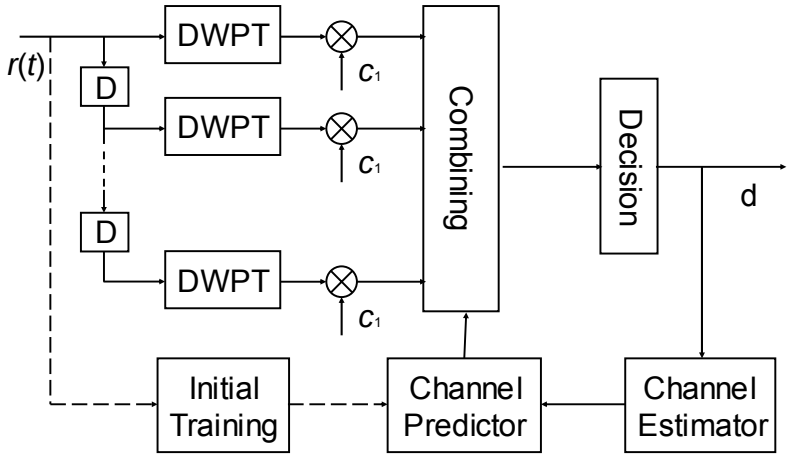

Figure 5.16 Receiver of the wavelet based MC-CDMA system for time-varying channels

The receiver design here is a time-domain algorithm. Therefore, the channel in any specific time is represented by its impulse response snapshot $h(n)$, where n takes on values from *0* to $N_c=N/4$, i.e., the delay spread of the channel is ¼ of the chip duration. Since the time-varying channel condition is considered in the following, another discrete variable m is introduced to represent the time parameter. The channel impulse response snapshot $h(n)$ at a specific time m can be written as a column vector $\mathbf{h}_m=[h(m,1), h(m,2), \ldots, h(m,N_c)]^T$. If a series of M channel impulse responses are considered, then the channel can be represented by

$$\mathbf{H}_m=\begin{bmatrix} h(m-M,1) & \cdots & h(m-1,1) \\ \vdots & \ddots & \vdots \\ h(m-M,N_c) & \cdots & h(m-1,N_c) \end{bmatrix}=\begin{bmatrix} \mathbf{h}_{m-M} & \cdots & \mathbf{h}_{m-1} \end{bmatrix}=\begin{bmatrix} \left(\mathbf{h}^1(m)\right)^T \\ \vdots \\ \left(\mathbf{h}^{N_c}(m)\right)^T \end{bmatrix} \quad (5.49)$$

where the vectors $\mathbf{h}^n(m)$ represent the values of the same sample in the time-varying impulse response over M snapshots of impulse responses. One approach to predict the next channel impulse response $\mathbf{h}_m$ from $\mathbf{H}_m$ is using one predictor for each sample n in the channel impulse responses so that

$$\hat{h}(m,n) = \left(\mathbf{h}^n(m)\right)^T \mathbf{v}_n(m) \tag{5.50}$$

where the vector $\mathbf{v}_n(m)$ is the nth predictor at time m. This requires N_c predictors where N_c is the length of the channel. For simplicity, in the following we use a common predictor for all points in the channel impulse response. Thus, $\mathbf{h}_m$ is predicted from $\mathbf{H}_m$ using only one length M vector of weights $\mathbf{v}(m)$ as

$$\hat{\mathbf{h}}_m = \mathbf{H}_m \mathbf{v}(m) \tag{5.51}$$

The weight vector $\mathbf{v}$ is indexed by m since it is updated adaptively. The simulation results suggest that one predictor is enough to make a fairly accurate prediction. The mean square averaged error $\xi(m)$ (5.53 below) can be used as a criterion of the prediction optimization. In the time-varying channel case, an adaptive method is needed to track the time variation of the channel. In this paper, the Recursive Least Squares (RLS) [55] method is used to update the weight vector $\mathbf{v}$. In each step, the updating of the weight vector can be summarized as

$$\mathbf{k}(m) = \frac{\lambda^{-1}\sum_{n=1}^{N_c} \mathbf{P}(m-1)\hat{\mathbf{h}}^n(m)}{1+\lambda^{-1}\sum_{n=1}^{N_c} \hat{\mathbf{h}}^n(m)\mathbf{P}(m-1)\hat{\mathbf{h}}^n(m)} \tag{5.52}$$

$$\xi(m) = \sum_{n=1}^{N_c}\left[\hat{h}(m,n) - \mathbf{v}^T(m-1)\hat{\mathbf{h}}^n(m)\right] \tag{5.53}$$

$$\mathbf{v}(m) = \mathbf{v}(m-1) + \mathbf{k}(m)\xi(m) \tag{5.54}$$

$$\mathbf{P}(m) = \lambda^{-1}\mathbf{P}(m-1) - \lambda^{-1}\sum_{n=1}^{N_c} \mathbf{k}(m)\left(\hat{\mathbf{h}}^n(m)\right)^T \mathbf{P}(m-1) \tag{5.55}$$

where the forgetting factor λ is a positive constant close to but less than *1*, $\mathbf{k}(m)$ and $\mathbf{P}(m)$ are the gain vector and inverse correlation matrix, respectively. The input to this predictor is the channel matrix $\mathbf{H}_m$. However, in practice the channel matrix is not directly available, and an estimated matrix $\hat{\mathbf{H}}_m$ is used

instead. The channel estimation is based on the detected symbol values. The corresponding channel impulse response $h(m,n)$ can be estimated by chip/WP-correlation as

$$\hat{h}(m,n) = \begin{bmatrix} c_{1,0}\mathbf{w} & \cdots & c_{1,N-1}\mathbf{w} \end{bmatrix} \begin{bmatrix} \mathbf{r}^0(n) \\ \vdots \\ \mathbf{r}^{N-1}(n) \end{bmatrix} \tag{5.56}$$

where $\mathbf{w} = \sum_{l=0}^{N-1} \hat{d}_{m,l} \begin{bmatrix} w_l(0) & \cdots & w_l(N-1) \end{bmatrix}$ is the locally generated waveform based on the detected symbols $\hat{\mathbf{d}}_m$, $\mathbf{c}_1$ is the user spreading code. At the mth step, $\hat{\mathbf{H}}_m$ is used to predict $\mathbf{h}_m$. This predicted $\hat{\mathbf{h}}_m$ is then used to detect the current symbols $\mathbf{d}_m$ which are transmitted through $\mathbf{h}_m$. Then the detected symbols $\hat{\mathbf{d}}_m$ are used in (5.56) to estimate $\mathbf{h}_m$. The estimated $\hat{\mathbf{h}}_m$ becomes part of $\hat{\mathbf{H}}_{m+1}$ for the next step.

In the initialization phase, the matrix $\mathbf{P}$ is initialized as an identity matrix multiplied by a small scalar, and the weight vector is initialized as a zero vector. A number of training symbols are used to obtain an initial set of estimated channel impulse responses and to train the predictor. The predictor is then used online and updated adaptively. In the simulation the initial training phase takes about 25 snapshots of channel impulse responses to converge, and the online updating of predictor weights remains effective for all subsequent channel impulse response snapshots.

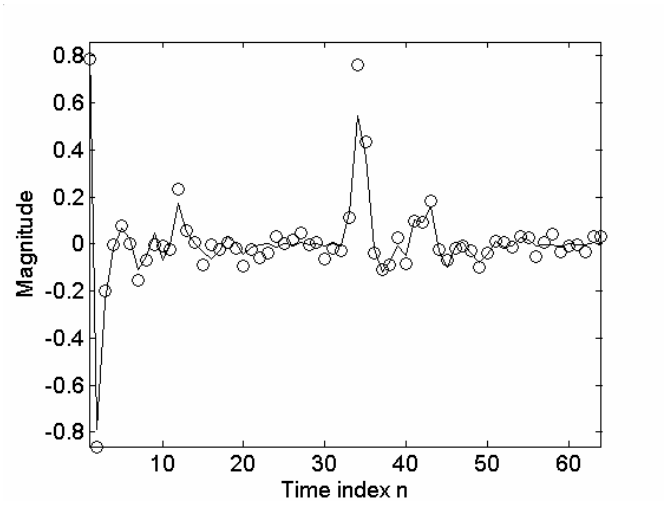

Figure 5.17 Channel prediction performance for one snapshot,

Eb/No=20 dB, training=26 steps, L=64, M=8, m=41

The proposed algorithm has been evaluated by means of simulations against field measurement channel impulse response data. In the simulation, the number of subcarriers is set to 64. The fast time-varying channel data are again those obtained from the Institute for Telecommunication Sciences [51]. In these field-measured channels the time delay between two adjacent impulse responses is 4.6 ms. The 64 samples of one impulse response snapshot correspond to a time duration of 3.2 us. The bit error rate is calculated by running the simulation for 100,000 symbols. The delay spread of the channel is assumed within ¼ of the symbol length. In the receiver, the strongest paths with 80% or more of the total energy are combined to form the decision variable. The number of input snapshots *M* for the channel predictor is set to 8. The initial training takes 26 snapshots and online updating of the weights lasts for 230 snapshots in our simulation but can be further continued with the same performance level.

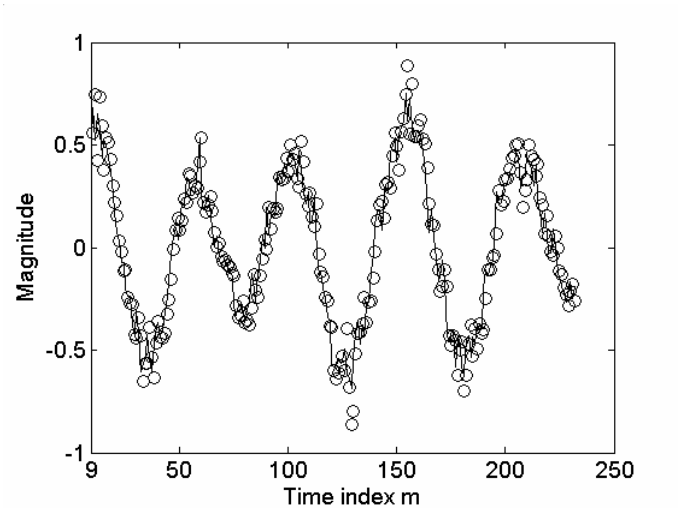

Figure 5.18 Channel tracking performance for one sample in channel impulse response snapshots, user number=40, Eb/No=20 dB, n=14

Figure 5.17 gives a plot of predicted channel impulse response $\hat{\mathbf{h}}_m = \left[\hat{h}(m,1) \quad \cdots \quad \hat{h}(m,N_c) \right]$ in comparison with the original channel impulse response $\mathbf{h}_m$. It can be seen that the predicted channel well resembles the original one so that when this predicted channel is used in the detection, a good BER performance can be achieved. The mean square error of the channel prediction is at the level of 5%.

The channel predictor should also track the channel variation properly. *Figure 5.18* gives a plot showing the tracking property of the channel predictor. In this figure the values of a specific sample in each of the channel impulse response snapshots are taken out and plotted together as $\hat{\mathbf{h}}^n = \left[\hat{h}(m-M,n) \quad \cdots \quad \hat{h}(m-1,n) \right]$. This plot is taken in a system with 40 active users and a bit energy to noise ratio Eb/No=20 dB. It can be easily seen that the predicted value follow the variation of the original channel data very well. Thus, this channel predictor can track the channel variation so that the detector can achieve a reasonable BER performance.

The proposed WP based multicarrier CDMA system has been compared with the DFT based system for the synchronous transmission case. Since the length of the channel is set to be ¼ of one symbol duration, in the DFT based system the data rate is 80% of the original data rate due to the cyclic prefix. The same BCH coding has been used to compare these two systems with the same data rate. The DFT based system uses the same channel prediction method as the WP based system for a fair comparison.

Figure 5.19 gives the performance comparison of the WP based system and the DFT based system. In the coded case, the WP based system still clearly outperforms the DFT based system. For asynchronous transmission case the improvement of the WP based system over the DFT based system is expected to be more significant, as we have seen in the time-invariant channel cases.

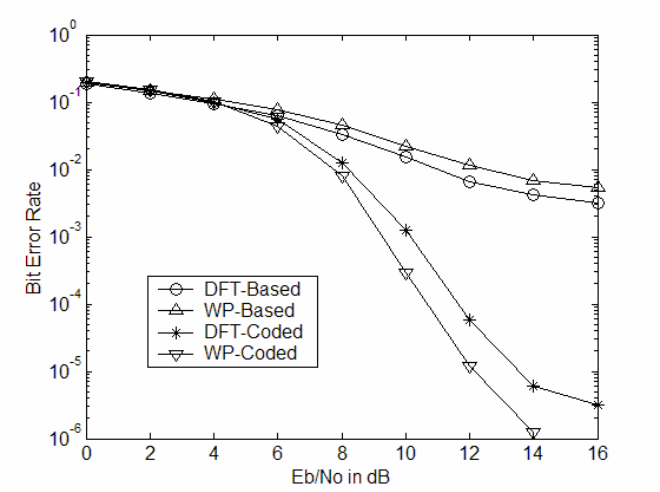

Figure 5.19 Performance Comparison for Time-Varying Channels, 30 active users

6. Wavelet Packet Domain Detection for The WP-MC-CDMA System

In the previous section the wavelet packet based multicarrier CDMA system has been introduced along with a time domain detection algorithm. This algorithm utilizes the time localization property of the wavelet packets and uses a RAKE combining structure to combine signals coming from different paths. In this section we will introduce a different wavelet packet domain detection algorithm for the synchronous WP-MC-CDMA system. This algorithm is based on wavelet packet domain signal processing. It also incorporates wavelet packet channel modeling discussed in Section 4 and channel prediction so that it can be used in a time-varying channel environment. The channel tracking/prediction and the signal detection are all done in the wavelet packet domain. The time and frequency localization properties of wavelet packets are utilized in a way different from the time domain detection. The performance of this detection algorithm has been proved effective by computer simulation. Lower bit error rate has been achieved than the FFT based MC-CDMA system with the same data rate for field measured time-varying channels. Also, the wavelet packet domain detection algorithm achieves more consistent performance than the time domain detection in more disperse channel conditions such as the 10-path NLOS channel. But a more important advantage of this algorithm is its low computational complexity, which will be discussed in the later part of this section.

The motivation of developing such a wavelet packet domain detection algorithm is briefly discussed in Section 6.1. Section 6.2 illustrates the system and channel model. The wavelet packet domain detection algorithm and performance analysis are presented in Sections 6.3 and 6.4, respectively. Simulation examples using field measured time-varying channels is given in Section 6.5 to validate the algorithm design and theoretical analysis.

6.1 Motivation for Wavelet Packet Domain Detection

As discussed before, wavelet packets have the property of both frequency and time localization, and they can approach the optimum time-frequency localization measure [41]. The utilization of this property in the wavelet packet based multicarrier CDMA systems has been investigated in the previous section, where a set of wavelet packets are used as the modulation waveforms in a multicarrier CDMA system. A time domain detection algorithm is designed to achieve time domain diversity by combining

multipath signals within one symbol (chip) duration so that the need for cyclic prefix is eliminated in this WP-MC-DS-CDMA system. Better bit error rate performance is achieved by utilizing the saved cyclic prefix overhead and the use of error correction coding.

As shown in Section 2, the basic idea of MC-CDMA system is using simple frequency domain combining instead of time domain equalization. In many cases frequency domain processing algorithms require less computation than time domain algorithms. In the conventional frequency domain signal processing approach, both the signal and the system (the channel) are represented in the frequency domain by means of (discrete) Fourier transform. In the wavelet packet based MC-CDMA system the signal is modulated using wavelet packets, thus is conveniently represented in the wavelet packet domain. To fully utilize the advantages of wavelet packets, in this section we investigate the possibility of combining wavelet packet modeling of communications channels with the wavelet packet signal design, to achieve a receiver/detection algorithm whose processing is totally in the wavelet packet domain.

This new detection algorithm is based on the wavelet packet channel modeling described in Section 4, where the channel impulse response is represented using an orthonormal wavelet packet set. Since the signal and the channel are both represented in the wavelet packet domain, the detection process can be simplified so that the resulted detector has a comparable computational complexity with the FFT based MC-CDMA detectors. The analysis described here is based on the wavelet packets formed from a full binary tree for the sake of simplicity. The general case of optimal pruning of the wavelet packet tree is out of the scope of this work but the basic design is still valid.

For the time-varying channel condition, a simple channel prediction method is used in the channel estimation. An RLS algorithm that is the same as that used in the previous section is used to predict the upcoming channel coefficients in the wavelet packet domain, and the predicted channel coefficients are in turn used in the detection process. This channel prediction is also performed in the wavelet packet domain. A decision feedback algorithm is used to estimate or update the current channel coefficients, which again will be used to predict future channels. This scheme utilizes the time-frequency localization property of wavelets in a different way from what has been used in Section 5.

Since the detection algorithm is intended to work in the wavelet packet domain in a way similar to the MC-CDMA detection system working in the frequency domain, the proposed system therefore takes a similar structure to that of the MC-CDMA, rather than the MC-DS-CDMA of the previous section.

Similar to the modulation method described in the previous section, this modulation does not require cyclic prefix either. The thus saved bandwidth can be used again either to increase transmission rate or to incorporate coding to reduce bit error rate (BER). The only drawback is that this approach is suitable for synchronous transmission only. Extension to asynchronous transmission cannot be worked out at this time.

6.2 System and Channel Model

6.2.1. System and Signal Model

The proposed system is based on the MC-CDMA structure, but using wavelet packet waveforms rather than sinusoid waveforms in the multicarrier modulation. As shown in *Figure 6.1*, the input bit is spread using the *k*th user's spreading code $\mathbf{c}_k$, then serial to parallel converted. The Inverse Discrete Wavelet Packet Transform (IDWPT) block is used to modulate the spread chips to N subcarriers, which are generated using a full binary wavelet packet tree. The signal is to be transmitted through time-varying multipath channels plus AWGN noise.

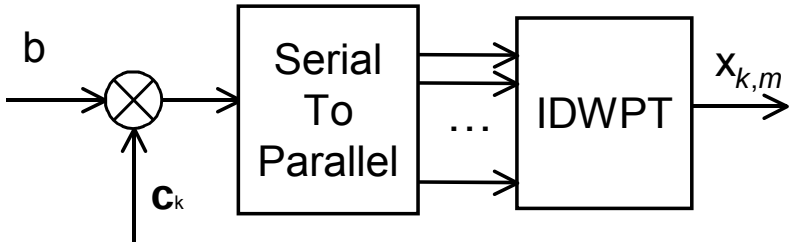

Figure 6.1 The baseband structure of the proposed system transmitter

The modulated signal $\mathbf{x}_{k,m}$ corresponding bit b_m of user k can be written as

$$\mathbf{x}_{k,m} = b_{k,m}\mathbf{W}_N\mathbf{c}_k \quad b_{k,m}\begin{bmatrix} s_{k,0} \\ s_{k,1} \\ \vdots \\ s_{k,N-1} \end{bmatrix}, \qquad b_{k,m} = \pm 1 \tag{6.1}$$

where $\mathbf{W}_N$ is the $N\times N$ orthogonal wavelet packet matrix defined in (4.4). $\mathbf{c}_k = \begin{bmatrix} c_{k,0} & \cdots & c_{k,N-1} \end{bmatrix}^T$ is the assigned spreading code for user k, which also has a length of N, as defined in (4.6). Since it is synchronous transmission, the multiuser signal is

$$\mathbf{x}_m = \sum_{k=1}^{K} b_{k,m} \mathbf{W}_N \mathbf{c}_k = \begin{bmatrix} x_0 \\ \vdots \\ x_{N-1} \end{bmatrix} \tag{6.2}$$

where K is the number of active users. Assuming that the channel delay spread L is much shorter than the symbol duration, i.e., $L<<N$, the received signal becomes

$$\mathbf{r}_m = \sum_{k=1}^{K} b_{k,m} \underbrace{\begin{bmatrix} s_{k,0} & & O \\ s_{k,1} & \ddots & \\ \vdots & \ddots & s_{k,0} \\ \vdots & & \vdots \\ s_{k,N-1} & \cdots & s_{k,N-L} \end{bmatrix}}_{N \times L} \begin{bmatrix} h_1 \\ h_2 \\ \vdots \\ h_L \end{bmatrix} + \mathbf{I}_{m-1} \square \sum_{k=1}^{K} b_{k,m} \mathbf{S}_k \mathbf{h} + \mathbf{I}_{m-1} \tag{6.3}$$

where $\mathbf{h}$ is the channel impulse response and $\mathbf{I}_{m-1}$ stands for the interference from the previous symbol b_{m-1}, which can be written as

$$\mathbf{I}_{m-1} = \sum_{k=1}^{K} b_{k,m-1} \underbrace{\begin{bmatrix} 0 & s_{k,N-1} & \cdots & s_{k,N-L} \\ & & \ddots & \vdots \\ & & & s_{k,N-1} \\ O & & & \mathbf{0} \end{bmatrix}}_{N \times L} \begin{bmatrix} h_1 \\ h_2 \\ \vdots \\ h_L \end{bmatrix} = \sum_{k=1}^{K} b_{k,m-1} \mathbf{S}_k^c \mathbf{h} \tag{6.4}$$

where $\mathbf{S}_k^c$ can be called the complementary matrix of $\mathbf{S}_k$.

6.2.2. Channel Modeling and Prediction

The time-invariant channel impulse response $\mathbf{h}$ can be modeled using a wavelet packet basis as [43]

$$\mathbf{h} = \sum_{i=0}^{L-1} g_i \mathbf{w}_i = \mathbf{W}_L \mathbf{g} \tag{6.5}$$

where $\mathbf{w}_i = \begin{bmatrix} w_{i,0} & \cdots & w_{i,L-1} \end{bmatrix}^T$ is the ith wavelet packet waveform, and the matrix $\mathbf{W}_L$ has the same form as $\mathbf{W}_N$ in (4.4) but is for length-L wavelet packets. This model is a discrete-time version of the model in (3.1). The wavelet packet domain channel coefficients $\mathbf{g}$ has a dimension of L. According to the wavelet packet properties, $\mathbf{g}$ can be calculated directly from $\mathbf{h}$ as

$$\mathbf{g} = \mathbf{W}_L{}^T \mathbf{h} \tag{6.6}$$

where $(\bullet)^T$ stands for matrix transposition.

In the later part of this section, the time-varying channel condition will also be considered, in which case the channel coefficients in the wavelet packet domain, **g**, becomes a function of time. The channel coefficients **g** at a specific time *m* can be written as a column vector $\mathbf{g}_m = [g(m,0), g(m,1), \ldots, g(m,L-1)]^T$. If a series of *M* snapshots of the channel are considered, then the channel can be represented as

$$\begin{aligned}\mathbf{G}_m &= \begin{bmatrix} g(m-M,0) & \cdots & g(m-1,0) \\ \vdots & \ddots & \vdots \\ g(m-M,L-1) & \cdots & g(m-1,L-1) \end{bmatrix} \\ &= \begin{bmatrix} \mathbf{g}_{m-M} & \cdots & \mathbf{g}_{m-1} \end{bmatrix} = \begin{bmatrix} \left(\mathbf{g}^0(m)\right)^T \\ \vdots \\ \left(\mathbf{g}^{L-1}(m)\right)^T \end{bmatrix}\end{aligned} \tag{6.7}$$

where the vectors $\mathbf{g}^n(m)$ represent the values of the same sample in the time-varying channel coefficients over *M* snapshots of the channel coefficients in the wavelet packet domain. One approach to predict the next channel coefficients $\mathbf{g}_m$ from $\mathbf{G}_m$ is using one predictor for each sample *n* in the channel coefficients so that

$$g(m,n) = \left(\mathbf{g}^n(m)\right)^T \mathbf{v}_n(m) \tag{6.8}$$

where the vector $\mathbf{v}_n(m)$ is the *n*th predictor at time *m*. This requires *L* predictors. For simplicity, here we use a common predictor for all samples in the channel coefficients. This is similar to that of Section 5, except now the modeling and prediction are done in the wavelet packet domain on wavelet packet channel coefficients. Thus, $\mathbf{g}_m$ is predicted from $\mathbf{G}_m$ using only one length *M* vector of weights $\mathbf{v}(m)$ as

$$\hat{\mathbf{g}}_m = \mathbf{G}_m \mathbf{v}(m) \tag{6.9}$$

The weight vector **v** is indexed by *m* since it is updated adaptively. The simulation results suggest that one predictor is enough to make a fairly accurate prediction for field measured fast time-varying channels. The mean square averaged error $\xi(m)$ (6.11) can be used as a minimization criterion for calculating **v**. In the time-varying channel case, an adaptive method is needed to track the time variation of the channel. As in the time domain detection algorithm described in Section 5, the Recursive Least Squares algorithm is used to update the weight vector **v**. But the input signal to this adaptive process is

the wavelet packet channel coefficients instead of the channel impulses themselves. In each step, the updating of the weight vector can be summarized as

$$\mathbf{k}(m) = \frac{\sum_{n=0}^{L-1} \mathbf{P}(m-1)\hat{\mathbf{g}}^n(m)}{\lambda + \sum_{n=0}^{L-1} \hat{\mathbf{g}}^n(m)\mathbf{P}(m-1)\hat{\mathbf{g}}^n(m)} \tag{6.10}$$

$$\xi(m) = \sum_{n=0}^{L-1} \left[\hat{g}(m,n) - \mathbf{v}^T(m-1)\hat{\mathbf{g}}^n(m) \right] \tag{6.11}$$

$$\mathbf{v}(m) = \mathbf{v}(m-1) + \mathbf{k}(m)\xi(m) \tag{6.12}$$

$$\mathbf{P}(m) = \lambda^{-1}\mathbf{P}(m-1) - \lambda^{-1} \sum_{n=0}^{L-1} \mathbf{k}(m)\left(\hat{\mathbf{g}}^n(m)\right)^T \mathbf{P}(m-1) \tag{6.13}$$

where the forgetting factor λ is a positive constant close to but less than *1*, $\mathbf{k}(m)$ and $\mathbf{P}(m)$ are the gain vector and inverse correlation matrix, respectively. The input to this predictor is the channel matrix $\mathbf{G}_m$. However, in practice the channel matrix is not directly available, and an estimated matrix $\hat{\mathbf{G}}_m$ is used instead. The estimation of the channel coefficients is based on the detected symbol values and will be discussed in the next section. At each step the detected symbol $\hat{b}_m$ is used to estimate $\mathbf{g}_m$. The estimated $\hat{\mathbf{g}}_m$ becomes part of $\hat{\mathbf{G}}_{m+1}$ for the prediction of $\mathbf{g}_{m+1}$. This predicted $\hat{\mathbf{g}}_{m+1}$ is then used to detect the next symbol b_{m+1} which is transmitted through $\mathbf{g}_{m+1}$. This proposed recursive scheme is shown in *Figure 6.2*.

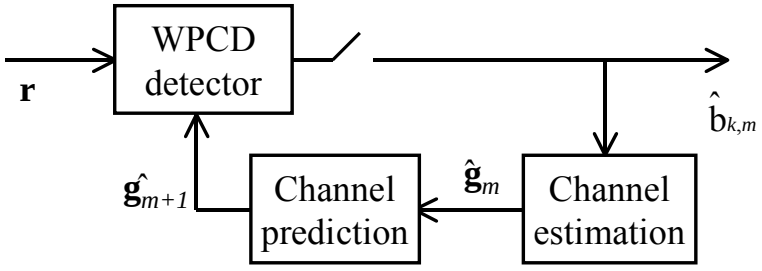

Figure 6.2 The WP combining detection receiver

In the initialization phase, the matrix **P** is initialized as an identity matrix multiplied by a small scalar, and the weight vector is initialized as a zero vector. A number of training symbols are used to obtain an initial set of estimated channel impulse responses and to train the predictor. After the initial training, the

predictor is then used online and updated adaptively using the transmitted information symbols without inserting any training symbols.

The accuracy of the wavelet packet domain channel prediction is in the same level as that of the time domain channel prediction, as will be shown in Section 6.5. However, since the detection algorithm derived in Section 6.3 is in the wavelet packet domain, it would require an extra wavelet packet transform if the channel prediction was done in the time domain. Therefore, the wavelet packet domain channel estimation and prediction is used for the sake of low computational complexity in the receiver design.

6.3 Wavelet Packet Domain Detection Algorithm

6.3.1 The Detection Algorithm

Without loss of generality, user 1 is assumed to be the desired user in the following. To take advantage of modeling the multipath channel using wavelet packet basis in the receiver design, we represent the row vector $\begin{bmatrix} s_{1,0} & 0 & \cdots & 0 \end{bmatrix}$ in (6.3) using the same channel modeling wavelet basis vectors as

$$\begin{bmatrix} s_{1,0} & 0 & \cdots & 0 \end{bmatrix} = \mathbf{f}_{1,0}\mathbf{W}_L^T \tag{6.14}$$

where the row vector $\mathbf{f}_{1,0}$ has a length of L. Other rows in the matrix $\mathbf{S}_1$ can also be represented in this way so that

$$\mathbf{S}_1 = \begin{bmatrix} s_{1,0} & & O \\ s_{1,1} & \ddots & \\ \vdots & \ddots & s_{1,0} \\ \vdots & & \vdots \\ s_{1,N-1} & \cdots & s_{1,N-L} \end{bmatrix} = \begin{bmatrix} \mathbf{f}_{1,0} \\ \mathbf{f}_{1,1} \\ \vdots \\ \mathbf{f}_{1,N-1} \end{bmatrix} \mathbf{W}_L^T \equiv \mathbf{F}_1\mathbf{W}_L^T \tag{6.15}$$

And the complementary matrix of $\mathbf{S}_1$ can be written as

$$\mathbf{S}_1^c = \begin{bmatrix} 0 & s_{k,N-1} & \cdots & s_{k,N-L} \\ & & \ddots & \vdots \\ & & & s_{k,N-1} \\ O & & & \mathbf{0} \end{bmatrix} = \begin{bmatrix} \mathbf{f}_{1,0}^c \\ \mathbf{f}_{1,1}^c \\ \vdots \\ \mathbf{f}_{1,N-1}^c \end{bmatrix} \mathbf{W}_L^T \equiv \mathbf{F}_1^c\mathbf{W}_L^T \tag{6.16}$$

Same representation can be applied to all other users, i.e., $\mathbf{S}_k = \mathbf{F}_k \mathbf{W}_L^T$ and $\mathbf{S}_k^c = \mathbf{F}_k^c \mathbf{W}_L^T$. The received signal without considering the AWGN noise can then be written as

$$\begin{aligned}
\mathbf{r}_m &= b_{1,m}\mathbf{S}_1\mathbf{h} + \sum_{k=2}^{K} b_{k,m}\mathbf{S}_k\mathbf{h} + \sum_{k=1}^{K} b_{k,m-1}\mathbf{S}_k^c\mathbf{h} \\
&= b_{1,m}\mathbf{F}_1\mathbf{W}_L^T\mathbf{W}_L\mathbf{g}_m + \sum_{k=2}^{K} b_{k,m}\mathbf{F}_k\mathbf{W}_L^T\mathbf{W}_L\mathbf{g}_m + \sum_{k=1}^{K} b_{k,m-1}\mathbf{F}_k^c\mathbf{W}_L^T\mathbf{W}_L\mathbf{g}_m \\
&= b_{1,m}\mathbf{F}_1\mathbf{g}_m + \sum_{k=2}^{K} b_{k,m}\mathbf{F}_k\mathbf{g}_m + \sum_{k=1}^{K} b_{k,m-1}\mathbf{F}_k^c\mathbf{g}_m \\
&= b_{1,m}\mathbf{F}_1\mathbf{g}_m + b_{1,m-1}\mathbf{F}_1^c\mathbf{g}_m + \sum_{k=2}^{K}\left(b_{k,m}\mathbf{F}_k + b_{k,m-1}\mathbf{F}_k^c\right)\mathbf{g}_m
\end{aligned} \tag{6.17}$$

The matrix $\mathbf{F}_1$ can be calculated beforehand, because $\mathbf{W}_N$, $\mathbf{c}_1$, and $\mathbf{W}_L$ are known. If the channel coefficient vector $\mathbf{g}_m$ can be estimated by $\hat{\mathbf{g}}_m$, a direct combining can be used to detect the data bit. Specifically, combining the received signal using the known coefficient vector $\mathbf{F}_1\hat{\mathbf{g}}_m$, and assuming $\hat{\mathbf{g}}_m \approx \mathbf{g}_m$, we have

$$\begin{aligned}
\hat{b}_{1,m} &= \mathbf{r}_m{}^H\mathbf{F}_1\hat{\mathbf{g}}_m \\
&= b_{1,m}\mathbf{g}_m^H\mathbf{F}_1^T\mathbf{F}_1\hat{\mathbf{g}}_m + b_{1,m-1}\mathbf{g}_m^H\mathbf{F}_1^{c,T}\mathbf{F}_1\hat{\mathbf{g}}_m + \sum_{k=2}^{K}\left(b_{k,m}\mathbf{g}_m^H\mathbf{F}_k^T + b_{k,m-1}\mathbf{g}_m^H\mathbf{F}_k^{c,T}\right)\mathbf{F}_1\hat{\mathbf{g}}_m \\
&\approx b_{1,m}\left\|\mathbf{F}_1\mathbf{g}_m\right\|^2 + b_{1,m-1}\mathbf{g}_m^H\mathbf{F}_1^{c,T}\mathbf{F}_1\mathbf{g}_m + \sum_{k=2}^{K}\left(b_{k,m}\mathbf{g}_m^H\mathbf{F}_k^T + b_{k,m-1}\mathbf{g}_m^H\mathbf{F}_k^{c,T}\right)\mathbf{F}_1\mathbf{g}_m
\end{aligned} \tag{6.18}$$

In (6.18), the second term represents the ISI and the third term (the sum) represents the MUI. Provided that $\left\|\mathbf{F}_1\mathbf{g}_m\right\|^2$ is large compared with the other two terms, the simple operation of (6.18) can then be used to detect the symbol $b_{1,m}$ with a small error probability. This operation can be called the wavelet packet domain combining. The error probability will be analyzed in the Performance Analysis subsection.

Based on (6.18), a simple channel estimator can be derived as

$$\hat{\mathbf{g}}_m = \frac{\hat{b}_{1,m}}{\left\|\mathbf{F}_1^T\mathbf{r}_m\right\|^2}\mathbf{F}_1^T\mathbf{r}_m \tag{6.19}$$

For the time-varying channel case, the receiver also needs a channel predictor since $\hat{\mathbf{g}}_m$ obtained from (6.19) can not be used in (6.18) for *m+1* to estimate $\hat{b}_{1,m+1}$, for which $\hat{\mathbf{g}}_{m+1}$ is needed. The RLS predictor of (6.10)-(6.13) and the recursive scheme of *Figure 6.2* are used to achieve the needed prediction and estimation.

Note that this approach applies to any orthogonal basis, including the Fourier basis. However, the interference terms in (6.18) depend highly on the correlation properties of the used basis. For the wavelet packet basis, this interference term is small due to the time-frequency localization property of wavelet packets. A detailed analysis is given in Section 6.4.

6.3.2 Computational Complexity

Since the receiver combines the demodulation and the despreading into a one-step process, it has a very low computational complexity. From (6.18) it can be easily seen that the wavelet packet domain detection algorithm needs to calculate the vector $\mathbf{F}_1\hat{\mathbf{g}}_m$ and the inner product of $\mathbf{F}_1\hat{\mathbf{g}}_m$ and $\mathbf{r}_m$. The vectors have a length of N, so the algorithm requires only $2N\times(L+2)$ real multiplications. The channel estimation (6.19) requires $N\times L$ multiplications. The channel predictor using the RLS algorithm requires $O(M^2)$ multiplications [54], where M is the length of the predictor.

The computational complexity of the time domain RAKE combining detection algorithm described in Section 5 depends on the complexity of DWPT. Typically it will require $2NL_fL_c$ to $NL_fL_c\log_2 N$ complex multiplications depending on the wavelet packet tree structure [22], where L_f is the length of the quadrature mirror filter of the wavelet packets and L_c is the number of combined paths. For the DFT-based MC-CDMA system, the computational complexity depends on the FFT algorithm ($N\log_2 N$ complex multiplications) and frequency domain combining (N complex multiplications) algorithm and de-spreading process (N multiplications). It typically requires $4N\log_2 N + 4N + N$ multiplications.

	Computational complexity	N=64, L=16 L_f=4, L_c=4
WP combining	2N(L+2)	2304
Time domain RAKE combining	$2NL_fL_c$ to $NL_fL_c\log_2 N$	8192 to 24576
DFT-based system	$4N\log_2 N+5N$	1856

Table 6.1 Computational complexity comparison in number of flops

Table 6.1 lists the computational complexities of all three approaches. It is clear that the proposed algorithm with wavelet packet domain combining has a much lower computational complexity than the time domain RAKE combining algorithm, and comparable computational complexity with the DFT-based system.

6.4 Performance Evaluation

Assuming perfect channel estimation, the performance of the combining detector described in the previous section depends on the relative strengths of three terms in (6.18), the desired signal part $b_{1,m}\left\|\mathbf{F}_1\mathbf{g}_m\right\|^2$, the multiuser interference part $\sum_{k=2}^{K}\left(b_{k,m}\mathbf{g}_m^H\mathbf{F}_k^T+b_{k,m-1}\mathbf{g}_m^H\mathbf{F}_k^{c,T}\right)\mathbf{F}_1\mathbf{g}_m$ which is equivalent to $\sum_{k=2}^{K}\left(b_{k,m}\mathbf{h}_m^T\mathbf{S}_k^T+b_{k,m-1}\mathbf{h}_m^T\mathbf{S}_k^{c,T}\right)\mathbf{S}_1\mathbf{h}_m$, and the inter symbol interference part $b_{1,m-1}\mathbf{g}_m^H\mathbf{F}_1^{c,T}\mathbf{F}_1\mathbf{g}_m$. Without loss of generality, $b_{1,m}=1$ is assumed, but $b_{1,m-1}$ and $b_{k,m}$, $b_{k,m-1}$ for $k\neq 1$ are random with values +1 or –1.

6.4.1 Interference Matrix $\mathbf{S}_k^T\mathbf{S}_1$

The matrix $\mathbf{S}_k^T\mathbf{S}_1$ plays a key role in the multiuser interference part since $\mathbf{S}_k^{c,T}$ has much fewer non-zero elements than $\mathbf{S}_k^T$. Therefore, in the following, we first evaluate $\mathbf{S}_k^T\mathbf{S}_1$. We have,

$$\begin{aligned}\mathbf{S}_k &= \begin{bmatrix}\mathbf{W}_N\mathbf{c}_k & \mathbf{W}_N^{+1}\mathbf{c}_k & \cdots & \mathbf{W}_N^{+(L-1)}\mathbf{c}_k\end{bmatrix} \\ &= \begin{bmatrix}\mathbf{W}_N\mathbf{c}_k & \mathbf{J}\mathbf{W}_N\mathbf{c}_k & \cdots & \mathbf{J}^{L-1}\mathbf{W}_N\mathbf{c}_k\end{bmatrix} \\ &= \begin{bmatrix}\mathbf{I} & \mathbf{J} & \mathbf{J}^2 & \cdots & \mathbf{J}^{L-1}\end{bmatrix} \otimes \mathbf{W}_N\mathbf{c}_k\end{aligned} \tag{6.20}$$

where $\mathbf{W}_N^{+i}$ stands for the matrix from $\mathbf{W}_N$ with rows down-shifted by *i*, and

$$\mathbf{J}^i = \begin{bmatrix}\mathbf{0} & & & O \\ 1 & \ddots & & \\ & \ddots & \ddots & \\ O & & 1 & \mathbf{0}\end{bmatrix} \tag{6.21}$$

has '1's in the *i*th sub diagonal, and '0's elsewhere, $\otimes$ stands for block-by-block multiplication. Therefore,

$$\begin{aligned}\mathbf{S}_k^T\mathbf{S}_1 &= \mathbf{c}_k^T\mathbf{W}_N^T \otimes \begin{bmatrix}\mathbf{I} \\ \mathbf{J}^T \\ \mathbf{J}^{2T} \\ \vdots \\ \mathbf{J}^{L-1,T}\end{bmatrix}\begin{bmatrix}\mathbf{I} & \mathbf{J} & \mathbf{J}^2 & \cdots & \mathbf{J}^{L-1}\end{bmatrix} \otimes \mathbf{W}_N\mathbf{c}_1 \\ &= \mathbf{c}_k^T\mathbf{W}_N^T \otimes \begin{bmatrix}\mathbf{I} & \mathbf{J} & \mathbf{J}^2 & \cdots & \mathbf{J}^{L-1} \\ \mathbf{J}^T & \begin{bmatrix}\mathbf{I} & 0 \\ 0 & 0\end{bmatrix} & \begin{bmatrix}\mathbf{J} & 0 \\ 0 & 0\end{bmatrix} & \cdots & \\ \mathbf{J}^{2T} & \begin{bmatrix}\mathbf{J}^T & 0 \\ 0 & 0\end{bmatrix} & \begin{bmatrix}\mathbf{I} & O \\ O & O\end{bmatrix} & & \\ \vdots & & \vdots & \ddots & \\ \mathbf{J}^{L-1,T} & & & & \end{bmatrix} \otimes \mathbf{W}_N\mathbf{c}_1\end{aligned} \tag{6.22}$$

In the case of an ideal channel, i.e., $\mathbf{h} = \begin{bmatrix}1 & 0 & \cdots & 0\end{bmatrix}^T$, the interference term $\sum_{k=2}^{K} b_{k,m}\hat{\mathbf{h}}_m^H\mathbf{S}_k^T\mathbf{S}_1\hat{\mathbf{h}}_m$ is determined by only the entry (1,1) of the matrix $\mathbf{S}_k^T\mathbf{S}_1$, which is always zero since $\mathbf{c}_k^T\mathbf{W}_N^T\mathbf{I}\mathbf{W}_N\mathbf{c}_1 = 0$.

Therefore, the multiuser interference as well as the multipath interference does not exist. However, in case of an actual multipath channel, the interference exists and the matrix $\mathbf{S}_k^T\mathbf{S}_1$ will determine the interference level. From (6.22) it is seen that $\mathbf{S}_k^T\mathbf{S}_1$ is determined by truncated auto- and cross-correlations of the basis functions. Therefore, orthogonality and time localization are the keys for good performance, whereas frequency localization is the key for the multicarrier operation. In other words, orthogonality as well as time and frequency localization properties of the basis functions is the key for this algorithm to work well for MC-CDMA signals.

		Diagonal	Off diagonal
WP basis	$\mathbf{S}_1^T\mathbf{S}_1$	54.36	3.61
	$\mathbf{S}_k^T\mathbf{S}_1$	0.48	1.85
Sinusoid basis, without pulse shaping	$\mathbf{S}_1^T\mathbf{S}_1$	52.96	2.69
	$\mathbf{S}_k^T\mathbf{S}_1$	2.20	2.93
Sinusoid basis, with pulse shaping	$\mathbf{S}_1^T\mathbf{S}_1$	57.13	4.25
	$\mathbf{S}_k^T\mathbf{S}_1$	1.96	3.41

Table 6.2 Mean values of the matrices $\mathbf{S}_k^T\mathbf{S}_1$ ***and*** $\mathbf{S}_1^T\mathbf{S}_1$

The matrices $\mathbf{S}_k^T\mathbf{S}_1$ for different '*k*'s have been evaluated by numerical method to determine the relative strengths of the desired signal and the interference. They have been calculated for Walsh code and Daubechies 10 wavelet packets. *Table 6.2* summarizes the relative average (mean) values of the matrix $\mathbf{S}_1^T\mathbf{S}_1$ corresponding to the desired signal, averaged over all *k* for 40 users, and of the matrices $\mathbf{S}_k^T\mathbf{S}_1$ corresponding to the interference term. This numerical evaluation has also been done for sinusoid basis, with and without pulse shaping. In the pulse shaping case, a raised cosine pulse shaping with α=1 is used. It can be seen clearly that for the wavelet packet based system, the largest elements of the matrix $\mathbf{S}_1^T\mathbf{S}_1$ are mostly in the main diagonal, which correspond to the useful signal. This explains the effectiveness of the proposed detection algorithm. For the matrix $\mathbf{S}_k^T\mathbf{S}_1$, which corresponds to the multiuser interference, both the off-diagonal elements and the diagonal elements are much smaller than the diagonal elements of $\mathbf{S}_1^T\mathbf{S}_1$. When the wavelet packet basis is replaced by the sinusoid basis, regardless of pulse-shaped or not, the mean diagonal and off-diagonal elements in the interference matrix $\mathbf{S}_k^T\mathbf{S}_1$ become larger. Due to usually a large number of users, the mean quantities determine the

interference level. Therefore, the interference level is decreased by using wavelet packet basis functions in the multicarrier modulation, which results in a lower bit error rate as can be seen in the simulations.

		Mean, LOS	variance σ^2, LOS	Mean, NLOS	variance σ^2, NLOS
WP basis	r_s	1	-	1	-
	r_i	0	0.072	0	0.077
Sinusoid basis, without pulse shaping	r_s	1	-	1	-
	r_i	0	0.2435	0	0.2844
Sinusoid basis, with pulse shaping (α=1)	r_s	1	-	1	-
	r_i	0	0.3042	0	0.3061

Table 6.3 Summary of the normalized interference term r_i

Table 6.3 gives the numerical values of the normalized interference term

$$r_i = \frac{b_{1,m-1}\mathbf{g}_m^H \mathbf{F}_1^{c,T}\mathbf{F}_1\mathbf{g}_m + \sum_{k=2}^{K}\left(b_{k,m}\mathbf{g}_m^H\mathbf{F}_k^T + b_{k,m-1}\mathbf{g}_m^H\mathbf{F}_k^{c,T}\right)\mathbf{F}_1\mathbf{g}_m}{\mathbf{g}_m^H\mathbf{F}_1^T\mathbf{F}_1\mathbf{g}_m} \tag{6.23}$$

The normalization is against $b_{1,m}\left\|\mathbf{F}_1\mathbf{g}_m\right\|^2$, denoted as r_s which has a normalized value of 1. In the evaluation of these two terms, 40,000 randomly generated 5-path Line-of-Sight (LOS) and Non-Line-of-Sight (NLOS) channels are used. The interference term r_i for wavelet packet basis functions has a much smaller variance (defined as σ^2) than the sinusoid basis functions as can be seen in this table. This is due to the smaller mean values of matrix $\mathbf{S}_k^T\mathbf{S}_1$ and the off diagonal elements of matrix $\mathbf{S}_1^T\mathbf{S}_1$ in *Table 6.2*. The interference term defined in (6.23) is actually the combination of the elements of matrix $\mathbf{S}_k^T\mathbf{S}_1$ and the off diagonal elements of $\mathbf{S}_1^T\mathbf{S}_1$, weighted by random channel coefficients.

6.4.2 Probability Density Function of The Decision Variable

The channel coefficient vector **g** is the orthogonal transform of the channel impulse response vector **h**. Therefore, all the individual items in **g** are Gaussian random variables. The quardrature analysis method used in Section 5 is still valid. The received signal in (6.17) plus AWGN is

$$\mathbf{r}_m = \sum_{k=1}^{K} b_{k,m}\mathbf{F}_k\mathbf{g}_m + \sum_{k=1}^{K} b_{k,m-1}\mathbf{F}_k^c\mathbf{g}_m + \mathbf{n}_m \tag{6.24}$$

where $\mathbf{n}_m = [n_m(0), n_m(1), \cdots, n_m(N-1)]^T$ denotes the additive white Gaussian noise at the *m*th symbol block. Assuming perfect channel estimation, i.e., $\hat{\mathbf{g}}_m = \mathbf{g}_m$, the decision variable, denoted as z, is therefore

$$z = \mathbf{r}_m{}^H\mathbf{F}_1\mathbf{g}_m = \sum_{k=1}^{K}\left(b_{k,m}\mathbf{g}_m^H\mathbf{F}_k^T + b_{k,m-1}\mathbf{g}_m^H\mathbf{F}_k^{c,T}\right)\mathbf{F}_1\mathbf{g}_m + \mathbf{g}_m^H\mathbf{F}_1^T\mathbf{n}_m \tag{6.25}$$

z is in general complex. Its real part is used to make the bit decisions. The Hermitian form of Re{z} is

$$\begin{aligned}\mathrm{Re}\{z\} &= \mathbf{g}_m^H\mathbf{Q}_0\mathbf{g}_m + \frac{1}{2}\left(\mathbf{g}_m^H\mathbf{F}_1^T\mathbf{n}_m + \mathbf{n}_m^H\mathbf{F}_1\mathbf{g}_m\right) = \begin{bmatrix}\mathbf{g}_m^H & \mathbf{v}_m^H\end{bmatrix}\begin{bmatrix}\mathbf{Q}_0 & \frac{1}{2}\mathbf{I}\\ \frac{1}{2}\mathbf{I} & O\end{bmatrix}\begin{bmatrix}\mathbf{g}_m\\ \mathbf{v}_m\end{bmatrix} \\ &= \mathbf{g}^H\mathbf{Q}\mathbf{g}\end{aligned} \tag{6.26}$$

where $\mathbf{g} = [\mathbf{g}_m^T \quad \mathbf{v}_m^T]^T$ is the extended channel coefficient vector, $\mathbf{v}_m = \mathbf{F}_1^T\mathbf{n}_m$ is the transformed noise vector, and

$$\mathbf{Q}_0 = \frac{1}{2}\sum_{k=1}^{K}\left(b_{k,m}\mathbf{F}_k^T + b_{k,m-1}\mathbf{F}_k^{c,T}\right)\mathbf{F}_1 + \frac{1}{2}\sum_{k=1}^{K}\mathbf{F}_1^T\left(b_{k,m}\mathbf{F}_k + b_{k,m-1}\mathbf{F}_k^c\right) \tag{6.27}$$

The probability density function of Re{z} can be obtained following the analysis process from (5.30)-(5.35) in Section 5, only with different matrices **V** and $\mathbf{Q}_0$. In particular, $\mathbf{Q}_0$ is given in (6.27) and **V** is given by

$$\mathbf{V} = E\left[(\mathbf{g}-\bar{\mathbf{g}})(\mathbf{g}-\bar{\mathbf{g}})^H\right] = \begin{bmatrix} \mathbf{V}_n & O \\ O & \sigma_1^2 \mathbf{F}_1^T \mathbf{F}_1 \end{bmatrix} \tag{6.28}$$

Since the channel coefficient vector $\mathbf{g}_m$ is the orthogonal transform of the channel impulse response vector $\mathbf{h}_m$, its entries are still identically distributed Gaussian random variables. Therefore, its covariance matrix of $\mathbf{V}_n$ is an identity matrix multiplied by the channel variance σ_0^2. Thus,

$$\mathbf{V} = \begin{bmatrix} \sigma_0^2 \mathbf{I} & O \\ O & \sigma_1^2 \mathbf{F}_1^T \mathbf{F}_1 \end{bmatrix} \tag{6.29}$$

so that

$$\mathbf{VQ} = \begin{bmatrix} \sigma_0^2 \mathbf{I} & O \\ O & \sigma_1^2 \mathbf{F}_1^T \mathbf{F}_1 \end{bmatrix} \begin{bmatrix} \mathbf{Q}_0 & \frac{1}{2}\mathbf{I} \\ \frac{1}{2}\mathbf{I} & O \end{bmatrix} = \begin{bmatrix} \sigma_0^2 \mathbf{Q}_0 & \frac{\sigma_0^2}{2}\mathbf{I} \\ \frac{\sigma_1^2}{2}\mathbf{F}_1^T \mathbf{F}_1 & O \end{bmatrix} \tag{6.30}$$

With the above VQ matrix, all computation thereafter would be identical to those of (5.30)-(5.35). *Figure 6.3* gives a plot of $p(z)$ for 5-path NLOS channel when AWGN is not included in the calculation. In comparison, the figure also gives a plot of $p(z)$ when sinusoid waveforms (without pulse shaping) are used instead of wavelet packets. It can be seen clearly from the figure that the wavelet packets result in a much smaller variance than sinusoid waveforms, indicating that the WP based system experiences a lower interference level than the DFT based system. This confirms the results in Tables 6.2 and 6.3. The bit error rate calculated based on above analysis will be compared with the simulation results in the next section.

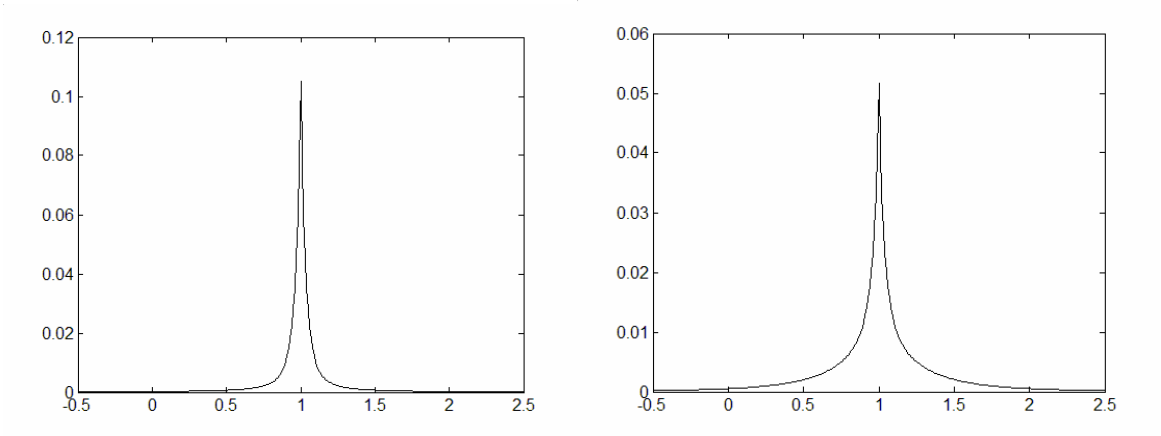

(a) WP waveforms ***(b) sinusoid waveforms***

Figure 6.3 pdf of decision variable z, 5 path NLOS Channel

6.5 Simulation Results and Discussion

The performance of this receiver design has been evaluated by simulation against both time-invariant and field measured time-varying channels. In the simulation, the number of subcarriers is set to 64. Daubechies 8 wavelet filter is used to form the wavelet packet basis from a level-six wavelet packet tree. Length 64 Walsh codes are used as spreading codes. The number of users is set to 40. The fast time-varying channel data are the same as that used in Section 5. The bit error rate is calculated by running the simulation for 1,000,000 symbols. The delay spread of the channel is assumed within ¼ of the symbol length. The number of input channel snapshots *M* for the channel predictor is set to 8. The initial training takes 26 snapshots, and online updating of the weights lasts for 230 snapshots in our simulation but can be further continued with the same performance level.

6.5.1 Performance in Time-Invariant Channel Conditions

In *Figure 6.4*, the system performance of the newly proposed WP-based system with wavelet packet domain combining, the WP-based system with time domain RAKE combining, and the DFT-based system with cyclic prefix have been compared. The channel is a 5-path real LOS channel, with the strongest path contributing half the channel energy. Note that the wavelet packet domain detection algorithm slightly but consistently performs better than the time domain RAKE combining algorithm of the WP-based system. The main reason for this performance gain of the new receiver design is the full

utilization of the channel coefficients in the WP domain, whereas in the time domain RAKE combining algorithm only the strongest paths are combined to form the decision variable. Also note that although both WP-based systems perform not as well as the DFT-based system, they do not need cyclic prefix. Since the length of the channel is set to be ¼ of one symbol duration, in the DFT-based system the data rate is 80% of the original data rate due to the cyclic prefix. Therefore, the two WP systems have 25% higher date rate than the DFT-based system. It can also be seen that the simulation result is consistent with the analytical result obtained in the last section.

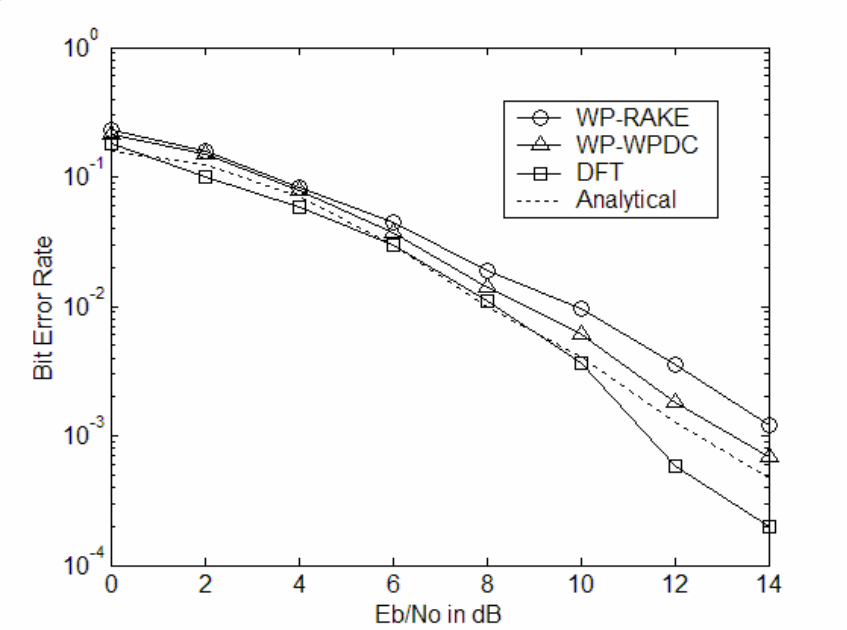

WP-RAKE = WP-based system with time domain RAKE combining

WP-WPDC = WP-based system with wavelet packet domain combining

DFT = DFT-based system with frequency domain combining

Figure 6.4 System performance for 5-path real LOS channel

Figure 6.5 gives the system performance for a 5-path real NLOS channel. In this case, the frequency domain combining receiver for DFT-based system and the wavelet packet domain combining algorithm for WP-based system perform similarly with those in *Figure 6.4*. However, the time domain RAKE combing algorithm performs slightly worse than in the LOS channel condition. This is because less

energy can be combined in the NLOS channel condition. The benefit of wavelet packet domain combining is clearer in this case.

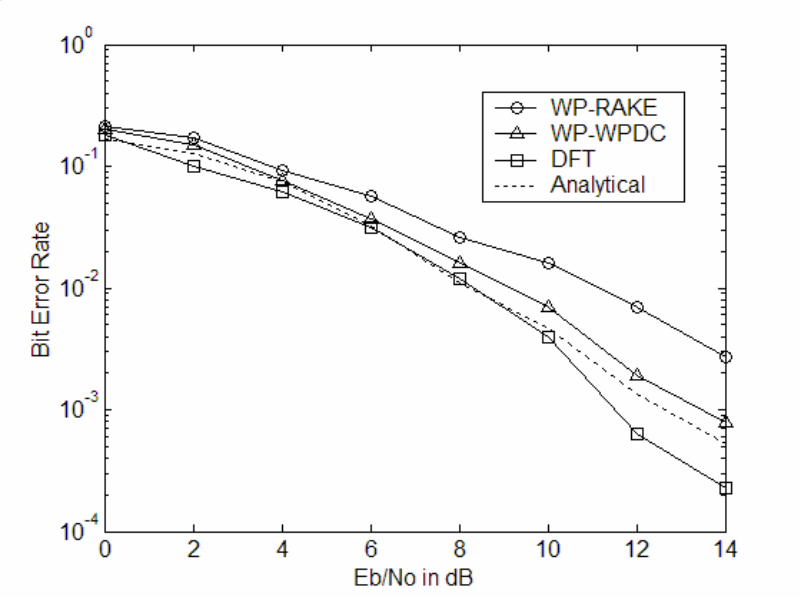

Figure 6.5 System performance for 5-path real NLOS channel

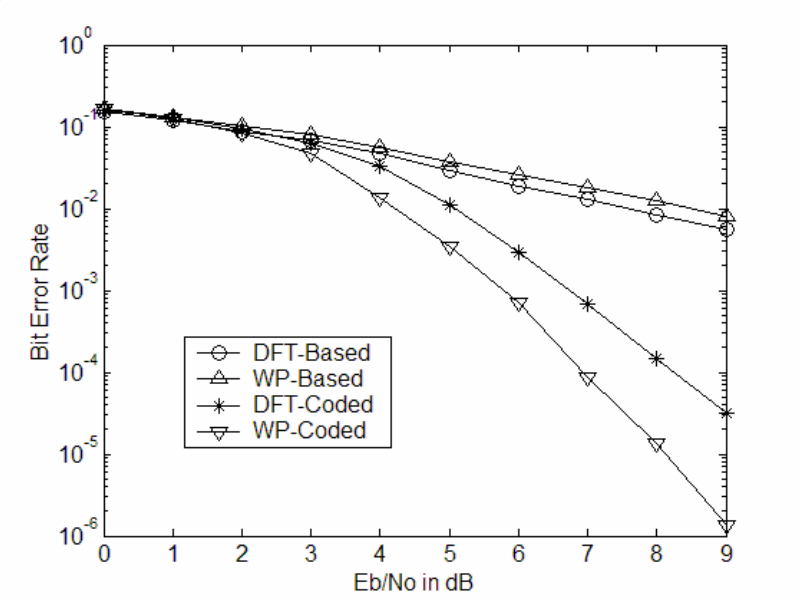

Figure 6.6 Performance comparison in 5-path real LOS channel condition

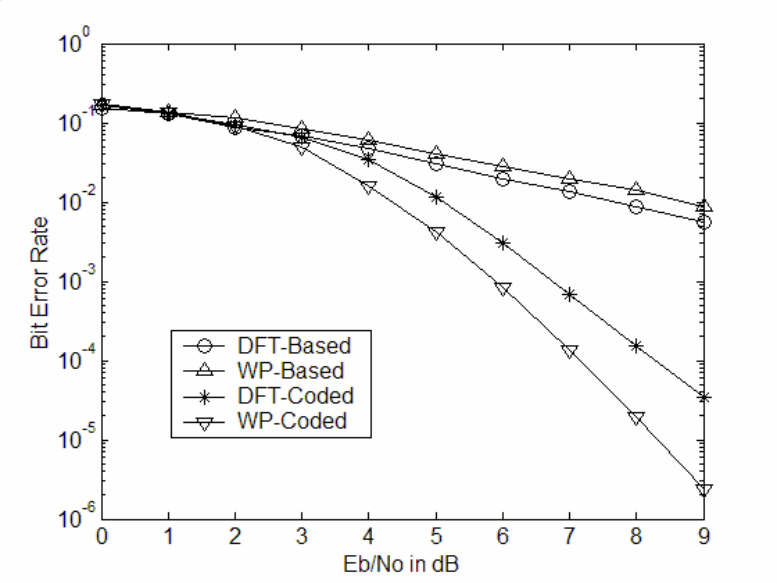

Figure 6.7 Performance comparison in 5-path real NLOS channel condition

To compare the performance of WP-based and DFT-based systems in a similar data rate, the BCH coding [54] used in the previous section is again used to the WP-based system. This coding achieves a decreased BER for the WP-based system accommodating the same data rate with that of DFT-based system. *Figures 6.6* and *6.7* give the performance comparison between the WP based system and the DFT based system for the case of *40* active users for 5-path LOS and 5-path NLOS channels, respectively. It can be seen that the coded WP based system achieves a much better BER performance than the coded DFT based system at the same data rate.

6.5.2 Performance in Time-Varying Channel Conditions

The system has also been evaluated in the time-vary channel condition. In this situation channel prediction has been used for all the compared systems. For the time domain RAKE combining and DFT-based systems, the channel predictor also uses 8 snapshots of channel impulse responses to predict the next snapshots. For the wavelet packet domain detection algorithm of WP-based system, the wavelet packet domain channel prediction method described in Section 6.2 is used.

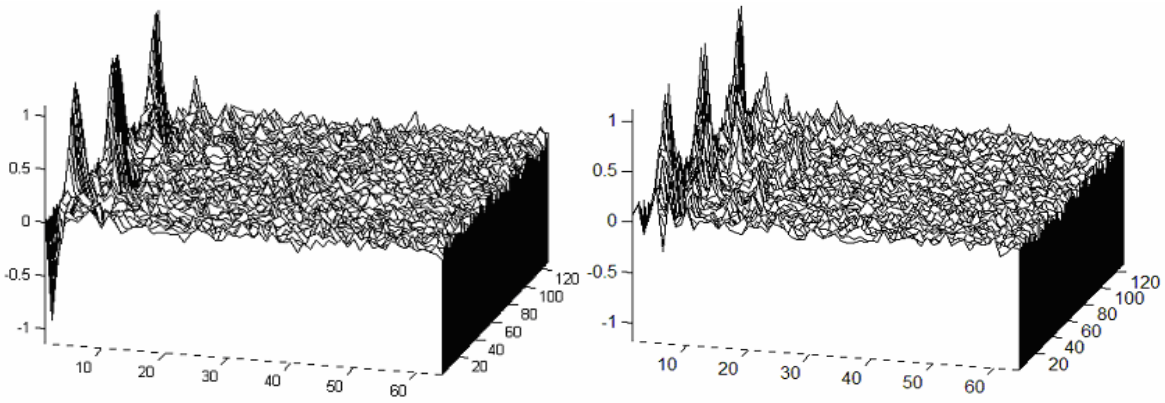

(a) real part of the channel ***(b) imaginary part of the channel***

Figure 6.8 A field measured time-varying channel, 128 snap-shots of impulse responses of length 64

Figure 6.8 gives an example complex baseband time-varying channel from the field measured channel data. The channel plotted in this figure can be effectively predicted and tracked using the method described in Section 6.2. *Figure 6.9* gives a plot of the predicted channel impulse response (the real part) in comparison with the original channel impulse response. The solid line stands for the original channel, and the circles stand for the predicted channel. Note that although the prediction is done in the wavelet packet domain, the given plot is in the time domain, i.e., given by channel impulse responses. It can be seen that the predicted channel well resembles the original one, similar to the time domain channel prediction algorithm used in the previous section. The mean square error of the channel prediction is at the level of 5%.

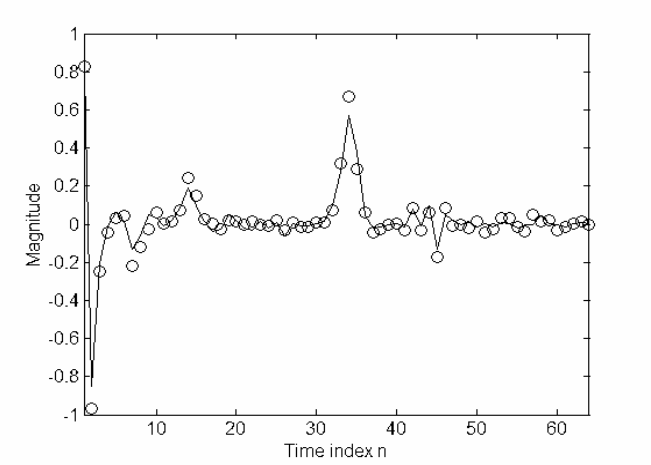

Figure 6.9 Channel prediction performance for one snapshot of the real part, Eb/No=20 dB, training=26 steps, L=64, M=8, m=40

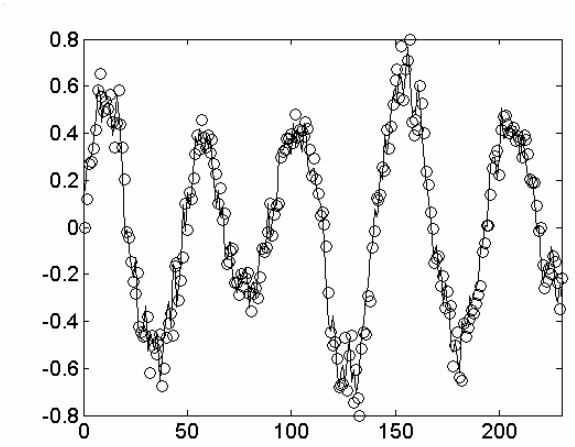

Figure 6.10 Channel tracking performance for one sample in channel impulse response, the real part

Figure 6.10 gives a plot showing the tracking property of the channel predictor. In this figure the values of a specific sample in a series of snapshots of the real part of the channel are taken out and plotted against time as $\hat{\mathbf{h}}^n = \left[\hat{h}(m-M,n) \quad \cdots \quad \hat{h}(m-1,n)\right]$. This plot gives the result obtained by the algorithm described in Section 6.2 in a system with 30 active users and a bit energy to noise ratio Eb/No=20 dB. As in the previous figure, the solid line stands for the original channel and the circles stand for the

predicted channel. It can be easily seen that the predicted channel follows the variation of the original channel very well.

The performance comparison of different systems on the above measured baseband complex channel is shown in *Figure 6.11*. Again, it can be seen that the coded WP-based system performs better than the coded DFT-based system, with both systems working at the same data rate.

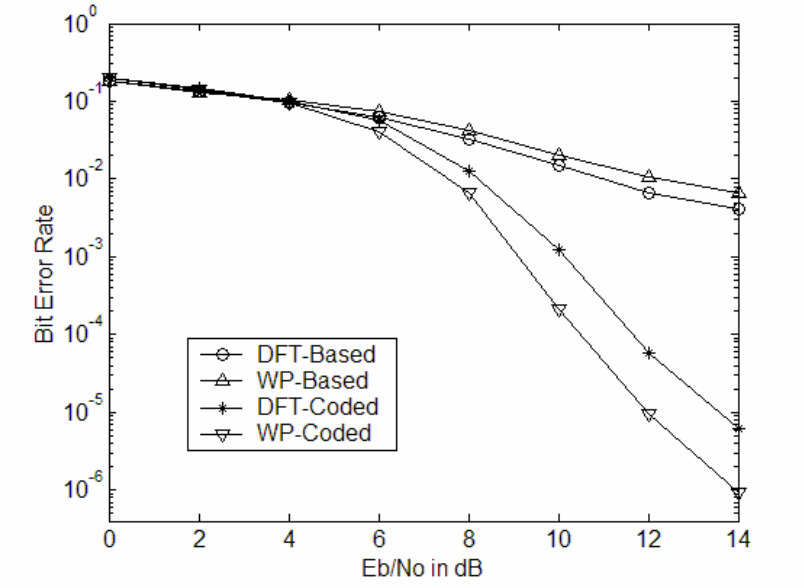

Figure 6.11 System performance for measured complex time-varying baseband channel

7. Conclusions

In this work we first developed a wavelet packet based doubly orthogonal signature waveform design for DS-CDMA communications. This new waveform design achieves better correlation properties than wavelet packets themselves. It combines the orthogonality of both Walsh code and wavelet packets. In this signature waveform design a number of shorter wavelet packets are cascaded to form a longer waveform. Therefore, by implementing fast wavelet packet transform of a shorter length it reduces the computational complexity of the receiver.

We have also developed system designs for wavelet packet based multicarrier CDMA communications. In this system design a set of wavelet packets are used as the modulation waveforms in a multicarrier CDMA system. The need for cyclic prefix is eliminated in the system design due to the good orthogonality and time-frequency localization properties of the wavelet packets. The received signals are combined in either the time domain or the wavelet packet domain to combat multipath interferences. Better bit error rate performance is achieved by utilizing the saved cyclic prefix overhead for error correction coding.

In the time domain detection algorithm, the orthogonality and time-frequency localization properties of wavelet packets are used to achieve time diversity by means of a RAKE combiner. In this wavelet packet based multicarrier CDMA system design, the channel delay spread is shorter than the chip duration. Thus the RAKE combining is working within one chip duration. This is different from that in the conventional CDMA receiver, where multipath signal with relative delay shorter than a chip duration can not be resolved.

For a system using wavelets or wavelet packets as modulation waveforms, it is desirable to have the communications channel represented in the same domain as that of the signal, for example, the wavelet packet domain. As the first attempt in this direction, a wavelet packet based time-varying channel model has been developed in Section 3. This channel model converts the time-varying channel impulse responses to a set of wavelet packet coefficients. These coefficients exactly represent the channel and have been used to develop a novel wavelet packet domain detection algorithm presented in Section 6. This new detection algorithm achieved a very low computational complexity since all the signal processing is done in a single wavelet packet domain.

For the time-varying channel condition, a channel prediction/estimation method is used in both the time domain RAKE receiver and the wavelet packet domain direct detection. An RLS algorithm is used to predict the upcoming channel coefficients, either directly in the time domain or in the wavelet packet domain. Simulation examples using statistical and field measured time-varying channels validate the theoretical analysis of the new channel model, the time domain detection algorithm, and the wavelet packet domain detection algorithm.

8. Publications Resulted From This Work

The following publications are resulted from this contract work:

[1] H. Zhang and H. Fan, "An indoor wireless channel model based on wavelet packets," *Proc. 34th Asilomar Conference on Signals, Systems, and Computers*, Pacific Grove, CA, Oct. 2000, pp.455-459.

[2] H. Zhang, H. Fan, and A. Lindsey, "A wavelet packet based model for time-varying wireless communication channels," *Proc. 3rd IEEE Signal Processing Workshop on Signal Processing Advances in Wireless Communications (SPAWC'01)*, Taiwan, March 2001, pp. 50-53.

[3] H. Zhang, H. Fan, and A. Lindsey, "Doubly orthogonal wavelet packets for CD-CDMA communication," *Proc. IEEE Statistical Signal Processing Workshop,* Singapore, Aug. 2001.

[4] H. Zhang, H. Fan, and A. Lindsey, "Over-loaded CD-CDMA system waveform design using doubly orthogonal wavelet packets," *Proc. IEEE Fall Vehicular Technology Conference,* Atlantic City, NJ, Oct. 2001.

[5] Hongbing Zhang, H. Howard Fan, and Alan Lindsey, "Wavelet packet waveforms for multicarrier CDMA communications," *Proc. of IEEE ICASSP 2002,* FL, USA, Vol. 3, pp. 2557-2560.

[6] Hongbing Zhang, H. Howard Fan, and Alan Lindsey, "Receiver design for wavelet based multicarrier CDMA communications," *IEEE Trans. on Vehicular Technology*, accepted for publication.

[7] Hongbing Zhang, H. Howard Fan, and Alan Lindsey, "Efficient Detection of WP-MC-CDMA Signals Using Wavelet Packet Time-Varying Channel Modeling and Prediction," submitted to *IEEE Trans. on Communications.*

9. References

[1] Shinsuke Hara and Ramjee Prasad, "Overview of multicarrier CDMA," *IEEE communication Magazine*, Vol. 35, no. 12, Dec. 1997, pp. 126-133.

[2] N. Yee, J-P. Linnrtz and G. Fettweis, "Multicarrier CDMA in indoor wireless radio networks," *Proc. of IEEE PIMRC'93*, Yokohama, Japan, Sept. 1993, pp. 109-113.

[3] K.Fazel and L. Papke, "On the performance of convolutionally-coded CDMA/OFDM for mobile communication system," *Proc. of IEEE PIMRC'93*, Yokohama, Japan, Sept. 1993, pp. 468-472.

[4] A. Chouly, A. Brajal, and S. Jourdan, "Orthogonal multicarrier techniques applied to direct sequence spread spectrum CDMA systems," *Proc. of IEEE GLOBECOM'93*, Houston, USA, Nov. 1993, pp. 1723-28.

[5] L. Vandendorpe, "Multitone spread spectrum multiple access communications system in a multipath Rician fading channel," *Proc. of IEEE ICC'94*, pp. 1638-1642.

[6] V. M. DaSilva and E. S. Sousa, "Performance of Orthogonal CDMA codes for quasi-synchronous communication systems," *Proc. of IEEE ICUPC'93*, Ottawa, Canada, Oct. 1993, pp. 995-999.

[7] Essam A. Sourour and Masao Nakagawa, "Performance of orthogonal multicarrier CDMA in a multipath fading channel," *IEEE Transactions on Communications*, vol. 44, no. 3, March 1996, pp. 356-367.

[8] Shiro Kondo and Laurence B. Milstein, "Performance of multicarrier DS CDMA systems," *IEEE Transactions on Communications*, vol. 44, no. 2, Feb. 1996, pp. 238-246.

[9] Richard Van Nee and Ramjee Prasad, *OFDM for Wireless Multimedia Communications*. Artech House, 2000.

[10] Helmut Bolcskei, Pierre Duhamel, and Rima Hleiss, "A subspace-based approach to blind channel identification in pulse shaping OFDM/OQAM systems," *IEEE Transactions on Signal Processing*, vol. 49, no. 7, July 2001, pp. 1594-1598.

[11] Chengyang Li and Sumit Roy, "Subspace based detection in MC-CDMA over dispersive channel," *Proc. of IEEE ICPWC2000*, pp. 98-103.

[12] Xiaojun Wu, Qinye Yin, Hanguo Zhang, and Ke Deng, "Time-domain multiuser detection for MC-CDMA systems without cyclic prefix," *Proc. of IEEE ICC2002*, pp. 921-925.

[13] Scott L. Miller and Bradley J. Rainbolt, "MMSE detection of multicarrier CDMA," *IEEE Journal on Selected Areas in Communications*, vol. 18, no. 11, Nov. 2000, pp. 2356-2362.

[14] D. N. Kalofonos, M. Stojanovic, and J. G. Proakis, "On the performance of adaptive MMSE detectors for a MC-CDMA system in fast fading Rayleigh channels," *Proc. of the ninth IEEE International Symposium on Indoor and Mobile Radio Communications*, 1998, vol. 3, pp. 1309-1313.

[15] Jean-Paul M. G. Linnartz, "Performance analysis of synchronous MC-CDMA in mobile Rayleigh channel with both delay and Doppler spreads," *IEEE Transactions on Vehicular Technology*, vol. 50, no. 6, Nov. 2001, pp. 1375-1387.

[16] J. A. Bingham, "Multicarrier modulation for data transmission: An idea whose time has come," *IEEE Communication Magzine*, May 1990, pp. 5-14.

[17] Stefan Kaiser, "On the performance of different detection techniques for OFDM-CDMA in fading channels," *Proc. of IEEE GLOBECOM'95*, Vol. 3, pp. 2059-2063.

[18] D. N. Kalofonos and J. G. Proakis, "Performance of the multi-stage detector for a MC-CDMA system in a Rayleigh fading channel," *Proc. of IEEE GLOBECOM'96*. vol. 3 pp. 1784-1788.

[19] Peter Jung *et al*, "Performance of multicarrier joint detection CDMA mobile communications systems," Proc. of IEEE VTC'97, vol. 3 pp. 1892-1896.

[20] Yi Sun and Lang Tong, "Channel equalization using one-tap DFE for wireless OFDM systems with ICI and ISI," *Proc. of IEEE SPAWC'99*, Annapolis, USA, May 1999, pp. 146-149.

[21] Stefan Kaiser and W. A. Krzymien, "Asynchronous spread spectrum multi-carrier multiple access systems with pilot symbol aided channel estimation," *Proc. of IEEE VTC'99*, Vol. 5, pp. 2701-2705.

[22] Stephane Mallat, *A Wavelet Tour of Signal Processing*, Academic Press, Massachusetts, 1997.

[23] Kenneth Hetling *et al*, "A PR-QMF (wavelet) based spread spectrum communications system," *Proc. of MILCOM'94*, vol. 3, pp. 760-764.

[24] Rachel E. Learned, Alan S. Willsky, and Don M. Boroson, "Low complexity optimal joint detection for oversaturated multiple access communications," *IEEE Trans. on Signal Processing*, vol. 45, no. 1, January 1997, pp113-123.

[25] Kon Max Wong, Jiangfeng Wu, Tim N. Davidson, and Qu Jin, "Wavelet packet division multiplexing and wavelet packet design under timing error effects," *IEEE trans. on Signal Processing*, vol. 45, no. 12, Dec. 1997, pp. 2877-2890.

[26] Weimin Yang, Guangguo Bi and T-S P. Yum, "A multirate wireless transmission system using wavelet packet modulation," *Proc. of VTC'97*, vol. 1, pp. 368-372.

[27] Andre Quinquis and David Boulinguez, "Multipath channel identification with WP," *IEEE Journal of Oceanic Engineering*, vol. 22, no. 2, April 1997, pp. 342-345.

[28] Fred Daneshgaran, M. Mondin and F. Davis, "Shaping the power spectrum of TCM codes using wavelet packet modulation," *Electronics Letters*, vol. 39-17, 1999, pp. 1459-61.

[29] H. Newlin, "Developments in the use of wavelets in communication systems," *Proc. of IEEE MILCOM'98*, Boston, USA, vol. 1, pp. 343-349.

[30] Gregory W. Wornell, "Emerging applications of multirate signal processing and wavelets in digital communications," *Proceedings of the IEEE*, vol. 84, no. 4, April 1996, pp. 586-603.

[31] Alan R. Lindsey, "Wavelet packet modulation for orthogonally multiplexed communications," *IEEE Trans. on Signal Processing*, vol. 45, no. 5, May 1997, pp.1336-1339.

[32] Kenneth Hetling, Gary Saulnier and Pankaj Das, "Spreading codes for wireless spread spectrum communications," *Proceedings of IEEE ICC'96*, vol. 1, pp 68-72.

[33] S. Gracias and V.U. Reddy, "An equalization algorithm for wavelet packet based modulation schemes," *IEEE Trans. on Signal Processing*, vol. 46, no. 11, November 1998, pp. 3082-3087.

[34] A. B. Sesay et al, "Waveform division multiple-access," *IEE Proceddings-I*, vol. 140, no. 3, June 1993, pp. 176-184.

[35] Kyung Chang *et al*, "Performance analysis of wavelet-based MC-CDMA for FPLMTS/IMT-2000," *Proc. of IEEE 4th International Symposium on Spread Spectrum Techniques and Applications*, 1996, Vol. 3, pp. 1356-1360.

[36] A Muayyadi and MNA Abu-Rgheff, "Wavelet-based MC-CDMA cellular systems," *Proc. of IEEE 6th International Symposium on Spread Spectrum Techniques and Applications*, 2000, Vol. 1, pp. 145-149.

[37] A. S. Madhukumar et al, "Performance enhancement of a wavelet based multicarrier DS-CDMA system through multistage interference cancellation," *Proc. of 34th Asilomar Conference on Signals, Systems and Computers*, 2000, Pacific Grove, USA, Vol. 2, pp. 1421-25.

[38] Kon Max Wong *et al*, "Performance of wavelet packet division multiplexing in impulsive and Gaussian noise," *IEEE trans. on Communications*, vol. 48, no. 7, July 2000, pp. 1083-1086.

[39] Yifeng Zhang and Jeffrey Dill, "Comparison of equalization techniques in a wavelet packets based multicarrier modulation DS-CDMA system," *Proc. of IEEE GLOBECOM'99*, Vol. 4, pp. 2152-2156.

[40] Rong Wang, Shixin Cheng and Jibo Wei, "Wavelet packet functions based coded MC-CDMA system and its performance," *Proc. of IEEE VTC 2000*, Tokyo, Japan, vol. 3, pp. 1933-1937.

[41] Akram Aldroubi and Michael Unser, "Families of wavelet transforms in connection with Shannon's sampling theory and the Gabor transform," *Wavelets: A Tutorial in Theory and Applications*, Edited by Charles K. Chui, Academic Press, 1992.

[42] Hongbing Zhang and H. Howard Fan, "An indoor wireless channel model based on wavelet packets," *Proc. of 34th Asilomar Conference on Signals, Systems and Computers*, 2000, Pacific Grove, USA, pp. 455-459.

[43] Hongbing Zhang, H. Howard Fan, and Alan Lindsey, "A wavelet packet based model for time-varying wireless communication channels," *Proc. of the third IEEE SPAWC Workshop*, March, 2001, Taiwan, pp. 50-53.

[44] C. Van Bouwel *et al*, "Wavelet packet based multicarrier modulation," *Proc. of IEEE Symposium on Communications and Vehicular Technology*, Oct. 2000, Leuven, Belgium, pp. 131-138.

[45] A. M. Sayeed and B. Aazhang, "Joint multipath-Doppler diversity in mobile wireless communications," *IEEE trans. on Communications*, vol. 47-1, Jan. 1999, pp. 123-132.

[46] Milos I. Doroslovacki and Howard H. Fan, "Wavelet-based linear system modeling and adaptive filtering," *IEEE Trans. on Signal Processing*, vol. 44, no. 5, May 1996, pp. 1156-1167.

[47] Ronald R. Coifman and Mladen Victor Wickerhauser, "Entropy-based algorithms for best basis selection," *IEEE Trans. on Information Theory*, vol. 38, no. 2, March 1992, pp. 713-718.

[48] Theodore S. Rappaport *et al*, "Statistical channel impulse response models for factory and open plan building radio communication system design," *IEEE trans. on Communications*, vol. 39, no. 5, May 1991, pp. 795-807.

[49] Homayoun Hashemi, "The indoor propagation channel," *Proc. of IEEE*, vol. 81, no.7, July 1993, pp. 943-967.

[50] Homayoun Hashemi, "Impulse response modeling of indoor radio propagation channels," *IEEE JSAC*, vol. 11, no. 7, Sept. 1993, pp967-977.

[51] P. B. Papazian, J. R. Hoffman, Y. Lo, "Phoenix, AZ, Washington, Sectors A, B, G", NTIA/ITS Mobile Radio Impulse Response Data 01-3[CD-ROM], 2000.

[52] Alan, R. Lindsey, "Generalized orthogonally multiplexed communication via wavelet packet bases," *Ph. D. Dissertation*, Ohio University, June 1995.

[53] William Wayne Jones, "A unified approach to orthogonally multiplexed communication using wavelet bases and digital filter banks," *Ph.D Dissertation*, Ohio University, August 1994.

[54] Stephen B. Wicker, *Error Control Systems for Digital Communication and Storage*, Prentice Hall, New Jersey, 1995.

[55] Simon Haykin, *Adaptive Filter Theory*, Prentice Hall, New Jersey, 3rd edition, 1996.

[56] Martin Toeltsch and Andreas F. Molisch, "Efficient OFDM transmission without cyclic prefix over frequency-selective channels," *Proc. of IEEE PIMRC 2000*, London, UK, vol. 2, Sept. 2000, pp. 1363-1367.

[57] Fred Daneshgaran and Marina Mondin, "Wavelets and scaling functions as envelope waveforms for modulation," *Proceedings of IEEE-SPIE*, pp. 504-507, 1994.

[58] Hongbing Zhang, H. Howard Fan, and Alan Lindsey, "Wavelet packet waveforms for multicarrier CDMA communications," *Proc. of IEEE ICASSP 2002*, Florida, USA, vol. 3, pp. 2557-2560.

[59] Hongbing Zhang, H. Howard Fan, and Alan Lindsey, "Receiver design for wavelet based multicarrier CDMA communications," submitted to *IEEE transactions on Vehicular Technology*.

[60] X. Wang, W. Lu and A. Antoniou, "Multiuser detection for multiple-access communications using wavelet packet transforms," Proc. of IEEE PACRIM'97, BC, Canada, vol. 2, pp. 607-610.

[61] D. Mihai Ionescu and Mark A. Wickert, "On the performance of a CDMA system with user signatures based on packet wavelets in multipath channels," *Proceedings of IEEE VTC'97*, vol. 1, pp. 392-396.

[62] G. L. Turin, "The characteristic function of Hermitian quadratic forms in complex normal variables," Biometrika, vol. 47, pp. 199-201, June 1960.